European Space Agency
Advanced Concepts Team

University of Liege
Faculty of Applied Sciences

Implications of the Pioneer Anomaly for the Laser Interferometer Space Antenna

Master thesis of Denis Defrère in order to obtain the degree of Civil Engineer in Physics. Orientation: Space Technologies.

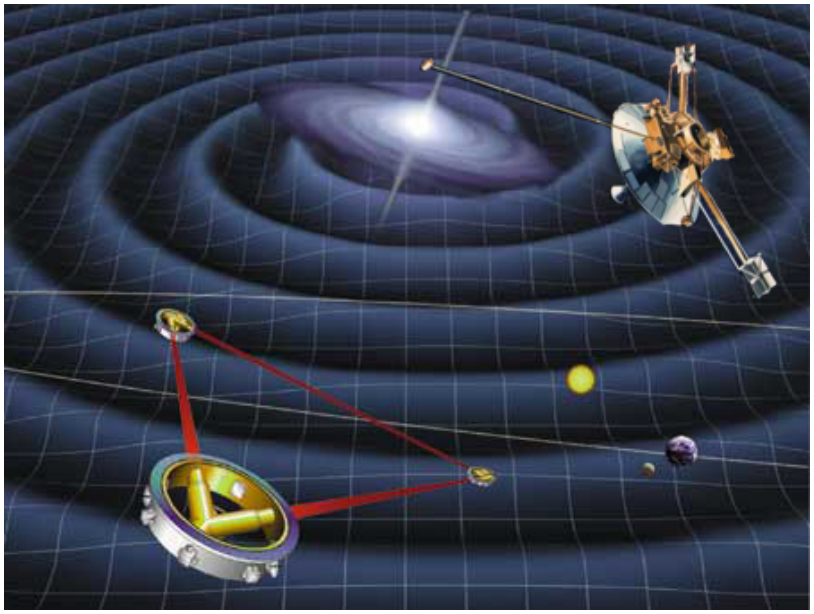

Supervised by
A. Rathke and J. P. Swings

Academic year
2004 – 2005

European Space Agency
Advanced Concepts Team

University of Liege
Faculty of Applied Sciences

Implications of the Pioneer anomaly for the Laser Interferometer Space Antenna

The Doppler tracking data from two deep-space spacecraft, Pioneer 10 and 11, show an anomalous blueshift, which has been dubbed "Pioneer anomaly". Whereas the effect is most commonly interpreted as a real deceleration of the spacecraft, it could as well indicate an unknown effect on the radio signal itself. Several authors have made suggestions how such a blueshift could be related to cosmology or to varying fundamental constants. We consider this interpretation of the Pioneer anomaly and study the impact of an anomalous blueshift on the Laser Interferometer Space Antenna (LISA), the first space-based gravitational wave observatory. The relative frequency shift (proportional to the light travel time and of the same magnitude as the Pioneer anomaly) for the LISA arm length is estimated to 10^{-16}, which is much bigger than the expected amplitude of the weakest measurable gravitational waves. Hence the effect could in principle be detectable.

The impact of the anomalous blueshift in the measurement band of LISA is considered both in the framework of phase noise cancellation in the frequency domain and time-delay interferometry. It is found that the blueshift does not spoil gravitational waves detection and is not detectable due to the small relative change of arm length in the frequency range of the measurement band. We also study the impact of the blueshift on timescales of a considerable fraction of the orbital period of LISA. Here the effect of the blueshift due to change of arm length of the interferometer can reach the magnitude of the LISA instrument noise. We discuss the possibility to detect the anomaly on these timescales by monitoring data of the laser stability.

Master thesis of **Denis Defrère**
In order to obtain the degree of
Civil Engineer in Physics
Orientation: Space Technologies

Board of examiners

J.P. SWINGS A. RATHKE Y. DE ROP P. ROCHUS

Agence Spatiale Européenne
Advanced Concepts Team

Université de Liège
Faculté des Sciences Appliquées

Influence de l'anomalie de Pioneer sur le "Laser Interferometer Space Antenna"

Les données télémétriques en provenance de deux sondes spatiales aux confins du système solaire, Pioneer 10 et 11, présentent un excès fréquentiel anormal, appelé anomalie de Pioneer. Bien que ce phénomène soit souvent interpreté comme une réelle décélération des sondes, il pourrait tout aussi bien indiquer un effet inconnu sur le signal lui-même. Plusieurs auteurs ont suggéré que cet effet proviendrait de l'expansion cosmologique ou d'une variation des constantes physiques fondamentales. Considérant ces interprétations, l'anomalie de Pioneer pourrait influencer la mission LISA (Laser Interferometer Space Antenna), le premier observatoire spatial d'ondes gravitationnelles. Le décalage relatif en fréquence (proportionnel au temps de vol du signal) sur les bras de LISA est estimé à 10^{-16}, ce qui est 4 ordres de grandeur supérieur à l'amplitude des plus faibles ondes gravitationnelles mesurables par LISA. L'effet pourrait donc en principe être détectable.

L'influence de cet excès fréquentiel est étudié dans le domaine de sensibilité de LISA par les méthodes interférométriques d'élimination des instabilités liées aux lasers. Cela permet de conclure que cet excès fréquentiel n'affecte pas la précision de mesure des ondes gravitationnelles et ne pourra pas être détecté dans la bande de sensibilité de LISA. Pour une période de détection plus longue, en dehors de la bande de sensibilité de LISA, l'inluence de l'anomalie est maximum, atteignant une amplitude comparable à celle des bruits instrumentaux de LISA. Cependant, pour une période d'observation plus longue, l' instabilité des lasers est moins efficacement éliminée et la possibilité de détection de l'anomalie est alors spécifiquement étudiée.

Travail de fin d'études présenté par
Denis Defrère
En vue de l'obtention du grade
d'Ingénieur Civil physicien
Orientation: techniques spatiales

Les membres du jury

J.P. SWINGS A. RATHKE Y. DE ROP P. ROCHUS

Acknowledgements

First of all, I would like to thank Andreas Rathke, responsible for fundamentals physics in the Advanced Concepts Team, for his time, guidance and teaching. We had daily discussions about this study which enhanced considerably my knowledge and my way to work. I am also very grateful to him for his kindness and encouragement during all this work.

I wish also to acknowledge Jean-Pierre Swings, my supervisor at University of Liege. Without him, I would never had the opportunity to perform this work.

Finally, I am also grateful to Pisart jury to have given me helpful funds and to Franco Ongaro for his intervention in the cost caused by my presentation of this work at the "Lasers, clocks and drag-free" conference (Bremen-May 2005).

Contents

Introduction **6**

1 The Pioneer anomaly **8**
1.1 Pioneer 10/11 missions: Overview 8
1.1.1 Mission status 8
1.1.2 Main characteristics of the spacecraft 9
1.2 The anomaly 9

2 LISA and Gravitational Waves **12**
2.1 Gravitational Waves 12
2.1.1 Physical characteristics 12
2.1.2 Astronomical sources 13
2.2 Laser Interferometer Space Antenna: LISA 15
2.2.1 The LISA concept 15
2.2.2 Spacecraft configuration 15
2.2.3 Lasers 17
2.2.4 Data extraction 17
2.2.5 Drag-free and attitude control 17
2.2.6 Ultrastable structures 18
2.2.7 The LISA orbits 18
2.2.8 Complementarity with the others detectors 19

3 An anomalous blueshift of light? **21**
3.1 The Pioneer anomaly as a blueshift 21
3.1.1 Magnitude of the blueshift 22
3.1.2 Comparison with the Berry phase model 25
3.1.3 Impact on LISA arms 27
3.2 Berry phase and gravitational waves 28
3.2.1 Doppler shift induced by the gravitational waves 28
3.2.2 Implications of the Berry phase and total Doppler shift 31

4 Implications for LISA **32**
4.1 Introduction 32
4.2 Interferometric measurement 32
4.3 The noises 34
4.3.1 Laser phase-noise 35
4.3.2 Shot noise 35
4.3.3 Acceleration noise 35
4.4 Frequency domain algorithm 37
4.4.1 The two-way Doppler signals 37
4.4.2 Laser phase noise cancellation 41

4.4.3 Theoretical performance of the algorithm . . . 43
4.4.4 Spectral leakage . . . 47
4.4.5 Outside the frequency band . . . 50
4.4.6 Conclusions of the frequency domain study . . . 51
4.5 Time delay interferometry . . . 52
4.5.1 Notation . . . 52
4.5.2 Signal and noise response functions . . . 53
4.5.3 Linear data combinations . . . 55
4.5.4 Gravitational wave sensitivity . . . 60
4.5.5 Conclusions of the TDI study . . . 61
4.6 Effect of orbital motion on Time Delay Interferometry . . . 62
4.6.1 The effects of rigid rotation . . . 62
4.6.2 The effects of flexing . . . 64

5 Conclusions **65**

Appendix **66**
A. Flight configuration . . . 66
B. Orbital noise . . . 69

References **70**

Glossary and Acronyms **73**

Introduction

The Pioneer anomaly refers to the discrepancy between the expected and observed frequencies received by outer Solar System spacecraft. The effect is clearly seen on the two Pioneer spacecraft, launched in the early seventies in opposite directions of the Solar System. These spacecraft are still the most precisely navigated deep space vehicles ever. The data from other deep space vehicles, like Galileo and the Voyagers, cannot confirm the anomaly because of relative proximity to the Sun and 3-axis spin-stabilization respectively, which make the effect harder to measure accurately. As of 2005, there is still no universally accepted explanation for the phenomenon. All internal sources of systematic errors have been studied and ruled out. Also to be rejected as an explanation, the effect of interplanetary dust, which was estimated to be too small. The inability to explain the anomalous acceleration of the Pioneer spacecraft with conventional physics has contributed to the growing discussion about its origin. The possibility that it could come from new physics or from a new effect of known physics is now being seriously considered.

The main difficulty in attempting an explanation of the anomaly in terms of new physics is that a modification of gravitation, large enough to explain the Pioneer anomaly, is in obvious contradiction with the planetary ephemeris. Hence the Pioneer anomaly can hardly be ascribed to a gravitational force since this would indicate a considerable violation of the *weak equivalence principle*. Recent works make the suggestion that the anomaly has nothing to do with the spacecraft motion but instead with an anomalous blueshift in the frequency of light. This blueshift could be caused by a *Berry phase*, a geometrical effect in the adiabatic evolution of the quantum state of a photon which propagates within an expanding space-time. Such a blueshift, proportional to the light-travel time, could be confirmed by a large gravitational wave observatory, like LISA (Laser Interferometer Space Antenna). This future ESA-NASA mission is aimed at detecting and studying low-frequency gravitational waves through their influence on the phases (or frequencies) of laser beams exchanged between three remote spacecraft. An additional Doppler shift on these laser beams could have consequences on the detection of gravitational waves and could reveal the Pioneer anomaly if it is measured. It is the purpose of this work to assess the implications of such a putative blueshift for LISA.

After a brief introduction of the Pioneer and LISA missions, we first estimate the anomalous frequency rate of change along the light path. By applying our result to LISA, it is found that the anomalous relative frequency shift for the LISA arm length is about 10^{-16}, which is much bigger than the expected amplitude of the weakest measurable gravitational waves. Hence the effect could in principle be detectable. Then, the main difficulty of this work was to establish to what extent suggested physical interpretations of the blueshift affect the gravitational wave propagation. Our results show the following:

1. The contribution of the anomaly within the *sensitivity band* of LISA is a second order term, below all instrument noises. We show explicitly that it is still the case after the cancellation of the leading noise source, the laser phase noise.

2. Outside the *sensitivity band* of LISA, the effect is bigger. It reaches the secondary noise

sources but it is still below the laser phase noise. In order to detect it, we investigate if the laser phase noise can be sufficiently cancelled by both frequency domain method and time delay interferometry (TDI).

Time delay interferometry and a frequency domain algorithm are the two methods developed to cancel the laser phase noise in the case of unequal arm length interferometers. This cancellation is necessary since the gravitational wave signatures in the data are overwhelmed by the laser phase noise, which is several orders of magnitude larger. For an equal arm length interferometer, this noise is easily removed as the signals from one laser experience the same delay in the arms. The instability of the laser is then exactly cancelled when the signals come back. Because of the orbital motion, LISA will obviously have unequal arm lengths and signals will not experience the same delays in different arms. In the frequency domain method, the problem is solved by using the signal of one arm to determine the laser phase noise. Then, the measured time series of the noise can be used to correct the interferometer response. In the case of TDI, the solution is to introduce appropriate time delays on the signals before combining them. Both methods are however developed for fixed interferometer in space and the continuous arm length changes, induced by the orbital motion of LISA, have to be specifically addressed. These are the main principles of the two methods cited above. The frequency domain method is the original baseline method of LISA, while Time Delay Interferometry is newer but not yet fully developed.

Finally, note that the last pages of this report give the meaning of technical terms, written in italic in the main text.

Chapter 1

The Pioneer anomaly

Since the beginning of the eighties, the signals received by two outer solar system spacecraft, Pioneer 10 and 11, have shown a clear discrepancy between the expected and the observed frequencies. Commonly, it is said that the spacecraft are slowing down. However, despite the growing number of publications on this phenomenon, its origin has not been yet figured out. It might come from external or internal sources of systematic errors, or from some unknown physical phenomena. In this section, we first describe briefly the Pioneer spacecraft before giving more details on the anomaly.

1.1 Pioneer 10/11 missions: Overview

1.1.1 Mission status

The pioneer 10 and 11 missions started the exploration history of the giants planets. Launched on 2 March 1972, Pioneer 10 was the first to explore Jupiter, which it encounters on 4 December 1973. On 5 April 1973, Pioneer 11 was launched to explore Saturn (see Fig. 1.1). Pioneer 11's primary mission was to be the backup for Pioneer 10. If Pioneer 10 failed before completing its Jupiter flyby, Pioneer 11 would have to repeat that flyby. Fortunately, Pioneer 10 didn't failed and Pioneer 11 has been allowed to go to Saturn.

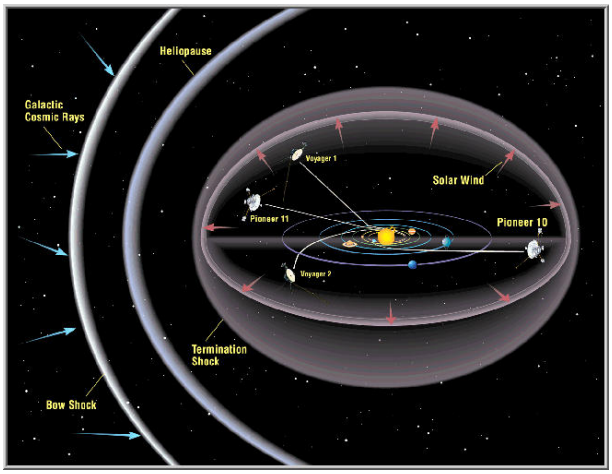

Figure 1.1: Hyperbolic orbits of the Pioneers.

After their encounters with the planets, the two spacecraft have followed hyperbolic escape orbits near the plane of the ecliptic to study the solar wind and the cosmic radiation. On 1 January 1987, Pioneer 10 was approximately 40 A.U. from the Sun, and receding with a nearly constant velocity of 12.8 km/s. The mission came officially to an end on March 31, 1997 for budgetary reasons. However, the Pioneer 10 radio system was still operating and occasional contacts with the spacecraft still occurred. The last contact with the spacecraft, very weak, took place on January 22, 2003 and a last unsuccessful attempt on February 7 the same year. Currently, Pioneer 10 is at more than 88 astronomical units from the Sun and gradually leaves the Solar System. In spite of that, the record of distance to Earth is held by Voyager 1, which was launched later. The operational life time of Pioneer 11 was shorter than that of its counterpart. In 1990, a switch failure in the radio system disabled the generation of coherent Doppler

signals. So, after that date, when the spacecraft was about 30 AU away from the Sun, no useful data have been generated for the trajectory investigations. Furthermore, by September 1995, its power source was nearly exhausted. Pioneer 11 could no longer make any scientific observations and routine mission operations were terminated. The last communication from Pioneer 11 was received in November 1995, when the spacecraft was at distance of about 40 AU from the Sun.

Finally, note that, in 2 million years, Pioneer 10 should reach the red star Aldebaran while in 4 million years, Pioneer 11 should pass close to the nearest star in the constellation Aquilla.

1.1.2 Main characteristics of the spacecraft

Pioneer 10 and 11 are identical in design. At launch, each had a total mass of 259 kg, including 36 kg of hydrazine propellant. They were designed to fit on the third stage of the Atlas-Centaur launch vehicle so that each spacecraft is 2.9 m long. The parabolic high gain antenna is made of aluminium honeycomb material and has a radius of 137 cm. The other main physical features of the spacecraft are the instrument compartment, which face the direction of travel and the two radioisotope thermoelectric generators (RTGs), which are attached to the compartment by booms of 300 cm length. The spacecraft is spin stabilized, and spins at a rate of roughly 4 or 7 rpm (revolution per minute), respectively. The spin axis is aligned with the high gain antenna axis, which is designed to point towards the Earth, roughly opposite the direction of travel.

Figure 1.2: Pioneer spacecraft [1].

The communication with the spacecraft is performed in the S-band frequencies (2.11 Ghz for the uplink from Earth). Phase coherence with the ground-transmitters is maintained by means of an S-band transponder with the 240/221 frequency turnaround ratio. The signals sent back to Earth have thus a frequency of 2.29 Ghz. The power source is Plutonium (^{238}Pu) with an half-life of 87.74 years. This provides the thermal source for the thermoelectric devices in the RTGs. These delivered about 160 Watts of electrical power at launch time. At present, less than about 65 Watts are still available, so that some instruments are switched off.

Finally, let us quickly list the main scientific instruments on board the Pioneer spacecraft. These are the plasma analyzer, the cosmic ray telescope, the meteorite detector, the ultraviolet photometer, the infrared radiometer and the imaging photopolarimeter.

1.2 The anomaly

The Pioneer anomaly refers to the observed deviation from expectations of the frequency received from various unmanned spacecraft visiting the outer Solar System, notably Pioneer 10 and 11. The effect is seen in tracking data, yielding information on the velocity and distance of the spacecraft, and was already observed before the Jupiter flyby of Pioneer 10 (about 5 AU from the Sun). However, the effect was explained by fuel leaks and mismatch in the solar radiation model. After the Jupiter flyby, these justifications become unsatisfactory because of the decrease of the solar radiation pressure and the lower level of gas leaks, due to the quiet state

of the spacecraft. In 1980, when Pioneer 10 passed a distance of $\sim$ 20 AU from the Sun, the acceleration contribution from solar-radiation pressure on the spacecraft (directed away from the Sun) had decreased to less than 4×10^{-10} m/s^2 and therefore, a search for an unmodeled acceleration of this level could start (see Fig. 1.3).

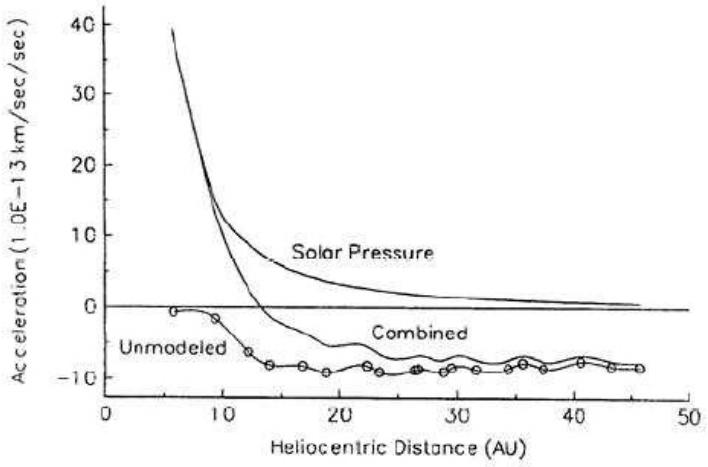

Figure 1.3: Unmodeled acceleration on Pioneer 10 as a function of distance from the Sun (bottom line) and calculated solar radiation acceleration (top line) [3].

Nevertheless, at the beginning, the anomaly was not seriously considered and it was only in 1994, since the anomaly has not disappeared, that an inquiry was initiated into its possible origins. The initial results of the study were reported in 1998 [1] and a detailed analysis appeared in 2002 [2], confirmed in the same year by an independent study [3]. In these investigations, contribution of all known sources of a possible systematic origin for the detected anomaly were specifically addressed. The explanations for the discrepancy that have been considered include:

- observational errors, including measurement and computational errors, in deriving the acceleration.
- a real deceleration:
  - by gravitational forces from unidentified sources such as the Kuiper belt.
  - drag from the interplanetary medium, including dust, Solar wind and cosmic rays.
  - gas leaks, including helium, produced by the Pu decay, escaping from the spacecraft radioisotope thermoelectric generators.
  - radiation pressure of sunlight and the spacecraft radio transmissions, or thermal radiation pressure from the radioisotope thermoelectric generators.
  - electromagnetic forces due to an electric charge on the spacecraft.
- New manifestation of known physics:
  - Gravitational interaction of the S-band radio signal with dust.
  - Interaction between the solar wind and the S-band radio signal.
- new physics
  - Interaction with *dark matter* of mirror type.

– Modified gravity.

However, the conclusion remained that there was an anomalous acceleration of $a^*=(8.74\pm1.33)\times 10^{-10}$ m/s^2 in the direction towards the Sun. This anomaly was constant in time for the whole measurement, i.e. between about 20 to 70 AU from the Sun. In Fig. 1.4 below, the two-way Doppler residuals (observed Doppler velocity minus modeled Doppler velocity) for Pioneer 10 are shown.

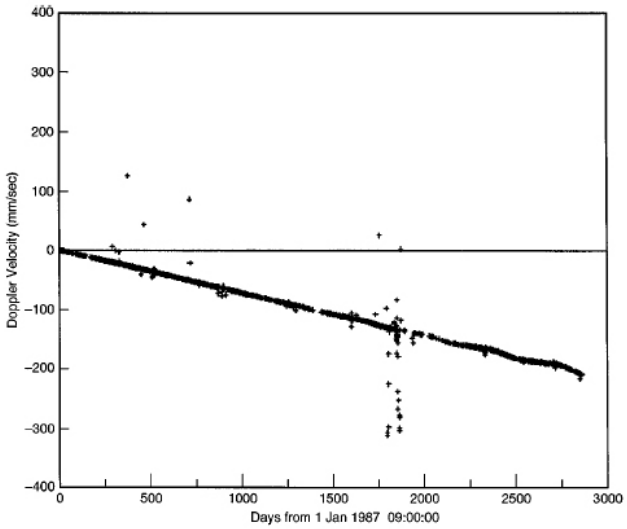

Figure 1.4: Anomalous velocity signal in two-way Doppler frequencies as a function of time [3]. 1 Hz is equivalent to 65 mm/s range change per second.

Data from other outer Solar system spacecraft is also indicative of a similar effect. This is the case of Galileo, which was dedicated to the study of Jupiter. However, because of its relative proximity to the Sun, firm conclusions cannot be drawn from it. Furthermore, the spacecraft that have gone sufficiently far from the Sun, like the Voyagers, are fully 3-axis spin-stabilized which makes the effect harder to be accurately measured.

The inability to explain the anomalous acceleration of the Pioneer spacecraft with conventional physics has contributed to the growing discussion about its origin. As of 2005, there is still no universally accepted explanation for this phenomenon; while it is possible that the explanation will be prosaic, such as thrust from gas leakage, the possibility of entirely new physics is also being considered. In addition, there is no new useful data to test the Pioneer anomaly because the Pioneer spacecraft are no longer providing data, Galileo was deliberately burned up in Jupiter's atmosphere at the end of its mission and currently operating spacecraft do not fulfill the high navigational requirements. In addition, many of the deep space missions that are currently being planned either will not provide the needed navigational accuracy and trajectory stability of under 10^{-10} m/s^2 or else they will have significant onboard systematics that mask the anomaly (e. g. Jupiter Icy Moons Orbiter). However, there would be the possibility to test the anomaly in non-dedicated missions to Neptune and beyond with Navigational precision about 15 times better than with Pioneer 10/11 [4].

Chapter 2

LISA and Gravitational Waves

The Laser Interferometer Space Antenna (LISA) is a mission jointly sponsored by the European Space Agency (ESA) and the National Aeronautics and Space Administration (NASA). LISA will be the first space-based gravitational wave detectors. Gravitational waves are a consequence of general relativity and can be intuitively understood as ripples in space-time, which produce a variation of the distance between free macroscopic bodies. LISA has been specially designed to detect gravitational waves from *massive black holes* (MBH) and galactic binaries in the frequency range 10^{-4} to 10^{-1} Hz where there are expected to be the most powerful. Once in orbit, LISA's observations will bring unprecedented information to better understand the fundamental physical laws of the Universe. As it will be useful all along this report, we begin this chapter by giving an overview of gravitational waves. Then, we briefly introduce the LISA concept, stressing the characteristics relevant for our study.

2.1 Gravitational Waves

2.1.1 Physical characteristics

According to General Relativity, space and time do not have independent existence but rather, are deeply intertwined. The physical world takes a geometric interpretation in terms of space-time which is more intuitive than the Newtonian picture of gravitation. Then, as a result of the Einstein field equations, massive bodies and energy influence this space-time. It is commonly said that they curve it. In this space-time, as Einstein showed in a paper that appeared in 1916 [5], a mass distribution moving in an asymmetric way will produce ripples travelling outwards. These ripples in space-time are called gravitational waves. These are fundamentally different from the familiar electromagnetic waves. While electromagnetic waves, created by the acceleration of electric charges, propagate in the framework of space and time, gravitational waves, created by the acceleration of masses, are waves of the space-time fabric itself. Unlike charge, which exists in two polarities, masses always come with the same sign. This is why the lowest order asymmetry producing electro-magnetic radiation is the dipole moment of a charge distribution, whereas for gravitational waves it is a change in the quadrupole moment of the mass distribution. Hence those gravitational effects, that are spherically symmetric, will not give rise to gravitational radiation. A perfectly symmetric collapse of a supernova will produce no waves, a non-spherical one will emit gravitational radiation. A binary system will always radiate.

In 1950, it was proved rigorously that gravitational radiation is in fact a physically observable phenomenon (c.f. [6] for the a review of the discussion at that time), that gravitational waves carry energy and that, as a result, a system that emits gravitational waves should lose energy. In accordance with this, in 1993, Hulse and Taylor were awarded the Nobel prize in physics for the indirect proof of the existence of gravitational waves by observing the decrease of the angular

momentum of the binary pulsar PSR 1913+16. This decrease, which indicates the emission of gravitational waves, was in perfect accordance with general relativity. It is interesting to note that already in 1805, Laplace, in his "Traité de Mécanique Céleste" stated that, if gravitation propagates with finite speed, the force in a binary star system should not point along the line connecting the stars, and the angular momentum of the system must slowly decrease with time.

Today, several ground-based gravitational wave detectors are about to become operational throughout the world to bring a direct detection, not yet achieved. A direct detection could be brought also by LISA which has been specifically designed for the detection of several kinds of sources predicted by current astrophysical theory (see next subsection). A gravitational wave passing through the Solar System creates a time-varying strain in space that periodically changes the distances between all bodies in a direction that is perpendicular to the direction of wave propagation. In particular, these could be the distances between shielded *proof masses* inside spacecraft that are separated by a large distance, as in the case of LISA. The main challenge is to achieve the very high accuracy needed to measure the relative length change. For example, the periodic change in distance between two *proof masses*, separated by 5×10^6 km, due to a typical *white dwarf* binary at a distance of 50 pc (*parsec*) is only about 10^{-10} m. This small change indicates the extreme stiffness of the space-time elastic medium and not a poor content in energy. For instance, a supernova in a not too distant galaxy could drench every square meter of earth with kilowatts of gravitational radiation intensity [8].

2.1.2 Astronomical sources

There are several expected sources of gravitational waves all over the frequency spectrum. This is illustrated in Fig. 2.1 below.

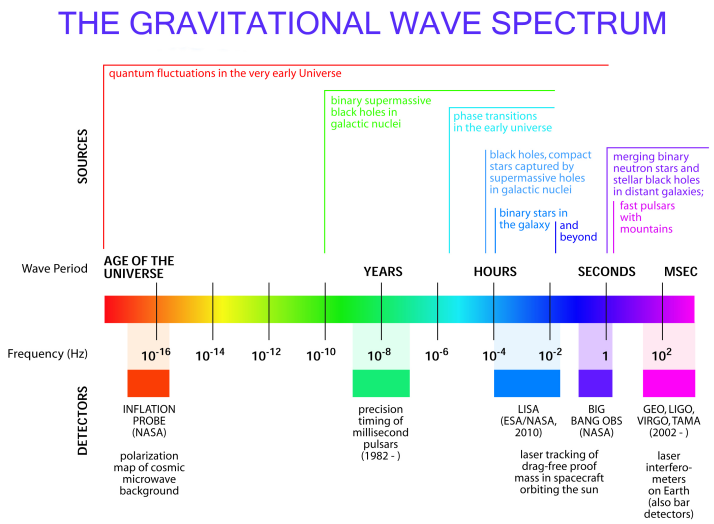

Figure 2.1: Spectrum of the expected sources of gravitational waves [51].

Mainly, there are two important categories of gravitational waves for LISA: the galactic binaries and the *massive black holes* (MBHs) expected to exist in the centres of most galaxies. Because the masses involved in typical binary star systems are small, a few solar masses[1], the observation of binaries is limited to our Galaxy. Galactic sources that can be detected by LISA include a wide variety of binaries, such as pairs of close *white dwarfs*, pairs of *neutron stars*, *neutron*

[1]The Solar mass ($\sim 10^{30}$ kg) will be denoted by $M_\odot$ in the following.

star and *black hole* ($5_{\odot}$- $20M_{\odot}$) binaries, pairs normal stars, normal star and *cataclysmic white dwarf* binaries, and possibly also pairs of *black holes*. It is likely that there are so many *white dwarf* binaries in our Galaxy that they cannot be resolved at frequencies below 10^{-3} Hz, leading to a confusion noise limit (see Fig. 4.16). LISA would also provide a lot of new information about the formation, growth, space density and surroundings of *massive black holes*. There is now compelling indirect evidence for the existence of MBHs with masses of 10^6 to $10^8 M_{\odot}$ in the centres of most galaxies, including our own. The most powerful sources are the mergers of MBHs in distant galaxies, with amplitude signal-to-noise ratios of several thousand for $10^6 M_{\odot}$ *black holes*. Observations of signals from these sources would test General Relativity and particularly black-hole theory to unprecedented accuracy. Note that not much is currently known about *black holes* with masses ranging from about 100 $M_{\odot}$ to $10^6 M_{\odot}$. LISA can provide unique new information throughout this mass range. Note also that there should exist background of gravitational waves coming from the beginning of the universe. If, just after the Big Bang, gravitational radiation was in thermal equilibrium with the other fields, then today its temperature would have been redshifted to about 0.9 K. This radiation peaks at frequencies inaccessible for LISA (see Fig. 2.1). Thus, if LISA sees a primordial background, it will be non-thermal.

This brief overview of gravitational waves sources can be summarized by Fig. 2.2 below.

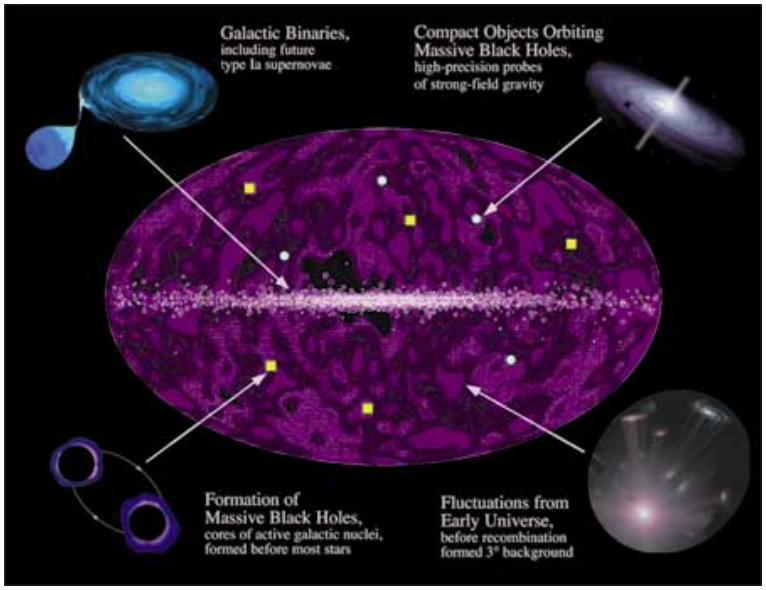

Figure 2.2: Image of the sky viewed by gravitational waves [51].

This figure shows the sky as seen from gravitational waves. The most important sources are the galactic binaries. Some are so well studied, especially the X-ray binary 4U1820-30, that they are one of the most reliable sources. If LISA would not detect the gravitational waves from known binaries with the intensity and polarisation predicted by General Relativity, it would shake the very foundations of gravitational physics.

2.2 Laser Interferometer Space Antenna: LISA

The Laser Interferometer Space Antenna is the first dedicated space-based gravitational wave observatory. So far the only space searches for gravitational waves have been made using measurements of radio signals, not optimized for gravitational wave searches, from spacecraft on their way to other planets (see [7] for the more recent results from Cassini). LISA will use an advanced system of laser interferometry and the most delicate measuring instruments ever made to directly detect gravitational waves. LISA is aimed at a launch in 2012 with a planned mission duration of 10 years. ESA is providing the three spacecraft and their propulsion modules, the gravitational reference sensors, some interferometry components and the laser subsystems. NASA is providing the launch vehicle and the spacecraft's telecommunications systems. NASA will also perform payload integration and testing. The mission will be operated from the Jet Propulsion Laboratory.

2.2.1 The LISA concept

LISA consists of three identical spacecraft, which have roughly the shape of a 2.2 m diameter cylindrical boxes, as shown in Fig. 2.3 on the right. These are freely flying (not connected to each other) five million kilometers apart, in an equilateral triangle. Together, the three spacecraft function as a *Michelson interferometer* with an additional redundant third arm. The arm length has been chosen to optimize the sensitivity of LISA at the frequencies of known and expected sources. An arm length increase higher than 5×10^6 km would begin to compromise the high-frequency sensitivity when the light in the arms travels for more than half of the gravitational wave period. An interferometer shorter would begin to lose the interesting low-frequency *massive black hole* sources. It would give less scientific information but would not be any easier to build or operate because the spacecraft and the interferometry would be essentially the same.

Figure 2.3: Cutaway of LISA's instrument [8]. The actual spacecraft will be protected with a cover.

The goal is to operate the observatory with very few interruptions for long periods, typically for a half or one year. This will provide near continuous data sets, which will be analysed to separate the gravitational wave signals resulting from many different astrophysical sources. The steady data acquisition may be interrupted for periods of adjustment such as making changes to the relative spacecraft velocity. It may also be interrupted by events such as solar flares which may cause disturbances to the *drag-free* sensor *proof mass*. Scientific data acquisition will be limited by the mission consumables which are sized to permit extended operations over 10 to 20 years.

2.2.2 Spacecraft configuration

In each spacecraft, the two telescope arms are identical and subtend an angle of 60°. The configuration is outlined in Fig. 2.3. Not shown are the top lid, serving as a thermal shield, and the down-link antennas. Each spacecraft will also always have the Sun shining on the same, the "upper", side, at an angle of incidence of 30°. Baffles, with end angles at 30°, will be added to prevent sunlight from entering the telescopes. This will provide a thermally very stable environment, necessary for the high precision required to detect gravitational waves. The

scientific package will be located inside the gold-coated Y-shaped tubular protection, serving as a thermal shield. This internal configuration is shown in detail in Fig. 2.4 below.

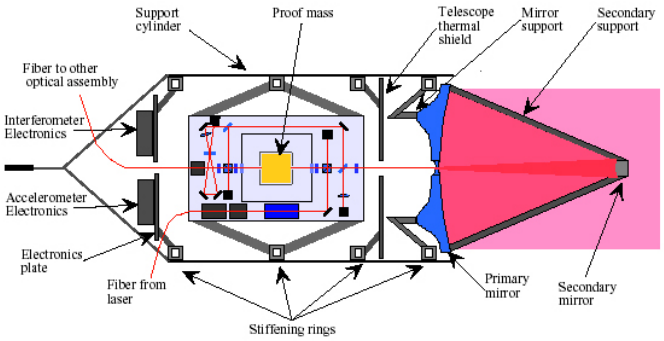

Figure 2.4: One of the two optical assemblies of the Y-shaped LISA payload [8].

Since it will useful for the following, we briefly describe below the important components for our study, beginning by the innermost.

The proof mass

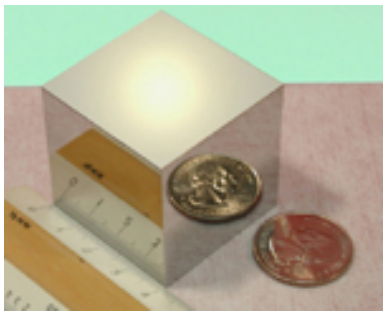

Figure 2.5: Highly polished test mass cubes [51].

The proof masses are considered the heart of the instruments as the interferometry between the spacecraft will be done with respect to them. They consist of cubes allowed to float freely within the spacecraft and shielded from external and internal disturbances so that they detect only the force of gravity. The cubes are highly polished to enable them to reflect laser light. In this way, they act as mirrors in the interferometer. The relative motion of these cubes on different spacecraft is what will detect passing gravitational waves. The test masses are essentially 40 mm cubes (see Fig. 2.5 on the left) with a mass of about 1.3 kg and made from an alloy chosen for its low magnetic susceptibility (90% Au, 10% Pt). These proof masses are also shown schematically in Fig. 2.4.

The optical bench

The optical bench is a rigid structure made of ultra-low expansion material in which, for rigidity, the optical components are embedded. All beams propagate in the central plane of this optical bench. The laser light is conducted onto the optical bench via an optical fibre (mono-mode, polarisation preserving). The light returning from the distant spacecraft is reflected on the *proof mass* before it is brought to interference with a fraction of the internally generated laser light. This configuration (see Fig. 2.4) will be very important when we will introduce the interferometric measurement and more details will be given.

The telescope

On right hand part of Fig. 2.4, the telescope on board of LISA's spacecraft is shown. It serves the dual purpose of transmitting the laser beam to the distant spacecraft and of receiving the light from that spacecraft. It is conceived as a *Cassegrain*, with a parabolic primary mirror of 300 mm in diameter, and a hyperbolic secondary mirror of 32 mm in diameter.

2.2.3 Lasers

The use of lasers is a natural choice for interferometric measurements since highly stable coherent signals are required. Lasers offer this high stability and have extremely narrow beams that can survive long journeys through space. In addition, the infrared frequency of the lasers has been chosen to render it immune from refraction caused by the charged particles plasma which permeates interplanetary space. It is intended to use solid-state diode-pumped monolithic miniature Nd:YAG (Neodymium-doped: Yttrium-Aluminium Garnet) ring lasers that generate a continuous 1 W infra-red beam with a wavelength of 1.064 μm. They allow LISA to deliver sufficient power at high efficiency, being compact, stable (in frequency and amplitude), and reliable at the same time. Each spacecraft has two 1 Watt lasers (actually four, two for redundancy), one master and one slave. A fraction of the light from the master laser (10 mW) is bounced off the back surface of its cube, and used as a reference to put the other local laser in slave mode. In this way, the main ($\sim$ 1 W) beams going out along each arm can be considered as having originated from a single laser.

2.2.4 Data extraction

At each spacecraft, the light coming from the neighbours has to be amplified before being sent back. This is due to the divergence of the beam over the $5{\times}10^6$ km between the spacecraft. Even though each outgoing beam is extremely narrow, a few micro radians, it is about 20 km wide when it reaches the distant spacecraft. The light sent out along an arm is received by the end spacecraft telescope, reflected on its cube, then amplified using its local laser, in such a way as to maintain the phase of the incoming light. The amplified light is then sent back. If the signal was simply reflected and sent all the way back, only about 200 photons per hour would reach the end spacecraft after the round-trip. The amplification brings the number back up to over 10^8 photons per second, which makes the signal detection straightforward using standard photodiodes.

2.2.5 Drag-free and attitude control

The purpose of the drag-free system is to shield the *proof masses* from interplanetary gas drag and solar radiation pressure, so that they follow trajectories which are determined only by gravity. The drag-free system consists essentially of a cavity containing sensors, which measure the position of the *proof mass* with respect to the outer spacecraft. The spacecraft in turn one has small thrusters which are fired so that it follows the *proof mass*, which then always remains centered in the cavity. Only a few micro-Newtons are required to operate the drag-free system. The delivered force must be smoothly controlable so that the varying disturbance forces can be matched without introducing a further disturbance from the thrust system itself. This is accomplished by accelerating ions in an electric field, and ejecting them to develop the thrust. The name Drag-Free spacecraft stems from the fact that there is no drag on the inner *proof mass*, and the drag on the main satellite is exactly compensated by the thrusters.

As an example, let us consider the momentum of the light from the Sun, which amounts to an average pressure of about 5×10^{-6} N/m^2. The internal dynamics of the Sun leads to small variations, of less than one percent, in this photon pressure, which occur at the low frequencies within LISA's *sensitivity band*. Although this variable photon pressure may seem rather small, if it were allowed to act on the *proof masses*, the resulting motion would be 10^4 times larger than the tiny motions due to gravitational waves that LISA is looking for. Then, the *drag-free* system has to come into operation to correct the relative motion induced by solar pressure blowing on the surface. This is done very precisely by monitoring the change in electrical capacitance between the *proof mass* and electrodes mounted at the spacecraft. The measurement is then

converted into a force-command, which instructs thrusters mounted on the outer structure of the spacecraft, to fire against the solar pressure and keep the spacecraft centred on the *proof mass*.

The LISA Pathfinder mission, an ESA technology demonstrator mission carrying the LISA Technology Package, will test the novel drag-free and attitude control technology needed for LISA. LISA Pathfinder is planned for launch in 2008.

2.2.6 Ultrastable structures

The thermal stability of the spacecraft is a very crucial point of the mission. Mostly, it is required to minimized the impact of the heat-load fluctuations induced by the small variations in the intensity of sunlight. In fact, this could lead to thermal gradients across the *optical bench*, which would upset the stability of the laser cavity. To obtain the required thermal stability, most structural elements are made from carbon-epoxy which has a thermal expansion coefficient of 4×10^{-7}/K. The *optical bench* is made from ultra-low expansion material, which has a temperature coefficient at least a factor 4 lower than the carbon-epoxy over the possible temperature range of the LISA payload. Furthermore, low emissivity coatings are used on most surfaces inside the spacecraft and a thermal shield surrounds the payload cylinder, in order to provide isolation from the temperature variations of the spacecraft skin that is exposed to the Sun. These shields are only effective against heat fluctuations faster than a few hours to half a day. The slower variations will pass through, thus making the sensitivity of LISA deteriorate rapidly below roughly 10^{-4} Hz. The use of carbon-epoxy structures also minimises any thermally-induced mechanical distortions which could produce physical changes in the optical path-length, as well as local gravitational disturbances on the *proof masses*.

2.2.7 The LISA orbits

Each spacecraft of LISA moves along an elliptic orbit, with major axis D = 2AU $\approx 3 \times 10^{11}$km, eccentricity e $\approx L/D\sqrt{3} \approx 1/100$ and inclination with respect to the ecliptic $i = L/D \approx 1°$. The heliocentric orbit was chosen because a more stable environment it provides without a clear cost disadvantage against the geocentric orbit. The three orbits (see Fig. 2.6) are displaced by 120° from each other along the ecliptic. With this special choice of orbits, the triangular geometry of the interferometer is largely maintained throughout the mission. More details are given in Appendix A.

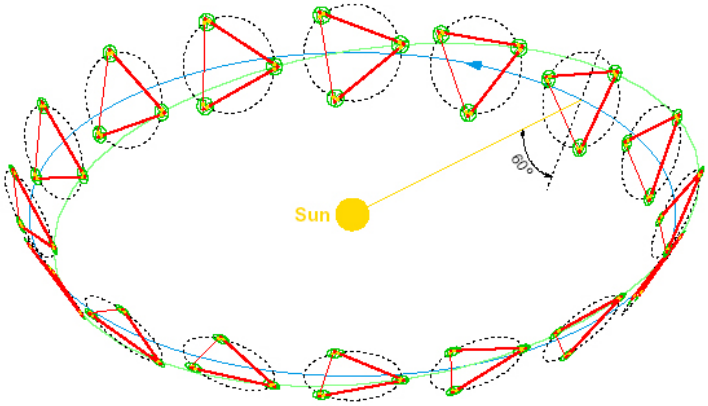

Figure 2.6: LISA configuration [8].

The centre of the triangle is located on the ecliptic (20° behind the Earth) and follows the Earth on its orbit around the Sun. Ideally, the constellation should be as far from Earth as possible in order to minimize gravitational disturbances. The choice of 20° is a practical compromise based on launch vehicle and telemetry capabilities. As the 3-spacecraft constellation orbits the Sun in the course of a year, the observed gravitational waves are Doppler-shifted by the orbital motion and amplitude-modulated by the non-isotropic sensitivity of the detector. This allows the determination of the direction of the source and investigation of some of its characteristics such as polarization. It is expected that the strongest LISA sources (from very distant *supermassive black holes*) should be resolvable to better than an arcminute; and even the weaker sources (galactic binaries) should be positioned to within one degree throughout the entire galaxy.

2.2.8 Complementarity with the others detectors

With the ground-based detectors, the frequency range of observation is limited to frequencies higher than 1 Hz because of the overwhelming seismic effects and terrestrial gravity-gradient noise. The range of frequencies spanned by ground- and space-based detectors are shown schematically in the figure below.

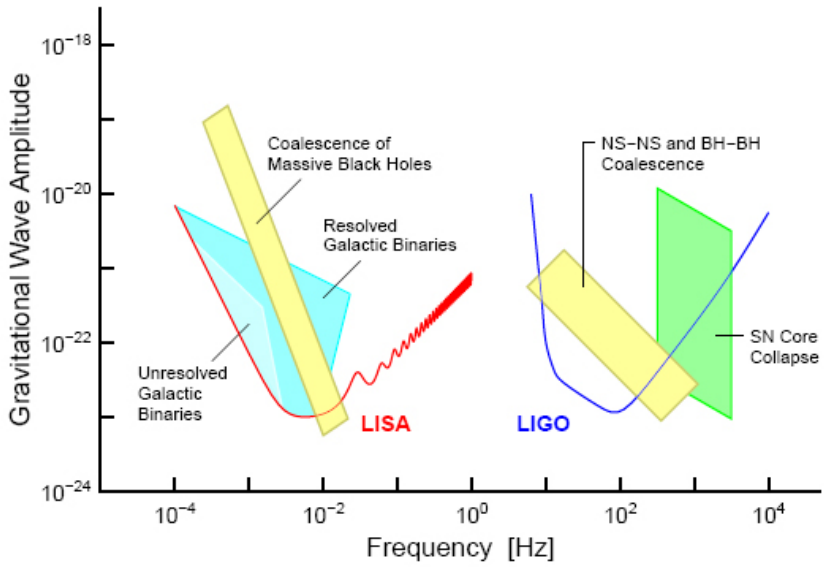

Figure 2.7: Frequency range of ground-and space-based detectors. Some typical sources are also indicated [8].

Ground-based interferometers are physically limited in length to a few km, restricting their coverage to events such as supernova core collapses and binary *neutron star* mergers. In the low-frequency band of LISA, sources are well known and signals are stable over long periods (many months to thousands of years). The low frequencies are very important in present astrophysical modelling and offer a range for great testing opportunity.

1. For systems involving Solar-mass objects, lower frequencies imply larger orbital radii, and the range down to 10^{-4} Hz includes sources with the typical dimensions of many galactic *neutron star* binaries, *cataclysmic binaries*, and some known binaries. These are the most certain sources.

2. For highly relativistic systems, where the orbital velocities approach the speed of light, lower frequencies imply larger masses ($M \simeq 1/f$), and the range down to 10^{-4} Hz reaches

masses of 10^7 $M_\odot$, typical of the *supermassive black holes* that are believed to exist in the centres of many, if not most, galaxies. Their formation and coalescences could be seen anywhere in the observable Universe and are among the most exciting of possible sources. Detecting them would test the strong-field limit of gravitational theory and illuminate galaxy formation and *quasar* models.

Both ground- and space-based detectors will also search for a cosmological background of gravitational waves. During the five-year lifetime of the mission, LISA is expected to yield 163 gigabytes of significant data for analysis. Since both kinds of detectors have similar energy sensitivities, their different observing frequencies are ideally complementary.

Chapter 3

An anomalous blueshift of light?

Among the proposed explanations of the Pioneer anomaly, most would have no significance for LISA. For example, this is the case for all based on systematics generated onboard the Pioneer spacecraft. Generally, if the anomaly corresponds to a real acceleration on the Pioneers, the anomaly should have no influence on LISA. This can be concluded from the fact that the LISA orbit is practically identical to the Earth's orbit. For the Earth itself an anomalous acceleration of the magnitude of the Pioneers would lead to an orbital perturbation which is beyond current observational limits (cf. [16]). Hence only a considerable violation of the *weak equivalence principle* (e. g. between bodies of different mass) could result in an anomalous acceleration on LISA but no on the Earth. Combining this requirement with the constancy of the Pioneer anomaly such an effect seems very hard to envisage. On the other hand, based on the coincidence in magnitude of the Pioneer anomaly and the Hubble acceleration, it was suggested that the Pioneer anomaly could be related to the cosmological expansion :

$$a^* \simeq cH\,, \tag{3.1}$$

where c is the speed of light and H the Hubble constant (71 ± 4 km/s Mpc). In this context, several studies [1, 11, 12, 13, 14]) have made the suggestion that the Pioneer anomaly is not caused by an anomalous force but rather by an effect on the frequency of light. Such an effect could be highly relevant for LISA, which is supposed to detect gravitational waves through the small frequency shift occurring on its arms.

3.1 The Pioneer anomaly as a blueshift

One of the obstacles for attempting an explanation of the Pioneer anomaly in terms of new physics is that a modification of gravitation, large enough to explain the Pioneer anomaly, is in obvious contradiction with the planetary ephemeris. This becomes particularly clear if one considers the orbit of Neptune. At 30 AU the Pioneer anomaly is visible in the Doppler data of both Pioneer 10 and 11. The influence of an additional radial acceleration of $8 \times 10^{-10}\mathrm{m/s^2}$ on Neptune is conveniently parameterised in a change of effective reduced Solar mass, $\mu_\odot$ felt by the planet. The resulting value, $\Delta\mu_\odot = 1.4 \times 10^{-4}\,\mu_\odot$, is nearly two orders of magnitude beyond the current observational constraint of $\Delta\mu_\odot = -1.9 \pm 1.8 \times 10^{-6}\,\mu_\odot$ [17]. Similarly Pioneer 11 data contradict the Uranus ephemeris by more than one order of magnitude. Thus, the Pioneer anomaly can hardly be ascribed to a gravitational force since this would indicate a considerable violation of the *weak equivalence principle*. In particular, planetary constraints rule out an explanation in terms of a long-range *Yukawa force* [2, 19]. Hence, more subtle explanations are to be attempted.

Amongst these several approaches have considered an origin of the anomaly in a blueshift of the radio tracking signal rather than in an acceleration of the spacecraft [11, 12, 13, 14]. For the concrete realisation several distinct models have been proposed. The work [11] considers the anomaly as a kinematical effect of the cosmological expansion. The anomaly arises from the fact that the coordinate system, in which local measurements are carried out, is not a synchronous one. The studies [12, 13] consider an adiabatic effect of the cosmic expansion on the phase of light viewed as the phase of a quantum state. Whereas [12] considers a closed path *Berry phase*, [13] drops the closed path requirement and considers an open path *Berry phase*. In [14] the anomaly arises from a time dependence of the local metric which leads to an effective time acceleration.

All of the above models to explain a blueshift of the Radio signals transponded by the Pioneers have to be considered as problematic. This is most obvious for the model of [11] where only a Robertson-Walker metric is considered and the influence of the gravitational field of the Sun is completely neglected. This seems too much of a simplification considering the predominant opinion that the local Schwarzschild geometry of the Solar system remains practically unaffected by the cosmological expansion (see [18] for a recent consideration of this problem and for references to the older literature). The problem is ameliorated a bit for the quantum effect considered in [12, 13] because in this case one could argue that the adiabatic evolution of quantum states is governed by a different metric than the non-adiabatic dynamics of large bodies. We will hence consider this model in more detail below. In [14] the embedding problem does not seem to spoil the model because both the cosmic and the local metric are treated as perturbations of a locally flat metric and can (at least formally) be superimposed linearly. In this model care has however to be taken that the effective time acceleration by the cosmic expansion does not lead to different velocities of light in different physical measurement processes (cf. [20] for a discussion of this problem in the context of varying speed of light theories.). Indeed the coordinate frame used by [14] seems to lead to a discrepancy between the speed of light as inferred from local Lorentz transformations and the speed of light inferred from the phase velocity of waves in vacuum.[1] In conclusions, the current theoretical models to explain the Pioneer anomaly in terms of a blueshift of light cannot yet be considered convincing. Despite of the deficiencies of the currently discussed models the idea that the Pioneer anomaly is cause by a blueshift of light is attractive because it automatically satisfies all constraints from planetary ephemeris.

3.1.1 Magnitude of the blueshift

To estimate the blueshift, which matches to the anomalous acceleration and without having to reevaluate the original data set, one can calculate the conversion between these quantities. For the Pioneer spacecraft, the Doppler tracking was used to determine the velocities. It consists in transmitting a radio wave towards the spacecraft and measuring its frequency change when it comes back. The wave-vector of the radio wave is a Lorentz vector and one can apply the transformation below to obtain the angular frequency of the signal from the spacecraft point of view (ω_1').

$$\begin{pmatrix} \frac{\omega_1'}{c} \\ k_x' \\ k_y' \\ k_z' \end{pmatrix} = \begin{pmatrix} \gamma & -\frac{v}{c}\gamma & 0 & 0 \\ -\frac{v}{c}\gamma & \gamma & 0 & 0 \\ 0 & 0 & 1 & 0 \\ 0 & 0 & 0 & 1 \end{pmatrix} \begin{pmatrix} \frac{\omega_1}{c} \\ k_x \\ 0 \\ 0 \end{pmatrix}, \tag{3.2}$$

where c is the speed of light, v the velocity of the spacecraft in the direction Earth-spacecraft (x-direction) and $\gamma = \frac{1}{\sqrt{1-\frac{v^2}{c^2}}}$. We have supposed without loss of generality that the signal is

[1] I thank A. Rathke for raising this issue.

propagating along the x-direction. Thus, we have:

$$\omega_1' = \frac{1-\frac{v}{c}}{\sqrt{1-\frac{v^2}{c^2}}}\omega_1 \,. \tag{3.3}$$

Moreover, the angular frequency of the signal transponded at the spacecraft differs from ω_1', depending on characteristics of the spacecraft. First, because of the phase coherent tracking system, an exact ratio exists between the transmission and reception frequencies. In the case of the S-band, the value of this ratio is 240/221. Second, the rotational movement of the spacecraft introduces a shift that is proportional to the spin rate. Therefore, the angular frequency of the signal transponded towards Earth is [3]

$$\omega_T = \left[R_T\omega_1' - \eta\omega_{spin}\right] \,, \tag{3.4}$$

where R_T is the spacecraft transponder turnaround ratio and ω_{spin}, the spacecraft spin angular frequency (note that η=1 + $\frac{240}{221}$). Finally, the angular frequency of the signal received (w_r) can be determined by applying again the Lorentz transformation.[2]

$$\begin{pmatrix} \frac{\omega_r}{c} \\ k_x" \\ k_y" \\ k_z" \end{pmatrix} = \begin{pmatrix} \gamma & -\frac{v}{c}\gamma & 0 & 0 \\ -\frac{v}{c}\gamma & \gamma & 0 & 0 \\ 0 & 0 & 1 & 0 \\ 0 & 0 & 0 & 1 \end{pmatrix} \begin{pmatrix} \frac{\omega_T}{c} \\ k_x' \\ 0 \\ 0 \end{pmatrix} \,. \tag{3.5}$$

Therefore, the relation between the frequency of the signals sent and received is given by

$$\omega_r = \left[R_T\frac{\left(1-\frac{v}{c}\right)}{\sqrt{1-\frac{v^2}{c^2}}}\omega_1 - \eta\omega_{spin}\right]\frac{1-\frac{v}{c}}{\sqrt{1-\frac{v^2}{c^2}}} \,. \tag{3.6}$$

The spin angular frequency of the spacecraft is very small (about $0.08Hz$) and one can neglect the term $\eta\omega_{spin}$ for our purposes. Eq. 3.6 then becomes

$$\omega_r = \left[R_T\frac{\left(1-\frac{v}{c}\right)^2}{1-\frac{v^2}{c^2}}\right]\omega_1 = R_T\frac{1-\frac{v}{c}}{1+\frac{v}{c}}\omega_1 \,. \tag{3.7}$$

If one differentiates this relation, the acceleration of the spacecraft appears. Explicitly, it can be decomposed into a sum of a nominal and anomalous acceleration like $\frac{d\vec{v}}{dt} = \vec{a} + \vec{a}^*$.[3] One obtains

$$\frac{d}{dt}\left[\frac{\omega_n+\omega^*}{\omega_1}\right] = \frac{-2R_T}{c\left(1+\frac{v}{c}\right)^2}(a+a^*) \,, \tag{3.8}$$

where ω_r is written as the sum of a nominal and an anomalous term. Of course, the nominal part of this expression is given by

$$\frac{d}{dt}\left[\frac{\omega_n}{\omega_1}\right] = \frac{-2R_T}{c\left(1+\frac{v}{c}\right)^2}a \,. \tag{3.9}$$

The last two equations allows us to determine the time derivative of the relative anomalous angular frequency

$$\frac{d}{dt}\left[\frac{\omega^*}{\omega_1}\right] = \frac{-2R_T}{c\left(1+\frac{v}{c}\right)^2}a^* \,. \tag{3.10}$$

[2]Here, we consider that the change in the relative velocity between Earth and the spacecraft during the tracking process is sufficiently small to be neglected.

[3]This decomposition can be done because, in the outer Solar System, the gravitational back reaction on the perturbation a^* is sufficiently small [15].

Then, to first order in $\frac{v}{c}$, this relation becomes

$$\frac{d}{dt}\left(\frac{\omega^*}{\omega_1}\right) = \frac{d}{dt}\left(\frac{\Delta\nu^*}{\nu_1}\right) = -2R_T\frac{a^*}{c} + \mathcal{O}\left(\frac{v}{c}\right), \tag{3.11}$$

which leads to the following anomalous frequency shift

$$\nu^* = -2R_T\nu_1\frac{a^*}{c}t\,, \tag{3.12}$$

where t is the one-way light-time to the spacecraft. This relation gives the value of the anomalous shift if we assume that the spacecraft is actually anomalously accelerated. Now, we suppose that there is no such acceleration on the spacecraft but, instead, a shift in the frequency of light that produces the same Doppler measurement on Earth. Following the same procedure as above, the angular frequency received on Earth, taking into account an anomalous shift, is given by

$$\begin{aligned}
\omega_r' &= \left[R_T\left(\omega_1 + \int_{path_1}\left(\frac{d\omega}{dt}\right)_1 dt\right)\frac{1-\frac{v}{c}}{\sqrt{1-\frac{v^2}{c^2}}} + \int_{path_2}\left(\frac{d\omega}{dt}\right)_2 dt\right]\frac{1-\frac{v}{c}}{\sqrt{1-\frac{v^2}{c^2}}} \\
&= \left[R_T\omega_1\left(1+\frac{1}{\omega_1}\left(\frac{d\omega}{dt}\right)_1 t\right)\frac{1-\frac{v}{c}}{\sqrt{1-\frac{v^2}{c^2}}} + \left(\frac{d\omega}{dt}\right)_2 t\right]\frac{1-\frac{v}{c}}{\sqrt{1-\frac{v^2}{c^2}}}\,,
\end{aligned} \tag{3.13}$$

where $path_1$ is the light path to the spacecraft and $(\frac{d\omega}{dt})_1$ the corresponding rate of change in the angular frequency. The frequency of the radio wave on the way back is equal to the first term of the square bracket and the second term is the anomalous corresponding shift. Moreover, in the second line of Eq. 3.13, the terms $(\frac{d\omega}{dt})_i$ are assumed to be constant and we can take them out of the integral. Finally, if we take the first term out of the square bracket, the equation becomes

$$\omega_r' = R_T\omega_1(1+b^*t)^2\frac{1-\frac{v}{c}}{1+\frac{v}{c}}\,, \tag{3.14}$$

where b^* is defined as

$$b^* = \frac{1}{\omega_1}\left(\frac{d\omega}{dt}\right)_1 = \frac{1}{\nu_1}\left(\frac{d\nu}{dt}\right)_1. \tag{3.15}$$

To find the value of b^*, we have to equal ω_r' from Eq. 3.14 to ω_r from Eq. 3.7, in which we write explicitly the velocity as the sum of a nominal and an anomalous part

$$R_T\omega_1(1+b^*t)^2\frac{1-\frac{v}{c}}{1+\frac{v}{c}} = R_T\frac{1-\frac{v+v^*}{c}}{1+\frac{v+v^*}{c}}\omega_1\,, \tag{3.16}$$

which leads to

$$\begin{aligned}
(1+b^*t)^2 &= \frac{1-\frac{v+v^*}{c}}{1+\frac{v+v^*}{c}}\frac{1+\frac{v}{c}}{1-\frac{v}{c}} \\
&\simeq \frac{1-\frac{v^*}{c}}{1+\frac{v^*}{c}} \\
&\simeq 1-2\frac{v^*}{c}\,,
\end{aligned} \tag{3.17}$$

where we have neglected the terms quadratic in v^*. If we replace b^* using Eq. 3.15, we get the following final expression

$$\frac{1}{\nu_1}\frac{d\nu}{dt} = -\frac{a^*}{c}\,. \tag{3.18}$$

This equation gives the physical variation of the frequency of light which corresponds to the anomalous acceleration. It is negative so the frequency is increasing on the way (i.e. it is a blueshift). Finally, note that similar expressions are obtained in the case of the gravitational frequency shift (Einstein effect). Indeed, for a signal moving in a gravitational field, the frequency is shifted as:

$$\frac{\Delta\nu^*}{\nu} = \frac{gt}{c}\,, \tag{3.19}$$

where g is the gravitational acceleration.

3.1.2 Comparison with the Berry phase model

A bit of theory

In the early eighties, Berry discovered a new peculiarity of the evolution of a quantum state [22] : the quantum eigen-state acquires an additional phase when the Hamiltonian of a system is adiabatically transported around a closed path in parameter space. This extra phase is called Berry phase. After the importance of Berry´s discovery was realised in many fields of physics, it was liberated from its restriction to periodic variations of the Hamiltonian [23]. Let us briefly describe the theory of the Berry phase.

Consider a quantum system driven by a slowly changing Hamiltonian $H(\mathbf{R(t)})$ where $\mathbf{R}$ is a set of external parameters. Then, the adiabatic approximation leads to the following solution to the Schrödinger equation:

$$|\Psi(t)>= \exp\left[-\frac{i}{\hbar}\int_0^t E_n(t)dt\right]\exp(i\gamma_n(t))|\Psi_n(\mathbf{R(t)})>\,, \tag{3.20}$$

where $|\Psi_n(\mathbf{R}(t))>$ are the instantaneous eigenstates of the Hamiltonian with non-degenerate eigenvalue $E_n(t)$. The first phase factor is the usual dynamical one. For closed-path in the parameter space, the extra phase factor $\exp(i\gamma_n(t))$ comes from the Berry phase given by

$$\gamma_n(C) = i\int_{\mathrm{R}(0)}^{R(t_f)} [<\Psi_n(\mathrm{R})|\nabla\Psi_n(\mathrm{R})>]\cdot d\mathrm{R}\,, \tag{3.21}$$

where ∇ denotes the gradient with respect to the parameter set $\mathbf{R(t)}$. It was then proposed that the same expression holds also for adiabatic evolution along an open path [25]. A more recent discussion of the open path Berry phase however comes to the conclusion that in this case a gauge potential has to be added to the Berry phase [26]. For an open path the Berry phase would then become

$$\gamma_n(C) = i\int_{\mathrm{R}(0)}^{R(t_f)} [<\Psi_n(\mathrm{R})|\nabla\Psi_n(\mathrm{R})> + iP_n(R)]\cdot d\mathrm{R}\,, \tag{3.22}$$

where a gauge potential $P_n(R)$ has now to be taken into account. This one is given by [26]:

$$P_n(R) = \frac{i}{2}\left[\frac{<\Psi_n(\mathrm{R}(0))|\nabla\Psi_n(\mathrm{R})>}{<\Psi_n(\mathrm{R}(0))|\Psi_n(\mathrm{R})>} - \frac{<\nabla\Psi_n(\mathrm{R})|\Psi_n(\mathrm{R}(0))>}{<\Psi_n(\mathrm{R})|\Psi_n(\mathrm{R}(0))>}\right]\,. \tag{3.23}$$

The work discussing the PA as the result of an open path Berry phase [13] does not consider such a gauge term.

The Pioneer anomaly as a Berry phase

Let us start by considering an expanding space-time with a Robertson-Walker metric

$$ds^2 = -c^2dt^2 + R(t)(dx^2 + dy^2 + dz^2)\,. \tag{3.24}$$

where $R(t)$ denotes the cosmological scale factor. Without loss of generality we consider photons that travel in the z-direction so that we can restrict our considerations to a two-dimensional line element and we drop the dx^2 and dy^2 in the following. The phases of these photons are given by

$$\begin{aligned} \varphi &= g_{\mu\nu}X^\mu K^\nu \\ &= \omega_0 t - kR(t)z\,, \end{aligned} \tag{3.25}$$

where $X^\mu \equiv (ct, z)$ is the position vector, $K^\mu \equiv (\frac{\omega}{c}, k)$ is the wave-vector and $g_{\mu\nu}$ is the space-time metric given by:

$$g_{\mu\nu} = \begin{pmatrix} -1 & 0 \\ 0 & R(t) \end{pmatrix} \tag{3.26}$$

Therefore, by using Eq. 3.25, we can write the wave function of one photon as

$$A_\mu(t) = N\epsilon_\mu e^{i(\omega_0 t - kR(t)z)}\,, \tag{3.27}$$

where N is a normalisation factor and ϵ_μ is the polarisation vector. Then, during their round-trip and according to [13], the photons acquire an extra phase given by (see Eq. 3.21)

$$\begin{aligned} \gamma &= i\int_{R(0)}^{R(t_f)} \left[A_\mu^* \frac{dA_\mu}{dR}\right] dR \\ &= kz\int_{R(0)}^{R(t_f)} \left[A_\mu^* A_\mu\right] dR \\ &= kz[R(t) - R(0)] \\ &\simeq kz\dot{R}(0)t \end{aligned} \tag{3.28}$$

where $A_{\mu,0} = A_\mu(R(0))$. Then, for a specific value of the phase we can express z by the time t

$$z = \frac{\omega_0 t}{kR(t)}\,. \tag{3.29}$$

Using this relation, the Berry phase can be written as

$$\gamma = \left(\omega_0 \frac{\dot{R}(0)}{R(t)}t\right) t \tag{3.30}$$

Then wave function of one photon is given by

$$A_\mu(t) = N\epsilon_\mu \exp i\left[\omega_0\left(1 + \frac{\dot{R}(0)}{R(t)}t\right)t - kR(t)z\right]\,. \tag{3.31}$$

Employing the definition of the Hubble constant,

$$H \equiv \frac{\dot{R}}{2R}\,, \tag{3.32}$$

where R and $\dot{R}$ are to be taken at the present time, and using $R(t) \simeq R(0)$ we can rewrite the photon wave function as

$$A_\mu(t) = N\epsilon_\mu e^{i[\omega_0(1+2Ht)t - kR(t)z]}\,. \tag{3.33}$$

The expression for the phase of the photon in Eq. 3.33 obviously also holds for superpositions of photons. Defining the frequency of a wave as the time derivative of the phase $\omega \equiv d\phi/dt$ we find the frequency shift induced by the Berry phase,

$$\dot{\omega} = 4\omega_0 H\,. \tag{3.34}$$

Assuming that this Berry phase causes the Pioneer anomaly one would expect an effect about four times as large as the observed anomaly (see Eqs. 3.1 and 3.18). It is however not surprising if the observed anomaly is smaller because a smaller effective Hubble constant might enter the adiabatic evolution. The question how big such an adiabatic effect could be is related to the averaging problem of cosmology (cf. [21]) and beyond the scope of this thesis. It is further worth noting that the effect derived above differs by a factor of four from the result found in [12]. A factor of two arises from dropping the requirement that the scale factor at the instant of emission and the instant of reception are the same. Another factor of two arises from an unusual definition of the phase velocity in [12], which seems inappropriate to make connection with experimental data.

It should be noted that the above considerations do not hold if the gauge potential (see Eq. 3.22) is taken into account. This term would exactly cancel the obtained *Berry phase* and there would be no influence of the cosmic expansion on the phase of a photon

$$\begin{aligned}
\gamma &= i\int_{R(0)}^{R(t_f)} \left[A_\mu^* \frac{dA_\mu}{dR} - \frac{1}{2}\left(\frac{A_{\mu,0}^* \frac{dA_\mu}{dR}}{A_{\mu,0}^* A_\mu} - \frac{\frac{dA_\mu^*}{dR} A_{\mu,0}}{A_\mu^* A_{\mu,0}} \right) \right] dR \\
&= kz\int_{R(0)}^{R(t_f)} \left[A_\mu^* A_\mu\right] dR - \frac{i}{2}\int_{R(0)}^{R(t_f)} \left[-ikz\frac{A_{\mu,0}^* A_\mu}{A_{\mu,0}^* A_\mu} - ikz\frac{A_\mu^* A_{\mu,0}}{A_\mu^* A_{\mu,0}} \right] dR \\
&= 0\,.
\end{aligned} \tag{3.35}$$

Even with this doubts, the model can serve as a generic example for the influence on various observables that one would expect from an anomalous blueshift of light.

3.1.3 Impact on LISA arms

As seen in the previous section, the anomalous blueshift is proportional to the light travel time of the signal. The effect would therefore be several orders of magnitude bigger on LISA arms than on ground-based detectors, which have arms limited to few km of length. The expected blueshift on the LISA arms can be calculated from Eq. 3.18 with the appropriate values of the parameters (5×10^6 km for the armlength and 3×10^{14} Hz for the frequency):

$$\Delta\nu^* = -\frac{a^*}{c^2} L\nu \cong 1.4 \times 10^{-2}\,\mathrm{Hz}\,. \tag{3.36}$$

This blueshift is very small compared with the nominal frequency (3×10^{14} Hz) but one can expect LISA to be able to measure it. Indeed, the corresponding relative change of the frequency is about 10^{-16} and the predicted value for the weakest gravitational waves detectable by LISA is about 10^{-22}. The impact on the frequency due to the anomaly is therefore 6 orders of magnitude higher. Hence the effect could in principle be detectable. The ability to measure the contribution of the anomalous blueshift will depend on the sensitivity of LISA (i. .e on the noise) at the frequencies where the anomaly is present. In the next chapter, we will give a quick overview of the noises that affect the sensitivity. This will allow us to study if the anomalous blueshift could be detected by introducing the blueshift in two proposed methods of data analysis.

3.2 Berry phase and gravitational waves

3.2.1 Doppler shift induced by the gravitational waves

When the solar system is crossed by a gravitational wave, the space-time metric fluctuates, depending on the amplitude and the polarisation of the wave. As a consequence, the light path between two free-falling bodies can change, leading to phase variation on the light exchanged between them. To start, let us consider a transverse and traceless gravitational wave which gives the following metric [37]

$$ds^2 = -c^2dt^2 + (1-h)dx^2 + (1+h)dy^2 + dz^2\,, \tag{3.37}$$

where c is the speed of light and $h = h(t-z)$ is the strain field of a train of plane gravitational waves propagating in vacuum parallel to the z axis. This geometry is outlined in Fig. 3.1 below.

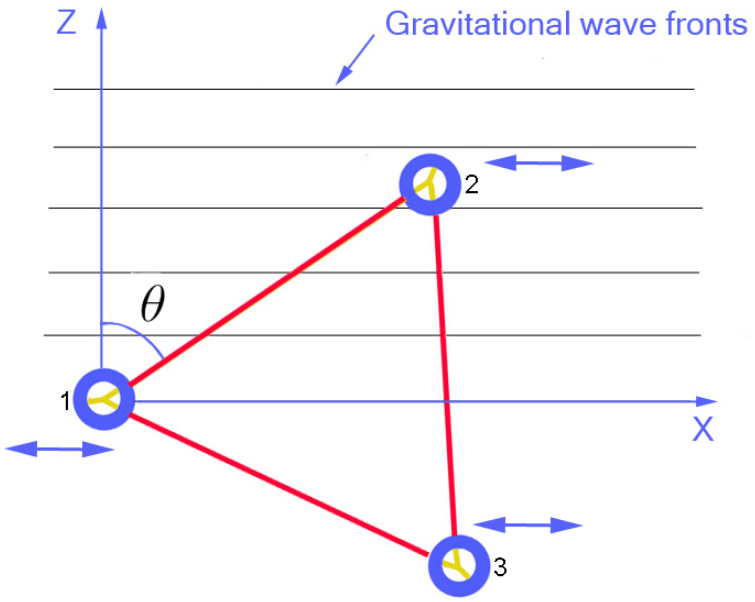

Figure 3.1: LISA and the gravitational wave geometry.

The double arrows indicate in which direction the LISA spacecraft will appear to move due to the gravitational waves. The amplitude of the distance variation will depend on the amplitude of the gravitational waves. Physically, as the gravitational waves passe the solar system, there is a geodesic deviation and a strain.
From Eq. 3.37, the metric tensor is

$$g_{\mu\nu} = \begin{pmatrix} -1 & 0 & 0 & 0 \\ 0 & 1-h & 0 & 0 \\ 0 & 0 & 1+h & 0 \\ 0 & 0 & 0 & 1 \end{pmatrix}. \tag{3.38}$$

To calculate the geodesics, we can use three Killing vectors in this space-time, which are obviously

$$V_1 = \hat{e}_x\,, \qquad V_2 = \hat{e}_y\,, \qquad V_3 = \hat{e}_t + \hat{e}_z\,, \tag{3.39}$$

where $\hat{e}_i$ indicates a unit vector along the ith direction. At the origin (see Fig. 3.1), a null vector is given by

$$\sigma_0 = (-\nu_0)\left[cdt - \left(1 + \frac{1}{2}h_0\right)\beta_0 - \alpha_0 dz\right]\,, \tag{3.40}$$

where ν_0 is the frequency of the signal emitted at spacecraft 1, $h_0 = h(t)$ and $\alpha_0^2 + \beta_0^2 = 1$. The null value of $\sigma_0 = g_{\mu\nu}\sigma^\mu\sigma^\nu$ is immediately verified. By projecting σ_0 onto an orthonormal triad at the origin, it is easily found that α_0 and β_0 are the locally measured direction cosines of the photon trajectory, with the z and x axes, respectively. At the reception at spacecraft 2, we can write σ again as

$$\sigma_1 = (-\nu_1)\left[cdt - \left(1 + \frac{1}{2}h_1\right)\beta_1 - \alpha_1 dz\right], \tag{3.41}$$

where ν_1 is the frequency observed at the spacecraft 2, h_1 is the gravitational wave strain at the same spacecraft and $\alpha_1^2 + \beta_1^2 = 1$. To determine the Doppler shift of a light signal propagating from spacecraft 1 to spacecraft 2, we can parallelly transport σ_0 along the photon trajectory, as it is done in [37]. To start, let us consider the null vector at the origin

$$g_{\mu\nu}\sigma^\mu\sigma^\nu \equiv \sigma_\nu\sigma^\nu = 0\,. \tag{3.42}$$

Then, the covariant derivatives of Eq. 3.42 is also equal to 0 and we have

$$[\sigma_\nu\sigma^\nu]_{;\mu} = 0\,, \tag{3.43}$$

where the semicolon indicates the covariant derivative. Then, since the ith Killing vector ($_iV$) satisfies the Killing equation

$${}_iV_{(\mu;\nu)} \equiv \frac{1}{2}\left[{}_iV_{\mu;\nu} + {}_i\,V_{\nu;\mu}\right] = 0\,. \tag{3.44}$$

We have the following equation which illustrates the constancy of the components of σ on the three ${}_iV$

$$\left(\sigma_{\mu i}V^\mu\right)_{;\nu}\sigma^\nu = 0 \qquad i = 1, 2, 3. \tag{3.45}$$

Eq. 3.45 leads to the following system of equations

$$\nu_0(1 + \frac{1}{2}h_0)\beta_0 = \nu_1(1 + \frac{1}{2}h_1)\beta_1\,, \tag{3.46}$$

$$\nu_0(1 - \alpha_0) = \nu_1(1 - \alpha_1)\,. \tag{3.47}$$

Dividing the square of Eq. 3.46 by Eq. 3.47 and using the relations between α and β, this system leads to the following result:

$$\frac{\nu_1 - \nu_0}{\nu_0} = \frac{1}{2}(1 + \alpha)(h_0 - h_1)\,. \tag{3.48}$$

In this equation, we use α for either α_0 and α_1, which differ only in first order. To the same approximation, the coordinates of the spacecraft 2 are $x = \frac{1}{2}\beta T$, $y = 0$ and $z = \frac{1}{2}\alpha T$ where T is the round-trip light time. Then, the gravitational wave strain h_1 is given by

$$h_1 = h(t + (1 - \alpha)T/2)\,. \tag{3.49}$$

Following the same method, we can calculate the Doppler shift of the returning photon. At spacecraft 2, a null vector of the photon re-emitted along the reverse direction is given by

$$\sigma_1' = (-\nu_1)\left[cdt + \left(1 + \frac{1}{2}h_1\right)\beta_1 + \alpha_1 dz\right]. \tag{3.50}$$

This photon is finally observed at reception at spacecraft 1

$$\sigma_2' = (-\nu_2)\left[cdt + \left(1 + \frac{1}{2}h_2\right)\beta_2 + \alpha_2 dz\right]. \tag{3.51}$$

This gives the following system by parallel transport:

$$\nu_1(1+\frac{1}{2}h_1)\beta_1 = \nu_2(1+\frac{1}{2}h_2)\beta_2\,, \tag{3.52}$$

$$\nu_1(1+\alpha_1) = \nu_2(1+\alpha_2)\,. \tag{3.53}$$

Finally, in the lowest order, the Doppler shift along the return travel time is given by

$$\frac{\nu_2-\nu_1}{\nu_1} = \frac{1}{2}(1-\alpha)(h_1-h_2)\,, \tag{3.54}$$

where $h_2 = h(t+T)$. This equation and Eq. 3.48 lead to the total Doppler shift of the returning photon of

$$\begin{aligned}\frac{\Delta\nu}{\nu} &\equiv \frac{\nu_2-\nu_0}{\nu_0} = \frac{1}{2}(1-\alpha)(h_1-h_2)+\frac{1}{2}(1+\alpha)(h_0-h_1)\\ &= \frac{1}{2}(1+\alpha)h(t)-\alpha h(t+(1-\alpha)T/2)-\frac{1}{2}(1-\alpha)h(t+T)\,.\end{aligned} \tag{3.55}$$

In particular, note that if the photons travel parallel to the gravitons (i.e. $\alpha = 1$), the Doppler shift is null. On the other hand, if the gravitational wave propagates normally to light-path of the photon, the Doppler shift is maximum and its value is given by

$$\frac{\Delta\nu}{\nu} = \pm\frac{1}{2}[h(t)-h(t-2l_i)]\,. \tag{3.56}$$

The "$\pm$" indicates that, in the plane transverse to the gravitational wave propagation, this expression has to be added to one direction and subtracted from the other. This is because the gravitational waves are area preserving in the transverse plane. Pictorially speaking, this means that if a wave increases the proper distance between two free masses that lie along a given direction, it will simultaneously decrease the distance between two free masses lying along the perpendicular direction in the transverse plane.[4] This is illustrated in the standard polarization diagram below.

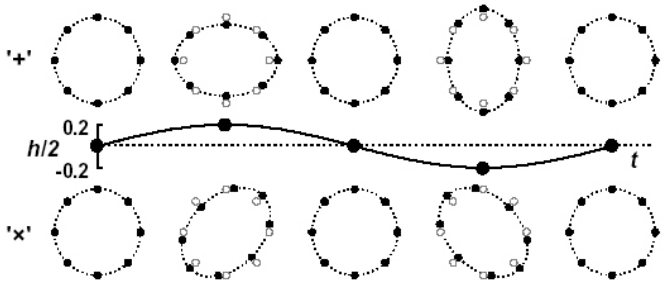

Figure 3.2: The 2 possible polarisations of gravitational waves [8].

This figure shows the effect of gravitational waves for two linearly independent polarisations on a ring of free particles arranged in a plane perpendicular to the direction of the wave. It is illustrated to scale how a wave with the dimensionless amplitude h = 0.2 distorts the original circle.

[4] In the case of LISA, the arms are not perpendicular but subtend an angle of 60°,i. e. $\alpha = 1/2$, and a factor of correction is necessary.

3.2.2 Implications of the Berry phase and total Doppler shift

In the previous section, the Doppler shift is calculated with the assumption that the propagation of the light signal is only perturbed by gravitational waves. Considering now an additional *Berry phase* on the photons, the expression 3.55 has to be modified. According to Section 3.1.1, the additional time dependance of the frequency is given by

$$\nu(t) = \nu_0(1 - \frac{a^*}{c}t)\,. \tag{3.57}$$

where ν_0 is the frequency at the signal emission and t the light travel time. In particular, in the expression of the one-way Doppler shift induced by gravitational waves,

$$\frac{\nu_1 - \nu_0}{\nu_0} = \frac{1}{2}(1+\alpha)(h_0 - h_1)\,, \tag{3.58}$$

the starting frequency (ν_0) can now be modified using Eq. 3.57. This leads to the following expression

$$\frac{\nu_1 - \nu_0}{\nu_0} = \frac{1}{2}(1+\alpha)(1 - \frac{a^*}{2c}T)(h_0 - h_1) - \frac{a^*}{2c}T\,. \tag{3.59}$$

where T is the two-way light time. Considering the example case of a Berry phase, the delay introduced on the propagation of a graviton can be neglected since the *Berry phase* arises in adiabatic evolution which can hardly hold for a gravitational wave with a frequency of 10^{-2} Hz compared to the THz frequency of the laser light.[5] Hence the argument of h_1 should remain unimpaired.

The same method can be applied to the returning signal and the final expression of the Doppler shift, including a Berry phase type contribution and the gravitational wave contributions, is given by

$$\begin{aligned}\frac{\Delta\nu}{\nu} &\equiv \frac{\nu_2 - \nu_0}{\nu_0} \\ &= \frac{1}{2}(1+\alpha)(1 - \frac{a^*}{2c}T)h(t) - \alpha(1 - \frac{a^*}{2c}T)h(t + (1-\alpha)T/2) \\ &\quad -\frac{1}{2}(1-\alpha)(1 - \frac{a^*}{2c}T)h(t+T) - \frac{a^*}{c}T\,.\end{aligned} \tag{3.60}$$

The anomaly appears in this equation in two different ways

1. As a multiplicative factor of the gravitational wave strain. The anomaly should thus have an impact in the *sensitivity band* of LISA. The effect is however at second order compared to the nominal gravitational wave contribution.

2. As an additional term proportional to the light travel time. If T is time dependent, as it will the case for LISA, the influence of the anomaly could appear at the different frequencies contained in T and at the null frequency anyway.

It is the purpose of the next chapter to assess how this Doppler shift affects the LISA measurement.

[5] The search for an anomalous blueshift of the gravitational wave itself could be carried out along the lines of that for massive graviton (see [27]) and will not be considered in this thesis.

Chapter 4

Implications for LISA

4.1 Introduction

In the previous chapter, we have shown that the pioneer anomaly could find its explanation in a blueshift in the frequency of light and we have calculated the corresponding effect on the arms of LISA. To understand how it could influence LISA, we begin this chapter by reminding the principles of interferometric measurement. We also give a quick overview on the different noise sources which spoil the measurements. Then, we show how the blueshift enters the data within and outside the *sensitivity band*. This is done both in the framework of phase noise cancellation in the frequency domain and time delay interferometry.

4.2 Interferometric measurement

Interferometry is a method to make very precise distance measurements. In the most widespread version, the *Michelson interferometer*, a laser signal is divided by a beam splitter. Then, the two divided beams are sent out along different paths and reflected back to the beam splitter, where the beams interfere to produce light fringe. The intensity of the fringe is then monitored to detect changes in the difference in the arm lengths. The advantage of the interferometer over a system where a single arm is used and where the returning light interferes with a fraction of the outgoing light to form the fringes, lies in the relative immunity of the interferometer to fluctuations in the phase of the laser. In a single-arm, jitter in the laser phase over the round-trip light time would cause the interference pattern to fluctuate, mimicking a change in the arm length. With an equal arm lengths interferometer, the phase fluctuations are transmitted equally along the two arms and, when the return beams finally combine, the fluctuations will be the same in both signals and will be cancel.

LISA will operate nearly in the same way. The round-trip journey between two neighbours spacecraft defines one arm of the large interferometer. However, because of the orbital motion, the arm lengths cannot be maintained equal and the laser phase noise is not totally cancelled. If the arm lengths are unequal by an amount of $\Delta L = L_1 - L_2$, then the residual laser phase noise will be given by

$$\Delta\phi(t) = p(t - 2l_1) - p(t - l_2) \approx 2\dot{p}(t - 2l_1)\Delta l\,, \tag{4.1}$$

where $p(t)$ is the laser phase noise and l_i the light time along the ith arm. If uncorrected, this residual noise can be dominant and can overwhelm the signature of gravitational waves.

The noises involved in LISA's measurement are very crucial for the sensitivity and needs to be carefully studied. In order to reliably distinguish the gravitational wave signals in the LISA's

data, a signal-to-noise ratio of 5 is generally required and also a geometric factor of $\sqrt{5}$ to allow for less optimal directions and polarizations [8]. These constraints leads to the sensitivity curve, as illustrated in Fig. 4.1 below.

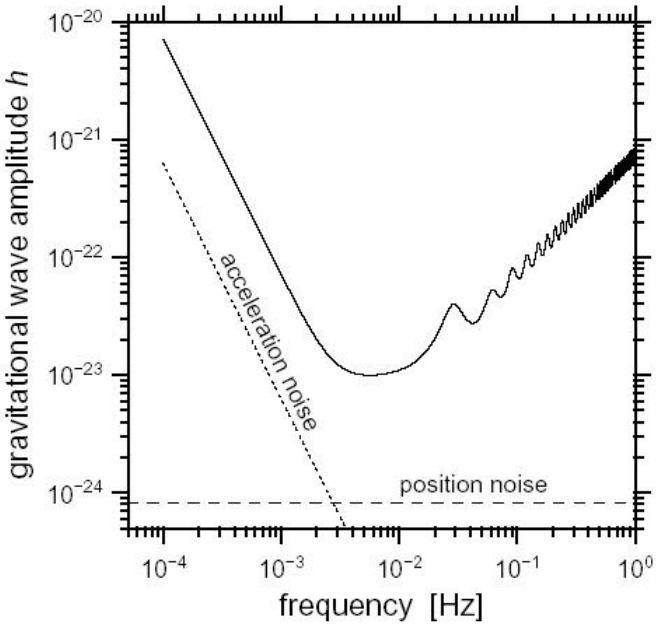

Figure 4.1: LISA sensitivity curve for one year integration time and a signal-to-noise ratio of 5, averaged over all possible source locations and polarizations [8].

In the case of LISA, the two arms do not subtend a right angle, but one of only 60°, thus decreasing the response by a factor sin 60°= 0.8660. Furthermore, the angle of incidence depends on the position of the source on the sky and on the momentary orientation of LISA, which undergoes a continuous change during its orbit around the Sun. The following figure gives an example of the rather complex dependence of the LISA response while orbiting the Sun.

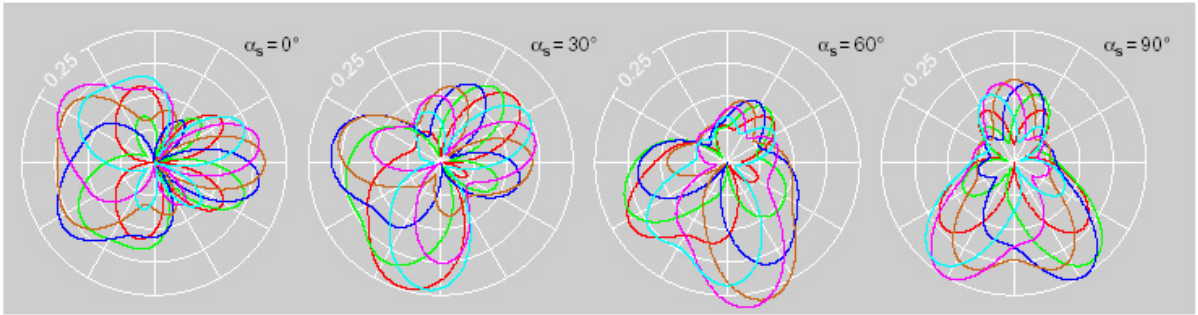

Figure 4.2: Magnitude of the normalized LISA transfer function in dependence upon the orbit azimuth for a source at declination 30° and azimuths of 0°, 30°, 60° and 90°, at a frequency of 45 mHz [8].

The figure outlines the orbit dependence for four different source azimuths and six different polarizations, considering for each a gravitational wave at the frequency of 45 mHz and a source

declination of 30° above the ecliptic. When averaged over the different angles of incidence of the gravitational wave in the course of one year, the antenna response is smoothed out considerably. Fig. 4.3 shows the frequency response of LISA for four different source declinations after averaging over the orbit and all possible source azimuths and polarizations.

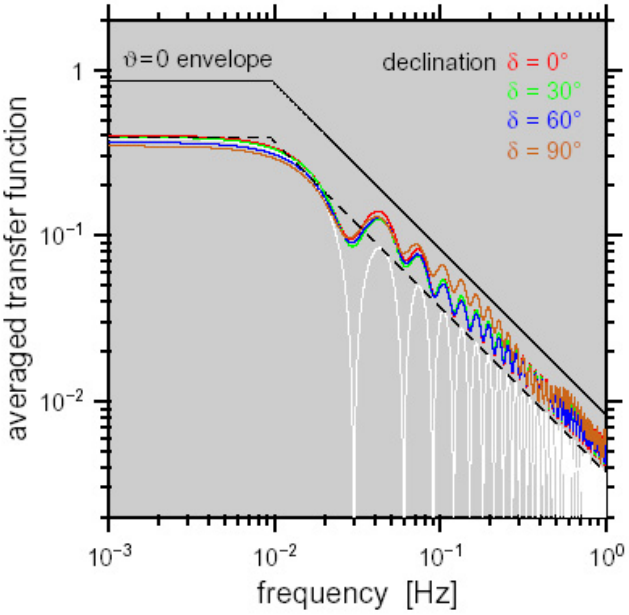

Figure 4.3: Magnitude of the normalized LISA transfer function in dependence upon frequency after averaging over the orbit and all possible source azimuths and polarizations [8].

4.3 The noises

A careful study of the noises involved in the LISA measurement is essential to determine the precision required for the detection of the gravitational waves. It is convenient to work in terms of signal-to-noise ratio which depends on several features of the expected signal, the characteristics of the noise and the duration of the measurements.

There are two different types of noise; the one due to residual forces which lead to undesirable accelerations on the *proof mass* and the one which fakes fluctuations in the lengths of optical paths. Obviously, it is impossible for a receiver spacecraft to distinguish between the Doppler shift cause by fluctuations in arm length or a true shift in the frequency of light. To be explicit, let us consider an interferometer with an arm of length L. Then, the phase difference between the outgoing and the returning signals is given by

$$\varphi = \frac{4\pi\nu L}{c}\,, \tag{4.2}$$

where ν is the frequency of the signal and c the speed of light. Thus, for slow changes in L and ν, we can see that, in the phase fluctuation $\delta\varphi$,

$$\delta\varphi = \frac{4\pi}{c}\left(\frac{\delta L}{L} + \frac{\delta\nu}{\nu}\right)\,, \tag{4.3}$$

the relative change of frequency and arm length have the same impact. In the following, we give a brief description of the dominant noises involving in the LISA measurement with their

power spectra. A complete study of the noises is carried out in [8] where they are summarized in useful noise budget tables.

4.3.1 Laser phase-noise

The laser system on-board of LISA consists of a diode-laser-pumped monolithic Nd:YAG ring laser which can generate a continuous infra-red beam at 1064 μm of up to 2W. This choice relies on its compact structure, reliability and high stability. The primary method of stabilization is to lock the laser frequency on to a *Fabry-Perot cavity*. Any change in the length of the cavity produces deviations from the nominal operational frequency. This is the laser phase noise. With the temperature fluctuations inside each spacecraft limited in the region of 10^{-3}Hz to approximately 10^{-6} K/$\sqrt{\text{HZ}}$ by three stages of thermal insulation, a cavity formed of ultra low expansion material allows a stability level of approximately 30 Hz/$\sqrt{\text{HZ}}$. If we compare this value to the maximum measurement noise level of 4pm/$\sqrt{\text{Hz}}$ (about 6×10^{-6} Hz/$\sqrt{\text{Hz}}$) in order to detect gravitational waves, it is clear that correction scheme is required to decrease the laser phase noise. A cancellation of about 10 orders of magnitude is necessary and this is the purpose of the frequency domain and time domain methods described in subsequent sections. According to [45], at the millihertz level, the power spectral density of the laser frequency noise is approximately given by

$$S_p(f) = 4 \times 10^{-38} f^{-4} \text{Hz}^{-1} \,. \tag{4.4}$$

At frequencies below the millihertz, the decrease in f^{-4} is still a good approximation until the relative change in the length of the cavity reaches roughly 10^{-3} where the power spectral density becomes flat.[1] Since the instability in the cavity are exactly transmitted to the laser below 10^{-3} Hz [45], the power spectral density would become flat near the Fourier frequency of 10^{-8} Hz (see Eq. 4.4).

4.3.2 Shot noise

Shot noise is due to the quantum-mechanical fluctuations in the arrival times of the photons. According to [8], for each single passage through an arm of length L, the power spectral density of the apparent optical path fluctuations is

$$S_n(f) = \frac{1}{2\pi} \frac{\lambda \hbar c}{P_{avail}} \,, \tag{4.5}$$

where P_{avail} is the light power available. For LISA, this one is very low due to beam spreading and the poor efficiency of optics and photodiode. The power spectral density commonly used for shot noise is given by [34]

$$S_n(f) = 5.3 \times 10^{-38} (f/1\text{Hz})^2 \text{Hz}^{-1} \,. \tag{4.6}$$

After having cancelled the laser phase noise by an appropriate algorithm, we will see that the sensitivity of LISA is limited by the shot noise near the frequency of 1 Hz.

4.3.3 Acceleration noise

Despite the fact that the *drag-free* environment will effectively shield the *proof masses* from outside influences, some residual acceleration noises will remain. In addition, the *optical bench*es themselves can undergo residual acceleration noises mainly due to thermal distortion. To be specific, the major sources of acceleration noises are

[1] Thanks to Oliver Jennrich for these information.

- The Lorentz force on charged *proof mass* from the fluctuating interplanetary field.
- Residual gas impacts on the *proof mass*.
- Thermal distortion of the spacecraft.
- Noise due to dielectric losses.
- Temperature differences across cavity.

A complete list of these acceleration noises with their magnitude is given in [8]. By accounting for all of them, the estimated total effect on one inertial sensor is $3 \times 10^{-15}\mathrm{ms}^{-2}/\sqrt{\mathrm{Hz}}$. The power spectral density for the acceleration noises is given by [34]

$$S_{\mathrm{acc}} = 2.8 \times 10^{-41}(1 + (f/3.10^{-3}\mathrm{Hz})^2)^2(f/10^{-4}\mathrm{Hz})^{(-8/3)}\mathrm{Hz}^{-1}\,. \tag{4.7}$$

After the cancellation of the laser phase noise, we will see that the acceleration noises are dominant in the low-frequency range of the *sensitivity band* of LISA.

4.4 Frequency domain algorithm

With precisely equal arm lengths, the interferometer allows the direct cancellation of the leading noise source, the laser phase noise. If uncorrected, this noise overwhelms the signature of the gravitational waves in the data. Unlike the ground-based interferometers, LISA will be unable to maintain precise arm length equality and an appropriate data analysis has to be performed. A first method in the frequency domain was introduced in [30]. In this section, we review this method, taking into account the anomalous blueshift. We also introduce additional noise sources, such as acceleration noise, which was not addressed in [30] and we update the value of laser and shot noise. Particularly, the main goals are to assess the impact on the gravitational waves detection and if we can distinguish the signature of the anomaly in the data.

4.4.1 The two-way Doppler signals

For simplicity, we assumed in this first method that each laser has the same fundamental frequency ν. This is different from LISA where the frequency of each laser may differ by several hundred of megahertz. However, it is useful to begin with this method to understand how the cancellation of the laser phase noise works for an unequal arm lengths interferometer and to have first interesting results. In addition, we assume, for the moment, the arm lengths to be constant and known exactly. We will remove this assumption later, and estimate the corresponding accuracy needed in order for the techniques still be effective.

Let us begin by outlining the geometry of the interferometer on the figure below.

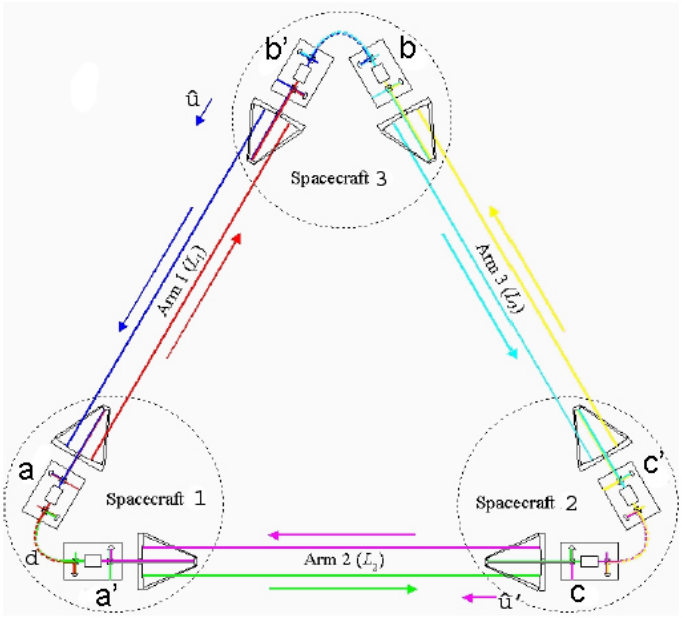

Figure 4.4: Geometry of the LISA formation [8].

Then, we define:

- p_m(t) as the phase noise of the mth laser, so that the phase of the mth laser is $P_m = \nu t + p_m(t)$.
- $l_i(t)$ as the one-way light-time for the signal along the ith interferometer arm, mainly

affected by slow drift velocities from the orbits and faster changes produced by gravitational waves.

- $\Delta\nu_i^*$ as the anomalous blueshift of light occurring during the travel on the ith arm.
- $n_i(t)$ as the shot noise on the ith laser.
- $a_i(t)$ as the residual acceleration of the ith spacecraft.

Each laser send a signal to its neighbour where a fraction of the local laser power being sent out is beating with the incoming signal. There are also two-way reference signal exchanges between the lasers on the same spacecraft to tie their phases.

Let us now look at the main effects which blur the phase of the signals.

1. The shot noise. Its effect is immediate at the time of reception, so that the response of the Doppler measurement at the ith laser is simply given by $n_i(t)$.

2. The acceleration noise. As already mentioned, the phase variation $\Delta\varphi$ of a signal depends on the path length x through
$$\Delta\varphi = \frac{2\pi\nu}{c}x\,, \tag{4.8}$$
where ν is the frequency of the signal. Therefore, the residual acceleration of the spacecraft appears on the second derivative of the phase of the signal. Obviously, the residual accelerations at the two spacecraft, at transmission and reception, have to be taken into account and we have the following expression
$$\Delta\varphi_a = \frac{2\pi\nu}{c}\int\int[\hat{u}\cdot\vec{a}_a(t) - \hat{u}\cdot\vec{a}_{b'}(t-l_1)]dt^2\,, \tag{4.9}$$
where a and b' are the end lasers of arm 1 and $\hat{u}$ is the unit vector along the same arm (see Fig. 4.4). Note that this equation is a first order estimate since it considers only the acceleration along the optical axis. The phase shift on the other arms can be obtained by the same way. Note that for the phase received at the kth laser, one can not simply switch the indices in 4.9 because the indexing is not symmetric against $\hat{u}$:
$$\Delta\varphi_{b'} = -\frac{2\pi\nu}{c}\int\int[\hat{u}\cdot\vec{a_{b'}}(t) - \hat{u}\cdot\vec{a_a}(t-l_i)]dt^2 \tag{4.10}$$

3. The anomalous blueshift. Its contribution on the phase of the signal can be derived from Eq. 3.36 and the relation between the frequency ν and the phase φ of a signal, i. e.
$$\nu = \frac{1}{2\pi}\frac{d\varphi}{dt} \tag{4.11}$$
This leads to the following contribution of the anomalous blueshift on the phase of the signal received:
$$\Delta\varphi_i^*(t) = 2\pi\int\Delta\nu_i^* dt \tag{4.12}$$

By taking into account all these factors, the phase of the signal sent by the kth laser and received at the ith is given by

$$\begin{aligned}\varphi_i(t) &= 2\pi\nu(t-l_i(t)) + 2\pi\int\Delta\nu_i^* dt + p_k(t-l_i) + n_i(t)\\ &\quad +2\frac{\pi\nu}{c}\int\int[\hat{u}\cdot\vec{a_i}(t) - \hat{u}\cdot\vec{a_k}(t-l_i)]dt^2\,,\end{aligned} \tag{4.13}$$

which becomes

$$\begin{aligned}\varphi_i(t) &= 2\pi\nu(t-l_i(t)) + 2\pi\alpha^* \int l_i(t)dt + p_k(t-l_i) + n_i(t) \\ &\quad +2\frac{\pi\nu}{c}\int\int[\hat{u}\cdot\vec{a_i}(t) - \hat{u}\cdot\vec{a_k}(t-l_i)]dt^2\,, \end{aligned} \tag{4.14}$$

by introducing the following expression for the anomalous blueshift,

$$\Delta\nu_i^* = -\frac{a^*}{c}\nu l_i(t) = \alpha^* l_i(t)\,. \tag{4.15}$$

At the reception, the incoming signal is beaten with the local laser to give the beat signal such as

$$\sin(\varphi_i(t)) + \sin(P_i(t)) = 2\sin(\frac{\varphi_i + P_i}{2})\cos(\frac{\varphi_i - P_i}{2})\,. \tag{4.16}$$

The high frequency sine term is too fast to be read. Therefore, on the ith arm, the phases of the beat signals read in the spacecraft photodiode are given by

$$\begin{aligned} s_i(t) &= \varphi_i(t) - P_i(t) \\ &= -2\pi\nu l_i(t) + p_k(t-l_i) - p_i(t) + 2\pi\alpha^*\int l_i(t)dt + n_k(t) \\ &\quad +2\frac{\pi\nu}{c}\int\int[\hat{u}\cdot\vec{a_i}(t) - \hat{u}\cdot\vec{a_k}(t-l_i)]dt^2 \end{aligned} \tag{4.17}$$

$$\begin{aligned} s_k(t) &= \varphi_k(t) - P_k(t) \\ &= -2\pi\nu l_i(t) + p_i(t-l_i) - p_k(t) + 2\pi\alpha^*\int l_i(t)dt + n_i(t) \\ &\quad -2\frac{\pi\nu}{c}\int\int[\hat{u}\cdot\vec{a_k}(t) - \hat{u}\cdot\vec{a_i}(t-l_i)]dt^2\,, \end{aligned} \tag{4.18}$$

where we have dropped the factor 1/2 and with the appropriate values for i and k. Finally, the main signal is essentially an integrated Doppler measurement at the central point. This one is formed by the combination

$$\begin{aligned} z_i(t) &= s_i(t) + s_k(t-l_i) \\ &= p_i(t-2l_i) - p_i(t) - 4\pi\nu l_i(t) + 4\pi\alpha^*\int l_i(t)dt + n_k(t) + n_i(t-l_i) \\ &\quad +2\frac{\pi\nu}{c}\int\int[\hat{u}\cdot\vec{a_i}(t) - 2\hat{u}\cdot\vec{a_k}(t-l_i) + \hat{u}\cdot\vec{a_i}(t-2l_i)]dt^2\,. \end{aligned} \tag{4.19}$$

In order to obtain $z_i(t)$, $s_k(t)$ is sent to the ith laser to be beaten with $s_i(t)$. Here, the beat signal is filtered in order to keep the gravitational waves contribution, i.e. by reading the cosine term in the expression of a beat (see Eq. 4.16). If unmodulated, the frequency of $s_k(t)$ is many order of magnitude lower than ν and one can neglect the corresponding anomalous blueshift.

Gravitational waves contribution

In Eq. 4.19, the terms in $l_i(t)$ account for the contributions of the orbital motion and the gravitational waves. At this stage, we explicitly write each contribution by splitting $l_i(t)$ into the nominal arm length and the contribution of the gravitational. According to Section 3.2.2, the

impact of a gravitational wave, transverse to the LISA plane and with appropriate polarization, on the two-way Doppler signal is given by

$$\frac{\Delta\nu}{\nu} = \pm\frac{1}{2}(1+\alpha^* l_i)[h(t) - h(t-2l_i)]\,, \tag{4.20}$$

where $\Delta\nu$ is the difference between the frequency of signal sent and received at the central spacecraft and h is the gravitational wave strain amplitude. The "$\pm$" indicates that this expression has to be added to one arm and subtracted from the other Then, using Eq. 4.11, we can calculate the corresponding contribution on the phase

$$\varphi_{\rm gw} = \pm\pi\nu\int(1+\alpha^*)[h(t) - h(t-2l_i)]dt\,. \tag{4.21}$$

By inserting this expression in Eq. 4.19, the explicit expression of the two-way Doppler signal becomes:

$$\begin{aligned} z_i(t) &= p_i(t-2l_i) - p_i(t) - 4\pi\nu l_i(t) + 4\pi\alpha^*\int l_i'(t)dt + n_k(t) + n_i(t-l_i) \\ &\quad +2\frac{\pi\nu}{c}\int\int[\hat{u}\cdot\vec{a_i}(t) - 2\hat{u}\cdot\vec{a_k}(t-l_i) + \hat{u}\cdot\vec{a_i}(t-2l_i)]dt^2 \\ &\quad \pm\pi\nu\int(1+\alpha^* l_i)[h(t) - h(t-2l_i)]dt\,, \end{aligned} \tag{4.22}$$

Eq. 4.22 shows the signal measured at the ith laser after it has propagated along one of the interferometer arm. In order to estimate the contribution of each term, it is useful to compute the power spectral density of $z_i(t)$. To begin, we restrict our study to the *sensitivity band* of LISA, i.e. from 10^{-4} Hz to 1 Hz, and we drop the two terms in $l_i(t)$ as the orbital motion has no impact at these frequencies. In Section 4.4.5 below, we will study what happens outside this frequency band. To compute the power spectral density, we can first calculate the Fourier transform [2] of Eq. 4.22

$$\begin{aligned} z_i(f) &= p_i(f)[e^{4\pi i f l_1} - 1] + n_i(f)[1 + e^{2\pi i f l_i}] + \nu a_i(f)\frac{[e^{4\pi i f l_1} + 2e^{2\pi i f l_1} + 1]}{2\pi c f^2} \\ &\quad \pm\nu(1+\alpha^* l_i)h(f)\frac{[e^{4\pi i f l_i} - 1]}{2if}\,, \end{aligned} \tag{4.23}$$

where we have assumed that $n_i(f) = n_k(f)$, $a_i(f) = a_k(f)$ and the worst case for the relative direction between $\vec{a}_{i,k}$ and $\hat{u}$. Here, we have to be careful because these expressions of the Fourier transform suppose that the observing time is infinite. In practice, the mission will operate a few years and thus, Eq. 4.23 only gives an estimate of the true spectrum. The error introduced is discussed in section 4.4.4.

[2] Here,we use the following formula:

$$F.T.[\int g(t)dt] \equiv -\frac{1}{2\pi i f}G(f)$$

where G(f) is the Fourier transform of g(t).

Assuming independent acceleration and shot noise, so that their power spectra add each other, we can plot Fig. 4.5 below by using the noise spectra given in Section 4.3.

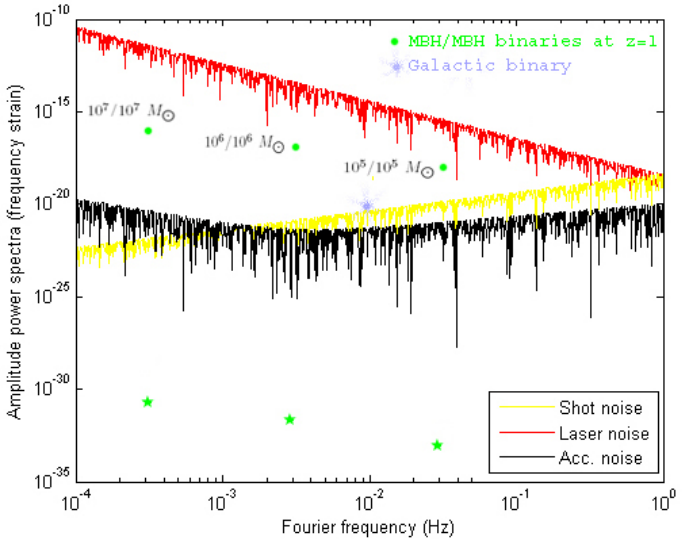

Figure 4.5: Spectra involved in the two-way Doppler signal. The upper green points indicates the expected signatures of some *massive black hole* binaries (MBH-MBH) located at z=1 and few months before coalescence. $M_\odot$ is equal to the Solar mass. The upper blue point represents the typical value for a *neutron star* binary in our galaxy. The lower points indicate the corresponding signature of the Pioneer anomaly.

From this figure, it is clear that in order to distinguish the signal of gravitational waves, even for the strongest one as MBH-MBH coalescence, the laser phase noise (in red) has to be cancelled to several order of magnitude. The following sections explain how handle this. The contribution of the Pioneer anomaly is shown by the lower points in Fig. 4.5 and it is well below the secondary noise sources, as shot noise (in yellow) and acceleration noise (in black). The anomaly should not have any impact since the noise cancellation algorithms of LISA is dedicated to the laser phase noise. However, these algorithms apply transfer functions to the secondary noises and anomalous term and it is not so obvious that, at the end, the effect is negligible. In the following section, the laser phase noise cancellation algorithm in the frequency domain is applied to $z_i(t)$ in order to see what really happen to the anomalous contribution.

4.4.2 Laser phase noise cancellation

The idea to cancel the laser phase noise is to compare the phases of signals which have propagated along different arms. To perform this data analysis, the phase of two lasers in the same spacecraft need to be tied. This can be done by using a reference signal, sent between them

$$\sigma_i(t) = -\nu d - \nu t + p_j(t-d) - p_i(t)\,, \tag{4.24}$$

where d is the light-time between the lasers i and j with $\{i,j\}$, chosen from $\{1,2\}$. The anomalous blueshift on this path is very small because the lasers are close to each other and we can neglect it. All the signals $s_i(t)$ and $\sigma_i(t)$ may be used to synthesize an interferometer in the data analysis. The differenced phase reference signal is given by

$$\sigma_2(t) - \sigma_1(t) = [p_1(t) + p_1(t-d)] - [p_2(t) + p_2(t-d)]\,. \tag{4.25}$$

In the frequency domain, this equation becomes

$$\sigma_2(f) - \sigma_1(f) = [p_1(f) - p_2(f)](1 + e^{2\pi i f d}) \,, \tag{4.26}$$

so, that knowing the light-time d, one can apply a linear filter to have the differenced laser phase noise:

$$\zeta(f) = p_1(f) - p_2(f) = \frac{\sigma_1(f) - \sigma_2(f)}{1 + e^{2\pi i f d}} \,. \tag{4.27}$$

The inverse Fourier transform of this equation yields $\zeta(t) = p_1(t) - p_2(t)$ which allows to tie the lasers of the same spacecraft together as if they were beams from a single laser. Now, we have all the signals needed to implement the noise cancellation algorithm. By combining $z_1(t)$ and $z_2(t)$ of Eq. 4.19 and using the reference signal $\zeta(t)$ of Eq. 4.27, one can write the interferometer signal in terms of the noise in one laser only

$$\begin{aligned}
\gamma(t) &\equiv z_1(t) - z_2(t) - \zeta(t - 2l_2) + \zeta(t) \\
&= p_1(t - 2l_1) - p_1(t - 2l_2) - 4\pi\nu\Delta l(t) + 4\pi\alpha^* \int \Delta l(t) dt + n_3(t) + n_1(t - l_1) \\
&\quad - n_4(t) - n_2(t - l_2) + 2\frac{\pi\nu}{c} \int\int [\hat{u}.\vec{a_1}(t) - 2\hat{u}.\vec{a_3}(t - l_1) + \hat{u}.\vec{a_1}(t - 2l_1)] dt^2 \\
&\quad + \pi\nu \int (1 + \alpha^* l_1)[h(t) - h(t - 2l_1)] dt - \pi\nu \int (1 + \alpha^* l_2)[h(t) - h(t - 2l_2)] dt \\
&\quad - 2\frac{\pi\nu}{c} \int\int [\hat{u}'.\vec{a_2}(t) - 2\hat{u}'.\vec{a_4}(t - l_2) + \hat{u}'.\vec{a_2}(t - 2l_2)] dt^2 \,.
\end{aligned} \tag{4.28}$$

For unequal arms, the algorithm to be used should lead to the minimization of the noise in Eq. 4.28. According to Fig. 4.5, this can be done by neglecting all the contributions against the phase noise, in which case the Fourier transform of $z_1(t)$ would be given in terms of the transform of $p_1(t)$ by

$$z_1(f) = p_1(f)(e^{4\pi i f l_1} - 1) \,. \tag{4.29}$$

We may therefore use $z_1(t)$ to generate an estimate $\tilde{p}_1(f)$ of $p_1(f)$

$$\tilde{p}_1(f) = \frac{z_1(f)}{e^{4\pi i f l_1} - 1} \,. \tag{4.30}$$

Computing the inverse Fourier transform gives estimates $\tilde{p}_1(t)$ and $\tilde{p}_2(t) = \tilde{p}_1(t) - \zeta(t)$ of the phase noise of the lasers. These estimates can then be used to predict the effect of the laser noise in the interferometer via

$$\tilde{z}_i(t) \equiv \tilde{p}_i(t - 2l_i) - \tilde{p}_i(t) \,, \tag{4.31}$$

and the resulting estimate,

$$\tilde{\gamma}(t) \equiv \tilde{z}_1(t) - \tilde{z}_2(t) \,. \tag{4.32}$$

This value of the estimate of the differenced interferometer signal can then be subtracted from $\gamma(t)$ to give a signal

$$\Delta(t) \equiv \gamma(t) - \tilde{\gamma}(t) \,, \tag{4.33}$$

which now does not contain the laser phase noise. This method will work as long as one remains far from the poles of Eq. 4.30, that is at frequencies well away from $f_n = n/2l_i$, where n is an integer. So, the gravitational wave detector will be relatively insensitive near these frequencies. Of course, this procedure breaks down near $f = 0$ but the laser phase noise contribution in

Eq. 4.29 goes to zero [40] as f decreases and the detector sensitivity remains unimpaired.

The procedure described above has however an inevitable sources of errors: the error in the knowledge of the actual time-of-flight of the signals in the two arms. In the following section, we discuss the limitations that this error places on the tolerances for the system.

4.4.3 Theoretical performance of the algorithm

Still following the method of [30], let us now look to the theoretical performance of the algorithm. The measurement of the position of the central and end masses of interferometer is not perfect and hence, errors arise on the actual light-time on each arm. Let δl_1 and δl_2 be such errors. Moreover, we assume, for sake of simplicity, that the phase reference signal $\zeta(t)$ in Eq. 4.27 is null, i.e. that p_1 and p_2 are identical.By using the method described in the previous section and taking into account the errors δl_1 and δl_2, one can reconstruct the laser phase noise

$$\tilde{p}_1(f) = \frac{z_1(f)}{e^{4\pi i f(l_1+\delta l_1)} - 1}\,, \tag{4.34}$$

with z_1 given by Eq. 4.23 which is reminded here after

$$\begin{aligned} z_1(f) &= p_1(f)[e^{4\pi i f l_1} - 1] + n_1(f)[1 + e^{2\pi i f l_1}] + a_1(f)[e^{4\pi i f l_1} + 2e^{2\pi i f l_1} + 1] \\ &\quad + \nu(1 + \alpha^* l_1)h(f)\frac{[e^{4\pi i f l_1} - 1]}{2if}\,. \end{aligned} \tag{4.35}$$

Note that here, $a_i(f)$ has the unit of radian instead of m/s^2 in Eq. 4.23. The conversion can be easily done by using Eq. 4.8 such as

$$4\pi^2 f^2 \varphi(f) = \frac{2\pi\nu}{c} a(f)\,. \tag{4.36}$$

Therefore, the estimate of the laser phase noise is given by

$$\begin{aligned} \tilde{p}_1(f) &= \left[p_i(f) + \nu\,(1 + \alpha^* l_1)\,\frac{h(f)}{2if}\right]\frac{[e^{4\pi i f l_1} - 1]}{[e^{4\pi i f(l_1+\delta l_1)} - 1]} \\ &\quad + a_1(f)\frac{[e^{4\pi i f l_1} + 2e^{2\pi f l_1} + 1]}{[e^{4\pi i f(l_1+\delta l_1)} - 1]} + \frac{n_1(f)[1 + e^{2\pi i f l_1}]}{[e^{4\pi i f(l_1+\delta l_1)} - 1]}\,. \end{aligned} \tag{4.37}$$

Then, the differenced Doppler signal, the Fourier transform of $\gamma(t)$ from Eq. 4.28, has the following form

$$\begin{aligned} \gamma(f) &= p_1(f)[e^{4\pi i f l_1} - e^{4\pi i f l_2}] + a_1(f)[e^{4\pi i f l_1} + 2e^{2\pi f l_1} + 1] - a_2(f)[e^{4\pi i f l_2} + 2e^{2\pi f l_2} + 1] \\ &\quad + \nu h(f)\frac{[e^{4\pi i f l_1} + e^{4\pi i f l_2} - 2]}{2if} + n_1(f)(1 + e^{2\pi i f l_1}) - n_2(f)(1 + e^{2\pi i f l_2}) \\ &\quad + \nu\alpha^* h(f)\frac{[l_1 e^{4\pi i f l_1} + l_2 e^{4\pi i f l_2} - l_1 - l_2]}{2if}\,. \end{aligned} \tag{4.38}$$

The reconstructed contribution of laser phase noise to this phase difference can be written in terms of $\tilde{p}_1(f)$

$$\tilde{\gamma}(f) = \tilde{z}_1(f) - \tilde{z}_2(f) = \tilde{p}_1(f)[e^{4\pi i f(l_1+\delta l_1)} - e^{4\pi i f(l_2+\delta l_2)}]\,.$$

If we substitute Eq. 4.37 into Eq. 4.39, the following expression for the estimated phase difference is obtained

$$\begin{aligned}\tilde{\gamma}(f) &= [p_1(f)+\nu(1+\alpha^* l_1)\frac{h(f)}{2if}]\frac{[e^{4\pi i f l_1}-1][e^{4\pi i f(l_1+\delta l_1)}-e^{4\pi i f(l_2+\delta l_2)}]}{[e^{4\pi i f(l_1+\delta l_1)}-1]}\\ &+a_1(f)\frac{[e^{4\pi i f l_1}+2e^{2\pi i f l_1}-1][e^{4\pi i f(l_1+\delta l_1)}-e^{4\pi i f(l_2+\delta l_2)}]}{[e^{4\pi i f(l_1+\delta l_1)}-1]}\\ &+n_1(f)\frac{[1+e^{2\pi i f l_1}][e^{4\pi i f(l_1+\delta l_1)}-e^{4\pi i f(l_2+\delta l_2)}]}{[e^{4\pi i f(l_1+\delta l_1)}-1]}\,. \end{aligned} \tag{4.39}$$

Finally, if we subtract from the actual phase difference, Eq. 4.39, this estimate, we get a signal, $\Delta(f)$, that has the following terms

$$\Delta(f) \equiv \gamma(f) - \tilde{\gamma}(f) = P(f) + A(f) + N(f) + H(f) + H^*(f)\,, \tag{4.40}$$

where $P(f)$, $A(f)$, $N(f)$, $H(f)$ and $H^*(f)$ are equal to

$$P(f) = 4\pi i f p_1(f)\left[\frac{\delta l_2(e^{4\pi i f l_1}-1)e^{4\pi i f l_2}-\delta l_1(e^{4\pi i f l_2}-1)e^{4\pi i f l_1}}{[e^{4\pi i f l_1}-1]}\right] \tag{4.41}$$

$$\begin{aligned}A(f) &= a_1(f)[e^{4\pi i f l_1}+2e^{2\pi i f l_1}+1]\frac{[e^{4\pi i f l_2}-1+4\pi i f\delta l_2 e^{4\pi i f l_2}]}{[e^{4\pi i f l_1}-1+4\pi i f\delta l_1 e^{4\pi i f l_1}]}\\ &-a_2(f)[e^{4\pi i f l_2}+2e^{2\pi i f l_2}+1]\end{aligned} \tag{4.42}$$

$$N(f) = n_1(f)[1+e^{2\pi i f l_1}]\frac{[e^{4\pi i f l_2}-1+4\pi i f\delta l_2 e^{4\pi i f l_2}]}{[e^{4\pi i f l_1}-1+4\pi i f\delta l_1 e^{4\pi i f l_1}]} - n_2(f)[1+e^{2\pi i f l_2}] \tag{4.43}$$

$$H(f) = 2\pi\nu h(f)\left[\frac{\delta l_2(e^{4\pi i f l_1}-1)e^{4\pi i f l_2}-\delta l_1(e^{4\pi i f l_2}-1)e^{4\pi i f l_1}}{e^{4\pi i f l_1}-1}+\frac{e^{4\pi i f l_2}-1}{2\pi i f}\right] \tag{4.44}$$

$$\begin{aligned}H^*(f) &= 2\pi\nu\alpha^* h(f)\frac{[l_2 e^{4\pi i f l_1}(e^{4\pi i f l_2}-1)\delta l_1 + l_1 e^{4\pi i f l_2}(e^{4\pi i f l_1}-1)\delta l_2]}{[e^{4\pi i f l_1}-1+4\pi i f\delta l_1 e^{4\pi i f l_1}]}\\ &+\nu\alpha^*\frac{h(f)}{2if}\frac{(l_1+l_2)(e^{4\pi i f l_1}-1)(e^{4\pi i f l_2}-1)}{[e^{4\pi i f l_1}-1+4\pi i f\delta l_1 e^{4\pi i f l_1}]}\,.\end{aligned} \tag{4.45}$$

Note that, for the case of an exact knowledge of the arm lengths ($\delta l_1 = \delta l_2 = 0$), the laser phase noise is totally cancelled. However, in practice, this is not the case due to the limited accuracy of ground tracking methods and the change of the arm lengths coming from the orbital motion. Then, we need to restrict the maximum value of the accuracies δl_1 and δl_2 in order to cancel sufficiently the laser phase noise, to a level below the gravitational waves signals. This will lead to the maximum time required before updating the round-trip light times during the implementation of the unequal-arm algorithm. It can be done by computing Eq. 4.40 which is the final result of this frequency domain algorithm. In addition, we can find useful results in the long-wavelength limit ($fl_1, fl_2 << 1$, i.e. $f \leq 10^{-2}$), although LISA will not operate exclusively in it. In this domain, the equation for $\Delta(f)$ becomes

$$\begin{aligned}\Delta(f) &\approx 4\pi i f p_1(f)\left[\frac{l_1\delta l_2 - l_2\delta l_1}{l_1}\right] + 4\frac{l_2}{l_1}a_1(f)\left[1-\frac{\delta l_1}{l_1}+\frac{\delta l_2}{l_2}\right] - 4a_2(f)\\ &+2n_1(f)\left[\frac{l_2+\delta l_2-\frac{l_2\delta l_1}{l_1}}{l_1}\right] - 2n_2(f) + 2\pi\nu h(f) l_2\left[2+\frac{\delta l_2}{l_2}-\frac{\delta l_1}{l_1}\right]\\ &+2\pi\nu h(f)\alpha^* l_1 l_2\left[1+\frac{l_2}{l_1}+\frac{\delta l_2}{l_2}-\frac{\delta l_1}{l_1}\right]\,.\end{aligned} \tag{4.46}$$

Gravitational wave component

In order to distinguish the gravitational waves signature in $\Delta(f)$, the gravitational wave term must dominate the others. This leads to a requirement on the accuracy with which the arm length must be determined in order for the data analysis algorithm correctly applied through

$$\left| p_1(f) \frac{f}{v} \left[\frac{\delta l_2 - \delta l_1}{l_2} + \frac{l_1 - l_2}{l_1 l_2} \delta l_1 \right] \right| \leq |h(f)| \,. \tag{4.47}$$

As an example, to be able to distinguish the gravitational wave of amplitude $10^{-20}\sqrt{\text{Hz}}$ from a galactic binary at the Fourier frequency of 10^{-2} Hz, the difference in arm length must be known to better than approximately 27 km and the individual arm length to about 275 km. Of course, the requirement on the length of one arm depends on the difference between l_1 and l_2. The more l_2 is different from l_1 the more precisely we must known the arm length (i.e. δl_i smaller, see the second term on the left side of Eq. 4.47). The corresponding requirement in time will depend on when, during the mission, this change takes place. However, a minimum value of the integration time can be given by considering the highest arm length rate of change (about 13 m/s according to Appendix A). This leads to an integration time to about 20000 s.

To illustrate this result, we have computed Eq. 4.40, which does not suffer from the long-wavelength assumption, with an integration time of 10000 seconds. In the worst case, this corresponds to a maximum uncertainty of about 130 km on the arm length. Indeed, if v_r is the relative velocity between 2 spacecraft (up to 13 m/s according Appendix A), during the integration time, the arm length change is $\delta l_1 = \frac{v_r}{c} \times t$.

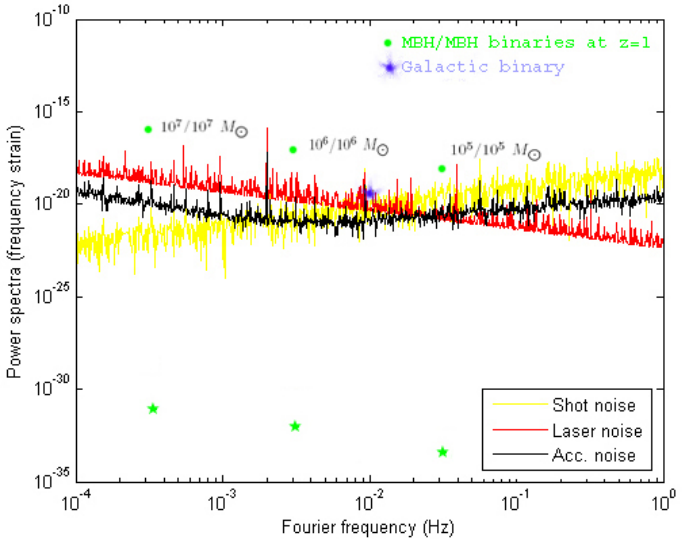

Figure 4.6: *Amplitude power spectrum* after the laser phase noise cancellation algorithm for an integration time of 10000s.

We can see that the noise cancellation process has effectively cancelled the laser noise below the gravitational waves component. Indeed, the gravitational waves from the MBH/MBH binaries can be clearly distinguished and the one of the galactic binary is just above the laser noise. On a other hand, the shot and acceleration noise are almost not affected by this algorithm and it would be useless to cancel the laser phase noise below these secondary noises. Therefore, even if we sufficiently cancel the laser noise, the contribution of the Pioneer anomaly would still be well below the other noises and can not be distinguishable.

Note that in order to derive the accuracies above, the light-time for the two arms have been taken to l_1=16.70 seconds and $l_2 = 1.1 \times l_1$ seconds. These arm lengths can be determined by combining ground tracking of the spacecraft with the observed arm length changes from the laser measurements or, alternatively, by computing the autocorrelation function[3] of each phase difference $z_i(t)$, $i = 1, 2$. Indeed, the autocorrelation of the laser phase noise has three maxima, at times zero and $\pm 2l_i$, and the other noise sources have autocorrelation time smaller than $2l_i$. Therefore, the arm length can be determined by searching the position of the $2l_i$ peak.

Pioneer anomaly contribution

To confirm the above result, we can apply the same procedure on the Pioneer component of Eq. 4.46. This leads to a requirement on the arm lengths, which allows the laser phase noise to be sufficiently cancelled

$$\left| \frac{2p_1(f)f}{\nu(l_1+l_2)} \left[\frac{\delta l_2 - \delta l_1}{l_2} + \frac{l_1 - l_2}{l_1 l_2} \delta l_1 \right] \right| \leq |\alpha^* h(f)| \,. \tag{4.48}$$

If we consider the effect on a strong gravitational wave, like the coalescence of MBH-MBH binary(typically of amplitude 10^{-16} $\sqrt{\text{Hz}^{-1}}$ at the Fourier frequency of $10^{-3.5}$ Hz), this relation leads to a requirement of about 1.3×10^{-8} m in the knowing of the difference in arm length! This precision can not be achieved in space. The result of the method is shown in Fig. 4.7. To plot this figure, we assume that the uncertainty on the arm length can be kept sufficiently low during the integration time necessary to reach 10^{-4} Hz. This assumption is obviously wrong for LISA but is useful to illustrate the performance of the cancellation method.

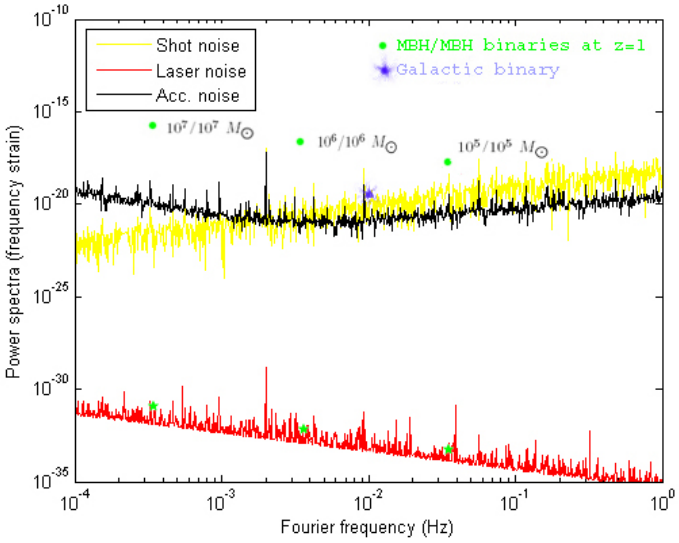

Figure 4.7: *Amplitude power spectrum* after the laser phase noise cancellation algorithm for an uncertainty on the arm length of 10^{-8} m.

We remark that, even if the laser noise could be sufficiently cancelled, the secondary noises remains well higher and the contribution of the anomaly would not be distinguishable.

[3]The autocorrelation function of a signal z(t) is defined as

$$\Gamma_{zz}(\tau, T) \equiv \lim_{T \to \infty} \frac{1}{2T} \int_{-T}^{T} z(t+\tau) z(t) dt$$

To conclude, with the assumption that we have the true spectrum of the arm lengths (see Eq. 4.23), there is no impact of the Pioneer anomaly on the gravitational wave detection in this Fourier frequency band. However, we have demonstrated that a certain minimal integration time is necessary to perform the laser phase noise cancellation sufficiently accurately. Therefore, the *spectral leakage* of the terms neglected in Eq. 4.23 needs to be specifically addressed.

4.4.4 Spectral leakage

The finite integration time required to sufficiently cancels the laser noise leads to the leakage of the power to other frequencies. In particular, the low-frequency terms neglected in the two-way signal $z_i(t)$, reminded here after, have now to be addressed.

$$\begin{aligned} z_i(t) &= p_i(t-2l_i) - p_i(t) - 4\pi\nu l_i(t) + 4\pi\alpha^* \int l_i(t)dt + n_k(t) + n_i(t-l_i) \\ &\quad +2\frac{\pi\nu}{c}\int\int[\hat{u}.\vec{a_i}(t) - \hat{u}.\vec{a_i}(t-2l_i)]dt^2 \pm \pi\nu\int[h(t)-h(t-2l_i)]dt \\ &\quad \mp\pi\alpha^*\int\int[h(t)-h(t-2l_i)]dt^2\,. \end{aligned} \tag{4.49}$$

In the previous algorithm, the power spectral density of terms in $l_i(t)$ has been dropped because their amplitudes are negligible in the *sensitivity band* of LISA for an infinite integration time (see Appendix A). Now, to be in accordance with our results, we have to limit the integration time to a fixed value T (typically 10000 s). For such a time scale, the arm length rate of change is nearly constant (see Appendix B) and depends on the position of the spacecraft along its orbit. We call the relative velocity v which can be up to 13 m/s. The approximation of the Fourier transform of $l_i(t)$ is then given by

$$\begin{aligned} \tilde{FT}.[l_i(t)] &= \frac{1}{c}\int_0^T (v_i t + 5\times10^9)e^{2\pi i f t}dt \\ &= v_i e^{i\pi Tf}\frac{\pi Tf\cos(\pi Tf) - \sin(\pi Tf)}{2\pi^2 i c f^2} + \left[v_i\frac{T}{2} + 5.10^9\right]e^{i\pi Tf}\frac{\sin(\pi Tf)}{\pi c f}\,. \end{aligned} \tag{4.50}$$

The details of the calculations are reported in Appendix B. With the given parameter values, one can see that the constant term (due to the nominal arm length, i.e. 5×10^9 m) is dominant. Here, we draw attention to the fact that intuition could lead to wrong interpretation. Indeed, one could think that the constant term of the arm lengths, being nearly the same for the two arms, would be removed by the algorithm. This is true when the signals from the two arms are subtracted but then, the signal from one arm is used to cancel the laser noise which reintroduces the constant term.

The *amplitude power spectrum* estimation can be computed by the periodogram method [47], i. e. by dividing the absolute value of the Fourier transform by the square root of the observing time. The complete Fourier transform of the two-way Doppler signal is now given by

$$\begin{aligned} z_1(f) &= p_1(f)\left[e^{4\pi i f l_1} - 1\right] + n_1(f)\left[1 + e^{2\pi i f l_1}\right] + a_1(f)\left[e^{4\pi i f l_1} + 2e^{2\pi i f l_1} + 1\right] \\ &\quad +4\pi\nu l_i(f) - \frac{2\alpha^*}{if}l_i(f)\,. \end{aligned} \tag{4.51}$$

In this equation, we have removed the contribution of gravitational waves, which has been studied in the previous section. As shown in Fig. 4.8, the nominal term in $l_i(t)$ is much higher than the phase noise but it can, in principle, be removed by preprocessing methods. We investigate this point at the end of this subsection. The different *amplitude power spectra* involved in Eq. 4.51 are shown in Fig. 4.8.

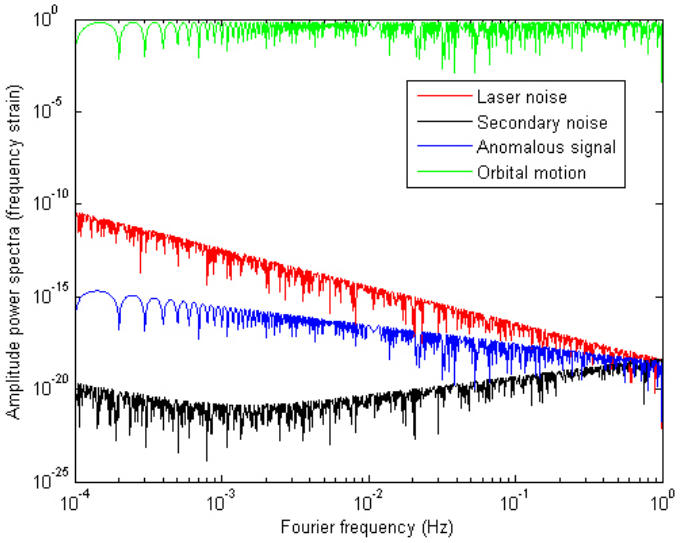

Figure 4.8: *Amplitude power spectra* contributing to the two-way Doppler signal. The signal of the Pioneer anomaly (in blue) is higher than the secondary noise sources (in black) but below the laser noise(in red).

A first important observation is that the signal from the Pioneer anomaly (in blue) is still well below the laser phase noise. This is important because the frequency domain cancellation algorithm required that the laser noise is dominant in the Fourier frequency band of interest. The method could thus be still implemented.

Frequency domain algorithm

By applying the algorithm to the new expression of $z_i(t)$, it is easy to find the corrected $\Delta(f)$ signal

$$\Delta^*(f) = P(f) + A(f) + N(f) + L(f)\,, \tag{4.52}$$

where $P(f)$, $A(f)$ and $N(f)$ are given in Section 4.4.2 and L(f) is written as:

$$L(f) = \frac{2\alpha^*}{if}\left[l_1'(f)\frac{1-e^{4\pi i f(l_2+\delta l_2)}}{e^{4\pi i f(l_1+\delta l_1)}-1} + l_2'(f)\right]. \tag{4.53}$$

In the long-wavelength approximation, $L(f)$ becomes

$$L(f) = \frac{2\alpha^*}{if}\left[-l_1'(f)\frac{l_2}{l_1}(1+\frac{\delta l_2}{l_2}-\frac{\delta l_1}{l_1}) + l_2'(f)\right] \tag{4.54}$$

These results are illustrated in Fig. 4.9 below. The integration time and the uncertainty on the arm length are respectively taken at the value 10000 s and 5000 m.

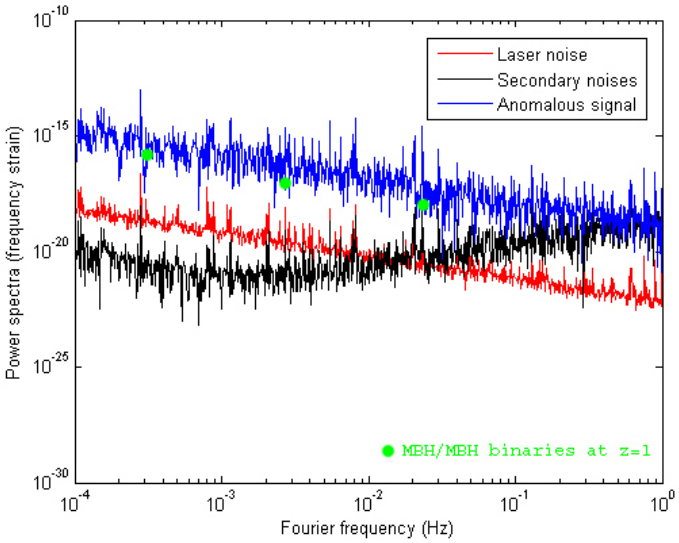

Figure 4.9: Spectra involved in $\Delta^*(f)$ for an integration time of 10000s. The signal of the Pioneer anomaly (in blue) remains higher than the secondary noise sources (in black) and most gravitational wave signals.

From this figure, it is clear that the cancellation algorithm might reveal the anomaly if an appropriate preprocessing treatment on the orbital motion term is performed. This point is discussed in the next subsection. On the other hand, even the strongest gravitational waves (the green points in the figure above come from MBH/MBH coalescences) would not be distinguishable.

Finally, note that the *spectral leakage* can be minimized by pre-multiplying the time-domain data sets by a window function before taking Fourier transform [34, 49]. With this preprocessing, the detection of gravitational waves remains unimpaired.

Pre-processing to remove the nominal orbit motion from the data

The crucial question of the previous method is how accurately we need to determine the arm length of LISA to sufficiently remove the nominal orbital motion term. According to Fig. 4.8, a cancellation of about 10^{15} orders of magnitude has to be performed. If we suppose that the arm length is known to a factor of $k \cdot l_i$, the Fourier transform of the one-way Doppler signal becomes

$$\begin{aligned} z_1(f) &= p_1(f)[e^{4\pi i f l_1} - 1] + n_1(f)[1 + e^{2\pi i f l_1}] + a_1(f)[e^{4\pi i f l_1} + 2e^{2\pi i f l_1} + 1] \\ &\quad + 4(1+k)\pi\nu l_i(f) - (1+k)\frac{2\alpha^*}{if} l_i(f)\,. \end{aligned} \tag{4.55}$$

Therefore, after the removal of this nominal orbital motion term, it remains $4k\pi\nu l_i(f)$ which should be sufficiently low to detect the anomaly. At 10^{-4} Hz, this corresponds to a knowledge of the arm length of about $10^{-15} \times 5.10^9$ m$= 5 \times 10^{-6}$ m which can not be achieved.

This discussion close the study within the *sensitivity band*. As it was already suspected when we derived Eq. 3.60, it is now evident that the Pioneer anomaly will not be detectable in the *sensitivity band* of LISA. The impact of the anomaly would nevertheless be bigger at the frequencies of the orbital motion.

4.4.5 Outside the frequency band

For long integration time, the arm length rate of change is not constant anymore. For the two first years of the mission, the arm lengths will change like shown on the left part of Fig. 4.10 below. For our purpose, we need the power spectrum of this orbital motion. This has been computed by taking the Fast Fourier Transform of each arm lengths. More details are given in Appendix A. The dominant frequencies of the arm length change due to orbital motion are shown in the right part of Fig. 4.10 below.[4]

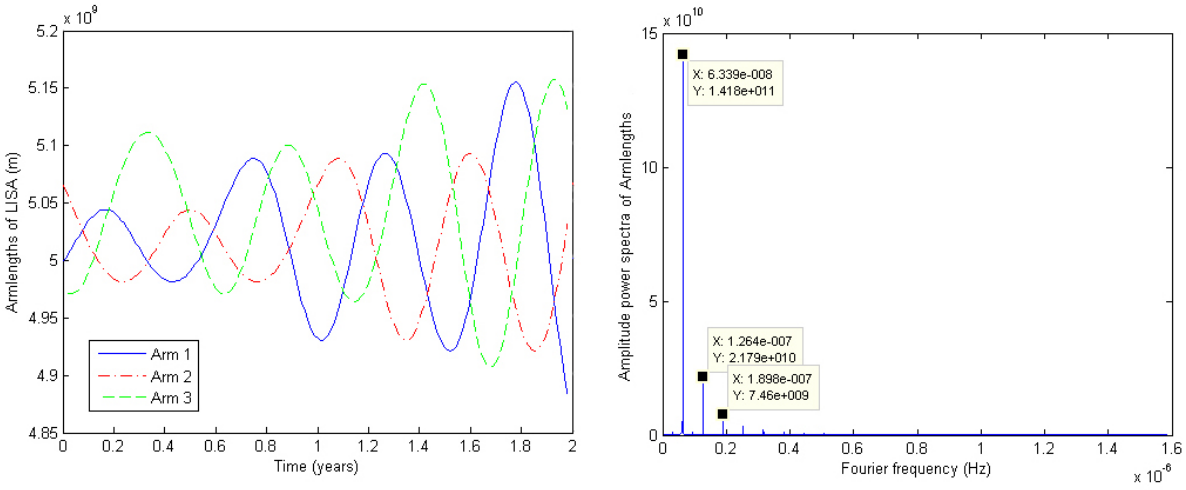

Figure 4.10: On the left, the 3 arm lengths of LISA during the first 2 years of the mission. On the right, *amplitude power spectrum* of arm length 1.

The dominant frequencies correspond to 6, 3 and 2 months and are shown with their amplitudes. Taking this spectrum into account, one can plot the two-way Doppler signal, Eq. 4.55, outside the *sensitivity band* of LISA (see Fig. 4.11).

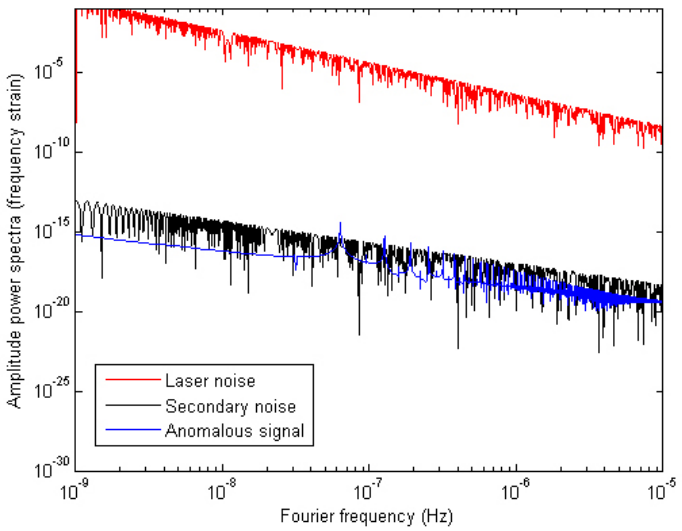

Figure 4.11: Two-way Doppler signal outside the *sensitivity band* of LISA.

[4]This spectrum was computed with an integration time of 10^6 years in order to minimize the *spectral leakage*. It was also computed without the continuous component of the arm length which is irrelevant in this case.

The term due to the Pioneer anomaly (in blue) is still below the laser phase noise and would be difficult to distinguish from the secondary noise (in black). Moreover, for the integration time required to reach these frequencies, the arm lengths change by much more than the accuracy needed to cancel sufficiently the laser noise. Indeed, from Eq. 4.46 and using Eq. 4.54, the maximum value of the uncertainty on the arm length would be about 2000m while change on this timescale will be of about 100000 km.

In conclusion, outside the *sensitivity band* of LISA, the laser noise can not be sufficiently cancelled and the Pioneer anomaly will not be detectable.

4.4.6 Conclusions of the frequency domain study

In the previous chapter, we have seen that, on the LISA's arms, the anomalous blueshift will have an amplitude several orders of magnitude higher than the weakest gravitational waves detectable. However, this "large" impact of the anomaly comes from the constant part of the arm lengths. Hence it is located at a null Fourier frequency while relevant gravitational waves for LISA are expected at Fourier frequencies between 10^{-4} and 1 Hz. In the *sensitivity band* of LISA, the effect of the anomaly is well below all the instrumental noises and should not have an impact. With the frequency domain method, we checked that it is still the case after the cancellation of the laser phase noise. Then, we explained that, because of the orbital motion, a limited integration time is required to sufficiently cancel the laser phase noise. With a finite observation time, power of the constant contribution of the anomaly can leak in the *sensitivity band*. We showed that, after the cancellation method, this contribution overwhelms the gravitational wave signature and therefore, could be detectable. However, this would require a precision in the knowledge of the arm lengths which can not be achieved.

Outside the *sensitivity band*, we showed that the contribution of the anomaly is just above the secondary noise sources but still below the laser phase noise. Hence there was a chance to detect the anomaly by removing the laser phase noise. However, at these timescales, the arm lengths change by much more that it is allowed to remove efficiently the laser phase noise. Therefore, we can conclude that the Pioneer anomaly has no impact on the gravitational wave detection and cannot be detectable with the frequency domain method.

4.5 Time delay interferometry

Time delay interferometry (TDI) is a noise cancellation technique performed in the time domain [34, 35, 36]. The basic principle of TDI consists in combining appropriate of one-way Doppler signals in order to remove the laser phase noise. As it will be shown below, these combinations have the interesting property to remove the Doppler shifts due to the no inertial motions of the optical-benches. The major question to be studied is how the Pioneer anomaly affects the TDI combinations. As the frequency domain study showed that the effect of the anomaly is negligible within the *sensitivity band*, we have focused our attention on the anomalous blueshift occurring at lower frequencies.

4.5.1 Notation

Fig. 4.12 below shows the overall geometry of the interferometer in the plane of the three spacecraft. These are equidistant from point O (distance L). Relative to O, the spacecraft are located by the coplanar unit vectors $\hat{p}_1$, $\hat{p}_2$ and $\hat{p}_3$. As indicated in the figure, the lengths between pairs of spacecraft are L_1, L_2 and L_3, with L_i being opposite of the ith spacecraft. Unit vectors along the lines connecting spacecraft pairs are $\hat{n}_1$,$\hat{n}_2$ and $\hat{n}_3$, oriented such as $L_1\hat{n}_1+L_2\hat{n}_2+L_3\hat{n}_3=0$. This terminology allows cyclic permutation of the indices in subsequent equations resulting in compact notation and facilitating coding of sensitivity calculations.

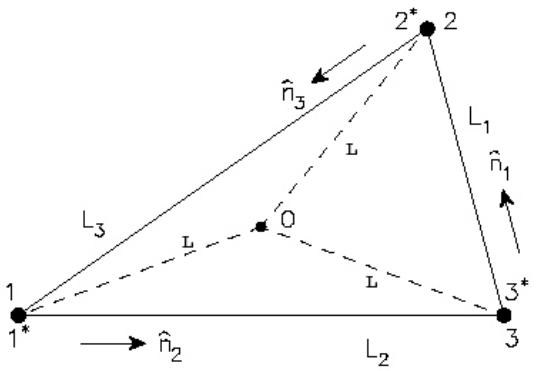

Figure 4.12: Schematic LISA configuration. At each vertex spacecraft, there are two *optical benche*s (denoted 1,1*,etc.).

In this method, it is convenient to formulate the instrumental responses in terms of observed relative frequency shifts rather than in terms of phase shifts[5], usually used in interferometry and in the frequency domain method. The Doppler data to be analyzed are now called $y_{ij} = \frac{\Delta\nu}{\nu_o}$, where $\Delta\nu$ is the frequency deviation from the center frequency ν_o. The subscripts label the transmitting and receiving spacecraft. The convention is that y_{31} is the beam received at spacecraft 1 and transmitted from spacecraft 2, y_{21} is the beam received at spacecraft 1 and transmitted from spacecraft 3, etc. Internal metrology signals to correct for *optical bench* motions are denoted by z_{ij} , with the same labelling convention described for y_{ij}. Delay of laser data streams, either by time-of-flight or in post-processing, is indicated by commas in the subscripts: $y_{31,23} = y_{31}(t - l_2 - l_3) = y_{31,32}$, etc ($l_i$ is the light-time on the i arm).

[5]These data are easily interconvertible by using Eq. 4.11.

4.5.2 Signal and noise response functions

The gravitational wave signal and the various noises, which enter the Doppler data, are given in section 4.4.1 in terms of phase shifts. In this subsection, we quickly remind them, updating the notations and giving the expressions in terms of relative frequency shifts. At the same time, we also give a more general expression of the gravitational wave contribution.

Gravitational wave signal transfer function

According to [37, 38], the contribution to the one-way Doppler relative shift y_{31} and y_{12} of a transverse and traceless plane gravitational wave having unit wave-vector $\hat{k}$ is given by

$$y_{31}^{gw}(t) = \left[1 + \frac{l}{l_3}(\mu_1 - \mu_2)\right](\Psi_3(t - \mu_2 l - l_3) - \Psi_3(t - \mu_1 l))\,, \tag{4.56}$$

$$y_{21}^{gw}(t) = \left[1 + \frac{l}{l_2}(\mu_3 - \mu_1)\right](\Psi_2(t - \mu_3 l - l_2) - \Psi_2(t - \mu_1 l))\,, \tag{4.57}$$

where $\mu_i{=}\hat{k}\cdot\hat{p_i}$, and Ψ_i is

$$\Psi_i(t) = \frac{1}{2}\frac{\hat{n_i}\cdot\mathbf{h(t)}\cdot\hat{n_i}}{1-(\hat{k}\cdot\hat{n_i})^2}\,, \tag{4.58}$$

and where $\mathbf{h}$(t) is the first order spatial metric perturbation at point O. In transverse traceless gauge, the gravitational wave strain $\mathbf{h}$(t) can be decomposed as $[h_+(\mathrm{t})e_+ + h_x(\mathrm{t})e_x]$, where the 3-tensors e_+ and e_x are transverse to $\hat{k}$ and traceless. With respect to an orthonormal propagation frame ($\hat{i}$,$\hat{j}$,$\hat{k}$), their components are

$$e_+ = \begin{pmatrix} 1 & 0 & 0 \\ 0 & -1 & 0 \\ 0 & 0 & 0 \end{pmatrix},\ e_x = \begin{pmatrix} 0 & 1 & 0 \\ 1 & 0 & 0 \\ 0 & 0 & 0 \end{pmatrix}. \tag{4.59}$$

In the derivation of Section 3.2, only the "+" polarization was considered.

Noise transfer function

As shown previously, the laser noise of the receiving spacecraft enters the Doppler data immediately at the time of reception, while the laser noise of the transmitting spacecraft enters one one-way delay earlier. Thus, we have

$$y_{ij}^{laser} = p_k(t - l_i) - p_j^*(t)\,, \tag{4.60}$$

where the laser phase noise is denoted by p and is now in unit of frequency strain.

Shot noise, n_{ij}^s, enters each Doppler time series in the reception process at spacecraft j. It is white phase noise so its effect on the derivative of phase, the Doppler time series, has a power spectral density proportional to f^2, where f is the Fourier frequency. Its effect is immediate at the time of reception, so that the responses of the Doppler observables are

$$y_{ij}^s = n_{ij}^s(t) \tag{4.61}$$

Let us look now closer to the light path of the signals inside the spacecraft to define an acceleration noise transfer function more suitable for LISA. The schematic geometry of the *proof-mass*-plus-*optical bench* assemblies for LISA spacecraft number 1 are shown in Fig. 4.13 below. The left-hand *optical bench* is taken to be bench number 1, while the right-hand bench is 1*. The photodetectors that generate the data y_{21}, y_{31}, z_{21}, and z_{31} at spacecraft 1 are shown.

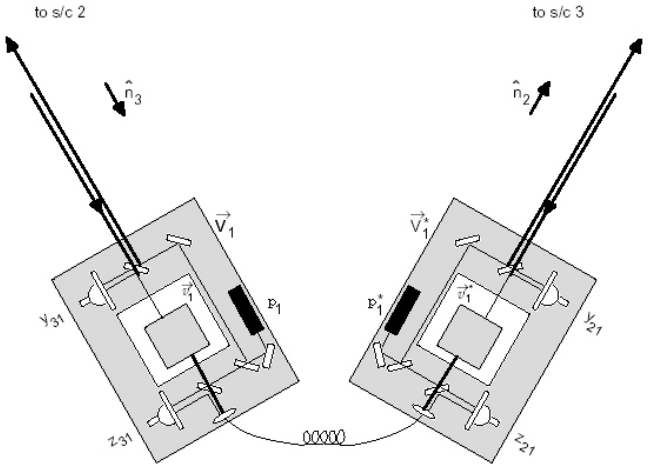

Figure 4.13: Schematic diagram of a LISA spacecraft [35]. The indices correspond to the spacecraft 1.

The random velocity vectors of the *proof masses* are respectively denoted $\vec{v}_i$ and $\vec{v}_i^*$, and the random velocities of their *optical bench*es are correspondingly denoted $\vec{V}_i$ and $\vec{V}_i^*$. An outgoing light beam transmitted to a distant spacecraft is routed from the laser on the local *optical bench* using mirrors and beam splitters; this beam does not interact with the local *proof mass*. Conversely, an incoming light beam from a distant spacecraft is bounced off the local *proof mass* before being redirected onto the photo-detector where it is mixed with light from the laser on that same *optical bench*.

With this configuration and using Eq. 4.8, the acceleration noise contributions to the relative frequency shifts are

$$y_{21}^{\rm acc} = -\hat{n}_2.\vec{V}_{3,2} + 2\hat{n}_2 \cdot \vec{v}_1^* - \hat{n}_2 \cdot \vec{V}_1^* \tag{4.62}$$

$$y_{31}^{\rm acc} = \hat{n}_3 \cdot \vec{V}_{2,3}^* - 2\hat{n}_3 \cdot \vec{v}_1 + \hat{n}_3 \cdot \vec{V}_1\,, \tag{4.63}$$

where the 2 multiplying $\vec{v}_i$ occurs because the signals are bouncing off the local *proof mass*.

Pioneer anomaly contribution

According to Section 3.1.1, the relative frequency shift due to the Pioneer anomaly is given by

$$y_{ij}^* = -\frac{a^*}{c} l_i(t) = \alpha^* l_i(t)\,, \tag{4.64}$$

where $\alpha^* \equiv \frac{a^*}{c}$. From the frequency domain method, it is clear that the contribution of the anomaly at the gravitational wave frequencies is undetectable and we focus the TDI study on the first order term.

Collecting all the contributions, the six time series (2 for each arm) of the total relative frequency shift are given by

$$y_{ij} = y_{ij}^{gw} + y_{ij}^{laser} + y_{ij}^{s} + y_{ij}^{\rm acc} + y_{ij}^{*}\,. \tag{4.65}$$

It will be shown in Section 4.5.3 that appropriate combinations of these one-way Doppler signals allow the laser noise cancellation.

Intra spacecraft metrology

To link the phases of adjacent benches, the present LISA design baseline foresees optical fibers transmitting signals between them. Because of the very small distance between the *optical bench*es on the same spacecraft, the time-delay effects for z_{ij} are ignored and we denote by $\eta_i(t)$ the frequency shifts upon transmission through the fibers. The light path is also shown in Fig. 4.13. Light to be transmitted from the laser on an *optical bench* is first bounced off the *proof mass* it encloses and then directed to the other *optical bench*. Upon reception it does not interact with the *proof mass* there, but is directly mixed with local laser light. This configuration allows the twelve Doppler data streams to be combined so as to eliminate all laser phase and *optical bench* noises and preserving the gravitational waves signature. Therefore, the relative frequency shift of the signals travelling inside spacecraft 1 are

$$z_{21} = p_1 + 2\hat{n}_3 \cdot (\vec{v}_1 - \vec{V}_1) + \eta_1 - p_1^* \tag{4.66}$$

$$z_{31} = p_1^* - 2\hat{n}_2 \cdot (\vec{v}_1^* - \vec{V}_1^*) + \eta_1 - p_1 \,. \tag{4.67}$$

As explained in the frequency domain method, the light time between the *optical bench*es on the same spacecraft is very short and an eventual blueshifting would be negligible.

TDI consists in forming appropriate combinations of the data series y_{ij} and z_{ij} in order to cancel the laser noise and reveal gravitational wave signatures. Note that in order to derive this technique, the arm lengths are assumed to be constant and known exactly. This assumptions leads to constraints on the maximum integration time which allows a sufficient cancellation of the laser phase noise. This maximum integration time is determined exactly like for the frequency domain method (appropriate calculations are made in [34]).

4.5.3 Linear data combinations

There are ten linear combinations which cancel the laser noises from all the spacecraft. These combinations are illustrated in Fig. 4.14 below and detailed just after that.

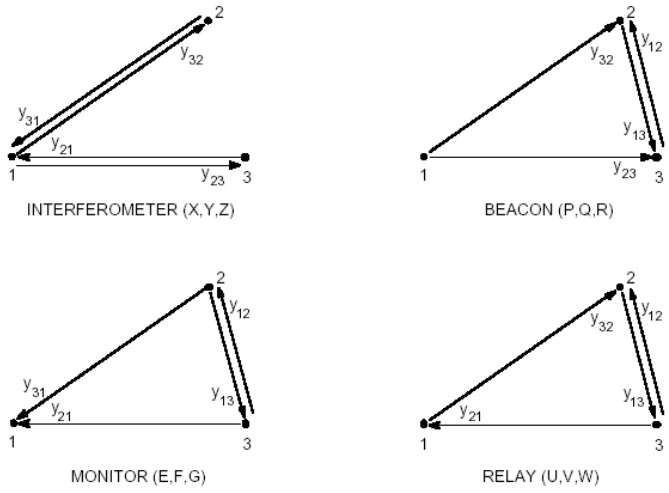

Figure 4.14: Schematic geometries of the data combinations [34].

These combinations are not independent, since they belong to a three-dimensional function space, but they have different spectral regions of sensitivity, and also can yield useful observables when different laser links are unavailable.

Unequal-arm length interferometric combinations

The nominal LISA configuration is the unequal-arm Michelson interferometer. There are three independent possible combinations (X,Y and Z). As can be verified by direct substitution of the laser noise contribution (Eqs. 4.60 and 4.66), they do not contain any laser noise are

$$\begin{aligned} X &= y_{32,322} - y_{23,233} + y_{31,22} - y_{21,33} + y_{23,2} - y_{32,3} + y_{21} - y_{31} \\ &\quad + \frac{1}{2}(-z_{21,2233} + z_{21,33} + z_{21,22} - z_{21}) \\ &\quad + \frac{1}{2}(+z_{31,2233} - z_{31,33} - z_{31,22} + z_{31})\,. \end{aligned} \tag{4.68}$$

Y and Z combinations are given by cyclic permutation of the indices. It is noteworthy that the *optical bench* motions (the V_i and V_i^*) are also cancelled.

In these combinations, each one-way signal occurs twice, at two different times; one term is added and the other subtracted. As a consequence, the Pioneer anomaly component disappears. Even the *spectral leakage* of the data has no impact because the terms which contain the anomaly are all cancelled. However, the results of the TDI will be useful for the following and we briefly show them. Explicitly, for X, the gravitational wave response is

$$\begin{aligned} X^{\rm gw} &= [1 - \frac{l}{l_3}(\mu_1 - \mu_2)](\Psi_3(t - \mu_1 l - 2l_3 - 2l_2) - \Psi_3(t - \mu_2 l - l_3 - 2l_2)) \\ &\quad -[1 + \frac{l}{l_2}(\mu_3 - \mu_1)](\Psi_2(t - \mu_1 l - 2l_2 - 2l_3) - \Psi_2(t - \mu_3 l - l_2 - 2l_3)) \\ &\quad +[1 + \frac{l}{l_3}(\mu_1 - \mu_2)](\Psi_3(t - \mu_2 l - l_3 - 2l_2) - \Psi_3(t - \mu_1 l - 2l_2)) \\ &\quad -[1 - \frac{l}{l_2}(\mu_3 - \mu_1)](\Psi_2(t - \mu_3 l - l_2 - 2l_3) - \Psi_2(t - \mu_1 l - 2l_3)) \\ &\quad +[1 + \frac{l}{l_2}(\mu_3 - \mu_1)](\Psi_2(t - \mu_1 l - 2l_2) - \Psi_2(t - \mu_3 l - l_2)) \\ &\quad -[1 - \frac{l}{l_3}(\mu_1 - \mu_2)](\Psi_3(t - \mu_1 l - 2l_3) - \Psi_3(t - \mu_2 l - l_3)) \\ &\quad +[1 - \frac{l}{l_2}(\mu_3 - \mu_1)](\Psi_2(t - \mu_3 l - l_2) - \Psi_2(t - \mu_1 l)) \\ &\quad -[1 + \frac{l}{l_3}(\mu_1 - \mu_2)](\Psi_3(t - \mu_2 l - l_3) - \Psi_3(t - \mu_1 l))\,, \end{aligned} \tag{4.69}$$

where Ψ_i, l, μ_i are given in terms of the wave properties and detector geometry (see Section 4.5.1 above). If the gravitational wave signal is a δ-function, it produces eight pulses in X, located at time, that depends on the arrival direction of the wave and the detector configuration: $\mu_1 l$, $\mu_2 l + l_3$, $\mu_3 l + l_2$, $\mu_1 l + 2l_3$, $\mu_1 l + 2l_2$, $\mu_3 l + l_2 + 2l_3$, $\mu_2 l + 2l_2 + l_3$ and $\mu_1 l + 2l_2 + 2l_3$.

The noises due to residual accelerations on the proof-mass remain and are dominant at low Fourier frequency. The transfer function in the X combination is

$$\begin{aligned} X^{\rm proof\ mass} &= \hat{n}_2 \cdot (-\vec{v}^*_{1,2233} + \vec{v}^*_{1,22} - \vec{v}^*_{1,33} + \vec{v}^*_1 + 2\vec{v}_{3,233} - 2\vec{v}_{3,2}) \\ &\quad + \hat{n}_3 \cdot (-\vec{v}_{1,2233} + \vec{v}_{1,33} - \vec{v}_{1,22} + \vec{v}_1 + 2\vec{v}^*_{2,223} - 2\vec{v}^*_{2,3})\,. \end{aligned} \tag{4.70}$$

The transfer function of shot noise is similar to Eq. 4.68 since shot noise enters the data series as $y^s_{ij} = n^s_{ij}(t)$

$$X^{\text{shot noise}} = n_{32,322} - n_{23,233} + n_{31,22} - n_{21,33} + n_{23,2} - n_{32,3} + n_{21} - n_{31}\,. \tag{4.71}$$

This equation also reflects that the shot noise in the z_{ij} are negligible since these Doppler measurements are performed at high signal-to-noise ratios.

Taking the Fourier transform of the shot and acceleration noise terms, it is easy to derive the following expression for the one-sided power spectral density

$$S_X = [8\sin^2(4\pi fL) + 32\sin^2(2\pi fL)]S_y^{\text{proof mass}} + 16\sin^2(2\pi fL)S_y^{\text{optical path}} \tag{4.72}$$

This equation is calculated by assuming independent individual proof-mass acceleration noises (with equal raw spectra), and independent shot noises. It is also assumed that the configuration of the interferometer is an equilateral triangle (L_1=L_2=L_3≡L). The results of these combinations are shown in Section 4.5.4.

The Sagnac combinations: α,β and γ

The α, β and γ are three different independent linear combinations of the Doppler data, which do not contain laser and *optical bench* noises. These are interesting for their simplicity and the six-pulse response to gravitational wave signals. The combination α is explicitly written (β and γ are given by cyclical permutation of the indices) as

$$\begin{aligned}\alpha \;=\;& y_{21} - y_{31} + y_{13,2} - y_{12,3} + y_{32,12} - y_{23,13} \\ & -\frac{1}{2}(z_{13,2} + z_{13,13} + z_{21} + z_{21,123} + z_{32,3} + z_{32,12}) \\ & +\frac{1}{2}(z_{23,2} + z_{23,13} + z_{31} + z_{31,123} + z_{12,3} + z_{12,12})\,.\end{aligned} \tag{4.73}$$

In this combination, the one-way signals are not used twice as for X,Y and Z combinations but occur in pairs. This means that for each one-way signal on a given arm, there is its counterpart travelling on the same arm and in the other direction. The result of this is again the cancellation of the Pioneer anomaly component. Note that it would not be the case if the anomalous frequency shift of light depends on the sense of travelling with respect to the Sun.

The gravitational wave response of α is:

$$\begin{aligned}\alpha^{\text{gw}} \;=\;& [1 - \frac{l}{l_2}(\mu_3 - \mu_1)](\Psi_2(t - \mu_3 l - l_2) - \Psi_2(t - \mu_1 l)) \\ & -[1 + \frac{l}{l_3}(\mu_1 - \mu_2)](\Psi_3(t - \mu_2 l - l_3) - \Psi_3(t - \mu_1 l)) \\ & +[1 - \frac{l}{l_1}(\mu_2 - \mu_3)](\Psi_1(t - \mu_2 l - l_1 - l_2) - \Psi_1(t - \mu_3 l - l_2)) \\ & -[1 + \frac{l}{l_1}(\mu_2 - \mu_3)](\Psi_1(t - \mu_3 l - l_1 - l_3) - \Psi_1(t - \mu_2 l - l_3)) \\ & +[1 - \frac{l}{l_3}(\mu_1 - \mu_2)](\Psi_3(t - \mu_1 l - l_1 - l_2 - l_3) - \Psi_3(t - \mu_2 l - l_1 - l_2)) \\ & -[1 + \frac{l}{l_2}(\mu_3 - \mu_1)](\Psi_2(t - \mu_1 l - l_3 - l_1 - l_2) - \Psi_2(t - \mu_3 l - l_3 - l_1))\end{aligned} \tag{4.74}$$

Note that here, a δ-function gravitational wave, would produce six pulses in α, depending also on the arrival direction of the wave and the detector configuration. Non inertial motions of the *proof-masses* do not cancel; this contribution to α is

$$\begin{aligned}\alpha^{\text{proof mass}} &= \hat{n}_1 \cdot (\vec{v}_{2,3} - \vec{v}_{2,12} + \vec{v}^*_{3,2} - \vec{v}^*_{3,13}) \\ &+\hat{n}_2 \cdot (\vec{v}_{3,13} - \vec{v}_{3,2} + \vec{v}^*_1 - \vec{v}^*_{1,123}) \\ &+\hat{n}_3 \cdot (\vec{v}_1 - \vec{v}_{1,123} + \vec{v}^*_{2,12} - \vec{v}^*_{2,3})\,, \end{aligned} \tag{4.75}$$

while the shot noise in α is similar to Eq. 4.73.

With the same assumptions than for the X,Y and Z combinations, we have the following expression of the one-sided power spectral density

$$S_\alpha = [8\sin^2(3\pi fL) + 16\sin^2(\pi fL)]S_y^{\text{proof mass}} + 6S_y^{\text{optical path}}\,. \tag{4.76}$$

Fully symmetric (Sagnac) combination

Another combination of all six one-way signals which exactly cancels laser and optical bench noises is the Sagnac combination:

$$\begin{aligned}\zeta &= y_{32} - y_{23,3} + y_{13,3} - y_{31,1} + y_{21,1} - y_{12,2} \\ &+\frac{1}{2}(-z_{13,21} + z_{23,12} - z_{21,23} + z_{31,23} - z_{32,13} + z_{12,13}) \\ &+\frac{1}{2}(-z_{32,2} + z_{12,2} - z_{13,3} + z_{23,3} - z_{21,1} + z_{31,1}) \end{aligned} \tag{4.77}$$

This combination has the property that each of the y_{ij} enters exactly once and is delayed by one of the one-way light times. However, as we can see by introducing Eq. 4.64, the contribution of the anomalous blueshift is also exactly cancelled. Like α, β and γ, this combination also has a six-pulse response to gravitational radiation:

$$\begin{aligned}\zeta^{\text{gw}} &= [1 - \frac{l}{l_3}(\mu_1 - \mu_2)](\Psi_3(t - \mu_1 l - l_3 - l_2) - \Psi_3(t - \mu_2 l - l_2)) \\ &-[1 + \frac{l}{l_2}(\mu_3 - \mu_1)](\Psi_2(t - \mu_1 l - l_2 - l_3) - \Psi_2(t - \mu_3 l - l_3)) \\ &+[1 - \frac{l}{l_1}(\mu_2 - \mu_3)](\Psi_1(t - \mu_2 l - l_1 - l_3) - \Psi_1(t - \mu_3 l - l_3)) \\ &-[1 + \frac{l}{l_3}(\mu_1 - \mu_2)](\Psi_3(t - \mu_2 l - l_3 - l_1) - \Psi_3(t - \mu_1 l - l_3)) \\ &+[1 - \frac{l}{l_2}(\mu_3 - \mu_1)](\Psi_2(t - \mu_3 l - l_2 - l_1) - \Psi_2(t - \mu_1 l - l_1)) \\ &-[1 + \frac{l}{l_1}(\mu_2 - \mu_3)](\Psi_1(t - \mu_3 l - l_1 - l_2) - \Psi_1(t - \mu_2 l - l_2))\,. \end{aligned} \tag{4.78}$$

A δ-function signal would produce six pulses in ζ, located at: $\mu_1 l + l_3 + l_2$, $\mu_2 l + l_1 + l_3$, $\mu_3 l + l_1 + l_2$, $\mu_3 l + l_3$, $\mu_2 l + l_2$ and $\mu_1 l + l_1$.
The proof mass noise for ζ is

$$\begin{aligned}\zeta^{\text{proof mass}} &= \hat{n}_1 \cdot (\vec{v}_{2,2} - \vec{v}_{2,13} + \vec{v}^*_{3,3} - \vec{v}^*_{3,21}) \\ &+\hat{n}_2 \cdot (\vec{v}_{3,3} - \vec{v}_{3,21} + \vec{v}^*_{1,1} - \vec{v}^*_{1,23}) \\ &+\hat{n}_3 \cdot (\vec{v}_{1,1} - \vec{v}_{1,23} + \vec{v}^*_{2,2} - \vec{v}^*_{2,13}) \end{aligned} \tag{4.79}$$

while the contribution of optical path noise is similar to Eq. 4.77 since shot noise enters the data series as $y^s_{ij} = n^s_{ij}(t)$. Finally, the power spectra of the acceleration and shot noise component of ζ, assuming equal and independent individual proof mass acceleration noises, equal and independent optical path noises, and the equilateral triangle configuration are

$$S_\zeta = 24\sin^2(\pi f L) S_y^{\text{proof mass}} + 6 S_y^{\text{optical path}}\,. \tag{4.80}$$

The (P,Q,R), (E,F,G) and (U,V,W) combinations

There are other interesting combinations which allow the laser and *optical bench* noises to be removed and thus, the detection of gravitational waves. These combinations

$$\begin{aligned} P &= y_{32,2} - y_{23,3} - y_{12,2} + y_{13,3} + y_{12,13} - y_{13,12} + y_{23,311} - y_{32,211} \\ &\quad + \frac{1}{2}(-z_{21,23} + z_{21,1123} + z_{31,23} - z_{31,1123}) \\ &\quad + \frac{1}{2}(-z_{32,2} + z_{32,112} + z_{12,2} - z_{12,112}) \\ &\quad + \frac{1}{2}(-z_{13,3} + z_{13,113} + z_{23,3} - z_{23,113})\,, \end{aligned} \tag{4.81}$$

with Q and R given by index permutation. The (E,F,G) and (U,V,W) combinations can be obtained the same way by using Fig. 4.14. All these can be useful in the case of selected subsystem failures. However, each one-way signal occurs twice and the Pioneer anomaly component disappears. The contribution of gravitational waves to P is given by

$$\begin{aligned} P^{gw} &= [1 - \frac{l}{l_3}(\mu_1 - \mu_2)](\Psi_3(t - \mu_1 l - l_2 - l_3) - \Psi_3(t - \mu_2 l - l_2)) \\ &\quad -[1 + \frac{l}{l_2}(\mu_3 - \mu_1)](\Psi_2(t - \mu_1 l - l_2 - l_3) - \Psi_2(t - \mu_3 l - l_3)) \\ &\quad -[1 + \frac{l}{l_1}(\mu_2 - \mu_3)](\Psi_1(t - \mu_3 l - l_1 - l_2) - \Psi_1(t - \mu_2 l - l_2)) \\ &\quad +[1 - \frac{l}{l_1}(\mu_2 - \mu_3)](\Psi_1(t - \mu_2 l - l_1 - l_3) - \Psi_1(t - \mu_3 l - l_3)) \\ &\quad +[1 + \frac{l}{l_1}(\mu_2 - \mu_3)](\Psi_1(t - \mu_3 l - 2l_1 - l_3) - \Psi_1(t - \mu_2 l - l_1 - l_3)) \\ &\quad -[1 - \frac{l}{l_1}(\mu_2 - \mu_3)](\Psi_1(t - \mu_2 l - 2l_1 - l_2) - \Psi_1(t - \mu_3 l - l_1 - l_2)) \\ &\quad +[1 + \frac{l}{l_2}(\mu_3 - \mu_1)](\Psi_2(t - \mu_1 l - 2l_1 - l_2 - l_3) - \Psi_2(t - \mu_3 l - 2l_1 - l_3)) \\ &\quad -[1 - \frac{l}{l_3}(\mu_1 - \mu_2)](\Psi_3(t - \mu_1 l - 2l_1 - l_2 - l_3) - \Psi_3(t - \mu_2 l - 2l_1 - l_2))\,. \end{aligned} \tag{4.82}$$

The proof mass noise contribution is

$$\begin{aligned} P^{\text{proof mass}} &= \hat{n}_1 \cdot (\vec{v}_{2,2} - 2\vec{v}_{2,13} + \vec{v}_{2,112} + \vec{v}^*_{3,3} - 2\vec{v}^*_{3,12} + \vec{v}^*_{3,123}) \\ &\quad + \hat{n}_2 \cdot (-\vec{v}^*_{1,23} + \vec{v}^*_{1,1123} + \vec{v}_{3,3} - \vec{v}_{3,311}) \\ &\quad + \hat{n}_3 \cdot (-\vec{v}_{1,23} + \vec{v}_{1,1123} + \vec{v}^*_{2,2} - \vec{v}^*_{2,112})\,. \end{aligned} \tag{4.83}$$

and the one-sided power spectral density of the noises is then given by

$$\begin{aligned} S_P &= [8\sin^2(2\pi f L) + 32\sin^2(\pi f L)] S_y^{\text{proof mass}} \\ &\quad + [8\sin^2(2\pi f L) + 8\sin^2(\pi f L)] S_y^{\text{optical path}}\,. \end{aligned} \tag{4.84}$$

4.5.4 Gravitational wave sensitivity

The gravitational wave sensitivity is defined as the wave amplitude required to achieve a given signal-to-noise ratio. With the transfer functions calculated for each combination and the raw spectra given in Section 4.3, the level of noise in each combination is plotted in Fig. 4.15 below.

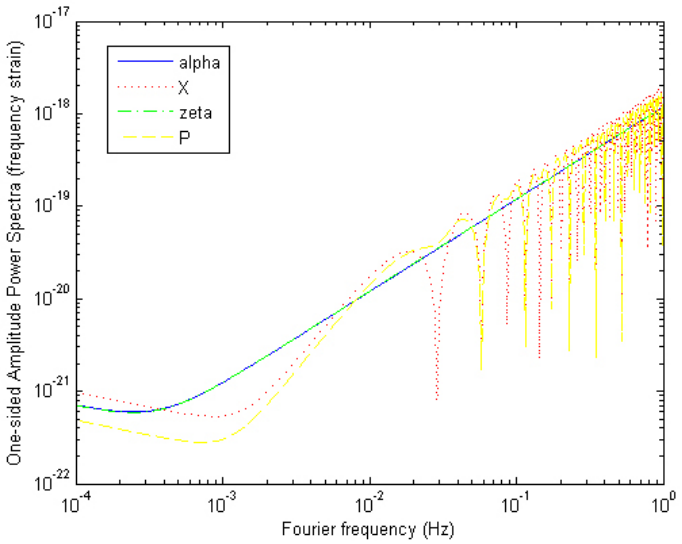

Figure 4.15: One-sided amplitude noise spectra for α, X, *zeta* and P for $L_1 = L_2 = L_3 = 10\sqrt{3}$ seconds.

This figure shows the *amplitude power spectra* of the noise in combinations X, ζ, α and P as a function of the Fourier frequency. Then, using the appropriate gravitational wave response from the previous section, the average sensitivity can be calculated in order to have a signal-to-noise ratio of 5 for 1 year observation (see Fig. 4.16 below).

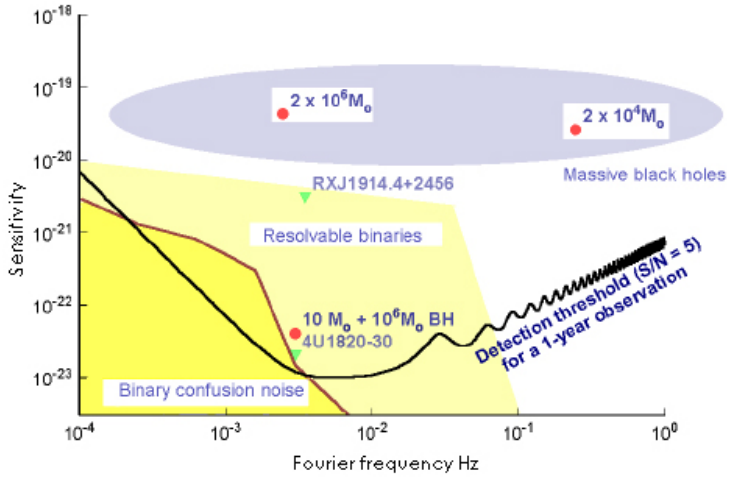

Figure 4.16: Sensitivity to gravitational waves for the unequal-arm combination X [8]. Several sources are also shown.

The sensitivity curve for the X combination is shown in with several expected sources. Specific sensitivity curves for the other combinations can be found in [35]. These are very similar to the X

combination with some minor differences such as the Fourier frequency of the optimal sensitivity. Note that the optimal sensitivity is slightly better than with the frequency domain algorithm. The heavy black curve shows the LISA sensitivity (or detection threshold), corresponding to a signal-to-noise ratio of 5 after a 1-year observation. At frequencies below 3 mHz, binaries in the Galaxy are so numerous that LISA will not resolve them, and they form a noise background called binary confusion noise. The area labelled "resolvable binaries" shows where LISA should resolve thousands of binaries that are closer to the Sun than most or that radiate at higher frequencies. The signals expected from two known binaries are indicated by the green triangles. Many other systems are known to be observable, but are not indicated here. Expected signals from coalescences of *massive black holes* in galaxies at redshifts of order z = 1 are also shown in the upper area. These signals may last less than 1 year and the region is drawn to indicate the expected signal-to-noise ratio above the LISA instrumental noise. There are also two signals indicated, for coalescences of binaries consisting of two $10^6 M_\odot$ and two $10^4 M_\odot$ *black holes*. In this case, the signal-to-noise ration could reach an amplitude of several thousand. While such events may occur only once per year, signals from small *black holes* falling into larger ones should be very common. Their strength is indicated by giving one example, where a 10 $M_\odot$ *black hole* falls into a 10^6 $M_\odot$ *black hole* at z = 1.

4.5.5 Conclusions of the TDI study

Several combinations of one-way Doppler signals, properly delayed, allow the cancellation of the laser phase noise while preserving the gravitational wave signal. This is called Time Delay Interferometry. The combinations have also the interesting property to cancel the *optical bench* noise. Taking into account an anomalous blueshift in the frequency of the laser light, we reviewed all the data combinations proposed in the LISA literature. The first order contribution due to the armlength changes by the orbital motion cancels exactly. Therefore, a study of the *spectral leakage* within the *sensitivity band* of the constant term will be useless. The second order contribution in the *sensitivity band* due to armlength changes by the gravitational waves remains but it has been clearly demonstrated in the frequency domain method that the effect is too small to be detected. Therefore, we come to the conclusion that the time delay interferometry, as presented in this section, would not reveal the anomaly. However, in orbit, the main assumption of TDI, the immobility of LISA, is not satisfied and the first order contribution of the anomalous blueshift might not be cancelled. This question is studied in the next section.

4.6 Effect of orbital motion on Time Delay Interferometry

The performance of time delay interferometry,as presented in previous section, is evaluated in the limit that LISA is fixed in space. However, each year, LISA will accomplish a complete rotation around its center and the symmetries available for a fixed detector will be broken. Because of this loss of symmetry, the contribution of the anomalous blueshift, occurring on each arm, could not be cancelled exactly in TDI combinations. In addition, the laser phase noise does not cancelled exactly either in these combinations and more complicated TDI combinations have been developed to overcome this problem (see [44, 43, 42]). In addition to the rotation, there is a complicated flexing of the arms in the detector. This is due to the orbital motion and the perturbations by planets. In this section, we consider these two effects and assess their impact on the contribution of the Pioneer anomaly in the TDI combinations.

4.6.1 The effects of rigid rotation

To take into account the effect of rigid rotation, let us first introduce a new notation for the arm lengths. Where, in first generation TDI, L_3 was the length of the arm between the first and the second spacecraft, we denote now by L_{12} the length travelled by the signal sent from spacecraft 1 and received at spacecraft 2. As before, the capital letters denote the lengths while small letters denote the light time. Similarly, the length travelled by the signal sent from spacecraft 2 and received at spacecraft 1 is called L_{21}. Unlike first generation TDI, L_{12} will now differ from L_{21}. This is outlined in Fig. 4.17 below.

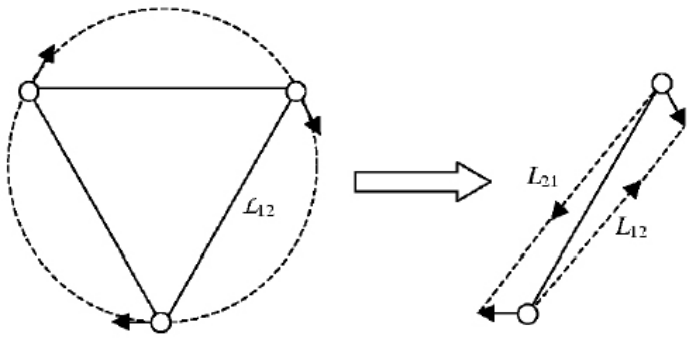

Figure 4.17: The rotation of the interferometer breaks the direction symmetry in the arm lengths [42].

Consider spacecraft 1 and 2 in the figure above. Since the interferometer is rotating in the clockwise direction, the spacecraft move during the signals are travelling along the arms. To be specific, if we define the length of the arm between spacecraft 1 and 2 to be $\mathcal{L}_{12}$ in the limit of no rotation, then the actual distance travelled by the signal from spacecraft 1 to spacecraft 2 will be $L_{12} < \mathcal{L}_{12}$. In the same manner, the signal from spacecraft 2 to spacecraft 1 will have to reach spacecraft 1 in its motion and will therefore travel a distance $L_{21} > \mathcal{L}_{12}$. We see now that the magnitude of an anomalous blueshift on one arm will depend on the direction in which the signal has travelled. Then, if the signals which have travelled on the same arm but in opposite direction are subtracted, it will remain a residual contribution of the anomalous blueshift. Let us now look what happen to each TDI combination.

The unequal-arm length interferometric combinations $X(t)$, $Y(t)$ and $Z(t)$, the contribution of the anomaly cancels exactly anyway. Indeed, if we take the $X(t)$ combination[6] reminded here

[6]For simplicity and without lost of generality, we drop the intra-spacecraft metrology (z_{ij} data).

after (the reasoning is the same for $Y(t)$ and $Z(t)$),

$$X = y_{32,322} - y_{23,233} + y_{31,22} - y_{21,33} + y_{23,2} - y_{32,3} + y_{21} - y_{31}\,, \tag{4.85}$$

we see that the one-way signals appear twice for a given direction, with opposite signs in the combination but are delayed by different times. Hence, for a rigid rotation where the relation $L_{ij}(t+\tau) = L_{ij}$ is always satisfied, the contribution of the anomaly is cancelled. An analysis of the (P,Q,R), (E,F,G) and (U,V,W) combinations leads to the same conclusion. For the Sagnac combinations (α, β, γ and ζ), it is different. Let us consider the ζ combination

$$\zeta = y_{32} - y_{23,3} + y_{13,3} - y_{31,1} + y_{21,1} - y_{12,2}\,. \tag{4.86}$$

In this combination, there are two signals from each arm, taken in opposite direction. Hence the effect of the anomaly is not totally removed. To assess the residual contribution, we can write the anomalous component in Eq. 4.86

$$\zeta^* = \alpha^*(l_{12} - l_{13} + l_{23} - l_{21} + l_{31} - l_{32})\,, \tag{4.87}$$

where $\alpha^* = -\frac{a^*}{c}$, as defined in the previous section. The term of this equation can be gathered in two parts: $l_{12}+l_{23}+l_{31}$, which is the total time around the interferometer in the counterclockwise direction and $l_{13}+l_{21}+l_{32}$, which is the total time in the clockwise direction. Even if the triangle were perfectly rigid, the times of flight would not be the same because of the rotation. Let us write the time of flight around the triangle in the limit of no motion as $\mathcal{L}_{tot}$, and the times of flight in the counterclockwise and clockwise directions as $\mathcal{L}_{tot}+\Delta l_-$ and $\mathcal{L}_{tot}+\Delta l_+$, respectively, when the triangle is rotating. Since the LISA constellation rotates in a clockwise direction (seen from the ecliptic pole), Δl_- will always be negative and Δl_+ will always be positive. Then, ζ^* can be re-written as

$$\zeta^* = \alpha^*(\Delta l_- - \Delta l_+)\,. \tag{4.88}$$

From [42], this difference is given by

$$\Delta l_- - \Delta l_+ = \Delta l_{\text{Sagnac}} = \frac{4A\Omega}{c^2} = \frac{2\pi\sqrt{3}L^2}{c^2 T}\,, \tag{4.89}$$

where Ω is the angular velocity of the rotating light path, A is the area enclosed by the light path, T is the period of rotation of the detector and L is a typical arm length. This time difference, $\Delta l_- - \Delta l_+$, is the Sagnac time shift for signal circulating around a closed path (often referred to *Sagnac effect*). By taking into account the LISA parameters (T=1 year and $L = 5 \times 10^9$m), this time difference is Δl_{Sagnac}=-10^{-4}s. Therefore, the residual effect of the anomaly on the combination ζ will be given by

$$\zeta^* = \alpha^*(\Delta l_- - \Delta l_+) \simeq 3 \times 10^{-22}\,. \tag{4.90}$$

The same conclusion can be drawn from the other Sagnac combinations. Then, the effect of the anomalous blueshift is to add a constant frequency shift in the Sagnac combinations, α, β, γ and ζ. The amplitude of this additional Doppler shift would be comparable to the weakest gravitational waves detectable by LISA. Indeed, it is shown in the previous section that, with TDI, the optimal sensitivity of LISA will be 10^{-23} (see Fig. 4.16). However, this optimal sensitivity occurs in a Fourier frequency range obviously far from the null Fourier frequency where the constant residual contribution of the anomaly has its impact. Hence this effect would not be detectable.

4.6.2 The effects of flexing

As we have seen in Section 4.4.5 (and is explained more in detail in Appendix A), the arms of LISA don't remain constant during the orbit. This is due to the orbital motion and the perturbations of the orbits by the planets. Unlike a pure rigid rotation, the arms are flexing and the important continuous symmetry, $L_{ij}(t+\tau) = L_{ij}(t)$ for any value of τ is no preserved. Now, we don't consider the TDI combinations in the framework of a fixed interferometer and we address the time varying light-times. Specifically, according to [42], the X combination becomes

$$\begin{aligned} X &= y_{12}\left[t - l_{31} - l_{13}^{(1)} - l_{21}^{(2)}\right] - y_{13}\left[t - l_{21} - l_{12}^{(1)} - l_{31}^{(2)}\right] + y_{21}\left[t - l_{31} - l_{13}^{(1)}\right] \\ &\quad - y_{31}\left[t - l_{21} - l_{12}^{(1)}\right] + y_{13}(t - l_{31}) - y_{12}(t - l_{21}) + y_{31}(t) - y_{21}(t)\,, \end{aligned} \tag{4.91}$$

where $l_{21} = l_{21}(\mathrm{t})$, $l_{31} = l_{31}(\mathrm{t})$, $l_{12}^{(1)} = l_{12}(t - l_{21})$, $l_{13}^{(1)} = l_{13}(t - l_{31})$, $l_{21}^{(2)} = l_{21}(t - l_{31} - l_{13}^{(1)})$ and $l_{31}^{(2)} = l_{31}(t - l_{21} - l_{12}^{(1)})$. In this equation, we have also changed the notation of the y_{ij} to be consistent with the l_{ij}. Now, y_{ij} is the signal received at the jth spacecraft and sent by the ith spacecraft. Taking into account Eq. 4.64, the contribution of the anomalous blueshift in the X combination is given by

$$\begin{aligned} X^* &= \alpha^*\left[l_{12}\left(t - l_{31} - l_{13}^{(1)} - l_{21}^{(2)}\right) - l_{13}\left(t - l_{21} - l_{12}^{(1)} - l_{31}^{(2)}\right) + l_{21}\left(t - l_{31} - l_{13}^{(1)}\right)\right] \\ &\quad + \alpha^*\left[-l_{31}\left(t - l_{21} - l_{12}^{(1)}\right) + l_{13}\,(t - l_{31}) - l_{12}(t - l_{21}) + l_{31}(t) - l_{21}(t)\right] \qquad (4.92) \\ &= \alpha^*\left[l_{12}^{(3)} - l_{13}^{(3)} + l_{21}^{(2)} - l_{31}^{(2)} + l_{13}^{(1)} - l_{12}^{(1)} + l_{31} - l_{21}\right]\,, \qquad (4.93) \end{aligned}$$

where $l_{12}^{(3)} = l_{12}(t - l_{31} - l_{13}^{(1)} - l_{21}^{(2)})$ and $l_{13}^{(3)} = l_{13}(t - l_{21} - l_{12}^{(1)} - l_{31}^{(2)})$. To evaluate the size of the residual effect of the anomaly in this equation, the time dependence in the arm lengths can be estimated using $l_{ij}^{(n)} = l_{ij}(t) - nV_{ij}l$, where V_{ij} is the rate of change arm length in seconds per second and l is a typical one-way light-time [42]. Including this expression in Eq. 4.92, we find

$$X^* = 4\alpha^*(V_{13} - V_{12})l = 6.47 \times 10^{-24}\,, \tag{4.94}$$

where, according to [42], we have used $V_{13} - V_{12} = 10$ (m/s)/c. This relation gives therefore the maximum effect of the blueshift due to the orbital motion. This Doppler shift is below the optimal sensitivity of LISA which is about 10^{-23}. Similarly results apply to all TDI combinations. Hence we conclude that the effect will not be detectable.

Chapter 5

Conclusions

The major outcome of this study is to state the inability of the future Laser Interferometer Space Antenna (LISA) to confirm the Pioneer anomaly as a blueshift in the frequency of light. Since only this interpretation is relevant for LISA, this conclusion applies to the Pioneer anomaly to its full extension.

This study was motivated by the fact that the anomalous blueshift on the arms of LISA could be several orders of magnitude bigger than the Doppler shift induced by the weakest measurable gravitational waves. The effect would however be overwhelmed by the laser phase noise and the cancellation methods developed to detect the gravitational waves have to be performed. In the *sensitivity band* of LISA, the anomalous blueshift would be well below all the instrumental noises, even after the laser phase noise cancellation. In addition, considering a finite observation time, the power from the dominant contribution of the anomaly leaks into the *sensitivity band*. This places a non-achievable requirement on the knowledge of the arm lengths of 5×10^{-6} m in order to detect the anomaly. Appropriate work in the frequency domain was then carried out to study the region beyond the *sensitivity band* where the anomaly has its largest impact. The results show that the anomaly cannot be revealed at these timescales since the arm lengths change by much larger distances than it is allowed to remove efficiently the laser phase noise.

Time delay interferometry, shows an even better immunity to the blueshift as it is cancelled perfectly in all the data combinations. Only from the rotation and flexion of the interferometer, a residual contribution of the anomaly would arise. This effect, outside the *sensitivity band*, would however be below the detection threshold of LISA. At the present day, the only way to test the Pioneer anomaly would be in non-dedicated missions to Neptune and beyond.

Appendix

A. Flight configuration

The performance of the laser phase noise cancellation methods, presented in this report, depends strongly on to what extent the three spacecraft of LISA maintain constant distances between them. The orbits of the three LISA spacecraft have thus been specially designed in order to minimise variations in the LISA arm lengths. In this Appendix, we briefly describe the method of [29] to get the expressions from the orbital motions of each spacecraft with respect to time. These expressions will allow us to compute the power spectra of each arm length.

To start, let us define $\alpha \equiv l/2R$, where $l \sim 5 \times 10^6$ km is the distance between two spacecraft and R=1 A.U. $\sim 1.5 \times 10^8$ km. The exact orbits of the three spacecraft are constructed so that to first order in the parameter α, the distances between any two spacecraft remain constant. The equation of an elliptical orbit in the (X-Y) plane is given by [29],

$$X = R(\cos\psi + e), \qquad Y = R\sqrt{1-e^2}\sin\psi\,, \tag{5.1}$$

where R is the semi-major axis of the ellipse, e the eccentricity and ψ the *eccentric anomaly*. The *eccentric anomaly* is related to the mean anomaly Ωt by

$$\psi + e\sin\psi = \Omega t\,, \tag{5.2}$$

where t is the time and Ω the average angular velocity. Note that on the left hand side of this relation, we have a positive sign instead of the usual negative sign. This is because the spacecraft is chosen to be at the aphelion at the zero time.

For the case of LISA, the geometry of the flight configuration is shown in Fig. 5.1.

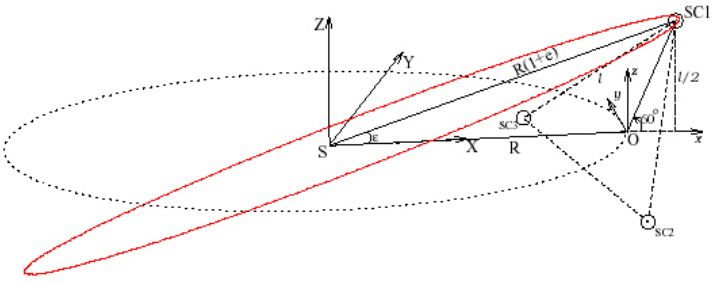

Figure 5.1: Orbit and geometry of LISA. SC1, SC2 and SC3 denote the three spacecraft. The barycentric frame is labelled (X, Y, Z).

The barycentric frame with coordinates (X, Y, Z) is chosen such that the ecliptic plane is X-Y and makes an angle of 60° with the plane of the LISA triangle. The centre of this triangle is

located on the reference orbit, which is assumed circular with a radius of 1 A.U. and centered on the Sun. The spacecraft 1 is chosen such as Z is maximum at $t = 0$. This means that at this point, $\psi = 0$ and $Y = 0$. Thus, to obtain the orbit of the first spacecraft, the orbit in Eq. 5.1 has to be rotated by a small angle ϵ about the Y-axis. In order to obtain the 60°, the spacecraft must have its Z-coordinate equal to $l/2$. Then, ϵ and e are obtained as:

$$\tan\epsilon = \frac{\alpha}{1+\alpha/\sqrt{3}} \tag{5.3}$$

$$e = \left(1+\frac{2}{\sqrt{3}}\alpha+\frac{4}{3}\alpha^2\right)^{1/2}-1\,, \tag{5.4}$$

and the orbit equations of spacecraft 1 are given by

$$X_1 = R(\cos\psi_1+e)\cos\epsilon, \quad Y_1 = R\sqrt{1-e^2}\sin\psi_1, \quad Z_1 = R(\cos\psi_1+e)\sin\epsilon\,. \tag{5.5}$$

The *eccentric anomaly* ψ_1 is implicitly given in terms of t by: $\psi_1 + e\sin\psi_1 = \Omega t$. The orbits of the 2 other spacecraft can be obtained by rotating the orbit of spacecraft 1 by 120° and 240° about the Z-axis. In addition, the phases ψ_2 and ψ_3 have to be adjusted so that the spacecraft are about the same distance l from each other. This lead to the following equations for the spacecraft k (k=2,3):

$$\begin{aligned} X_k &= X_1\cos\left[\frac{2\pi}{3}(k-1)\right] - Y_1\sin\left[\frac{2\pi}{3}(k-1)\right] \\ Y_k &= X_1\sin\left[\frac{2\pi}{3}(k-1)\right] + Y_1\cos\left[\frac{2\pi}{3}(k-1)\right] \\ Z_k &= Z_1\,, \end{aligned} \tag{5.6}$$

where the phase ψ_1 must be replaced by the appropriate phase ψ_k, implicitly given by:

$$\psi_k + e\sin\psi_k = \Omega t - (k-1)\frac{2\pi}{3}\,. \tag{5.7}$$

Using these equations of the spacecraft orbits, we can now plot the evolution of the arm lengths during the two first years of the mission (see Fig. 5.2 below). With these orbits, the inter-

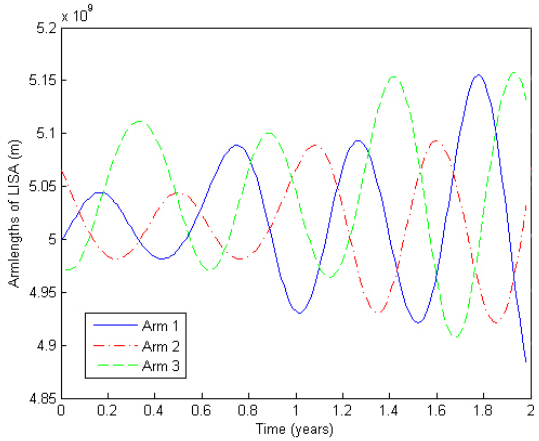

Figure 5.2: The 3 arm lengths of LISA during the first 2 years of the mission.

spacecraft distance can vary up to 100000 km. In the first order in α, it can be shown that the arm lengths remain constant along the orbit [29]. Note that, if we take the first derivative of the

arm length evolutions with respect to time, we obtain the arm length rates of change. These can be up to 13 m/s during the first year. Without correction manoeuvres, they will grow every year.

Finally, we can compute the power spectra of the arm length evolutions. This can be done by dividing the square of the Fast Fourier Transform (FFT) by the number of points used for computing the FFT. The *amplitude power spectrum* for the first armlength is shown in Fig. 5.3 below.

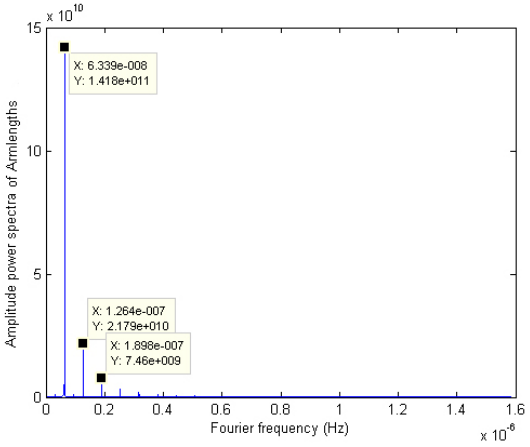

Figure 5.3: *Amplitude power spectrum* of arm length 1.

The dominant frequencies correspond to several months and are outside the *sensitivity band* of LISA.

B. Orbital noise

For short integration time relative to the period of the orbital motion, the arm length rate of change is nearly constant and the approximate Fourier Transform is then given by:

$$\begin{aligned}\widetilde{F.T.}[l_i'(t)] &= \frac{1}{c}\int_0^T (v_i t + 5.10^9)e^{2\pi i f t}dt \\ &= \frac{1}{c}\int_{-\infty}^{+\infty} \mathrm{rect}(\frac{t-\frac{T}{2}}{T})(v_i t + 5.10^9)e^{2\pi i f t}dt\,, \end{aligned} \tag{5.8}$$

where rect(t) is the rectangle function equal to 1 in $[-\frac{1}{2},\frac{1}{2}]$ and 0 elsewhere. Then, by introducing the new variable τ, define as

$$\tau = \frac{t-\frac{T}{2}}{T} \tag{5.9}$$

Eq. 5.8 becomes:

$$\begin{aligned}\widetilde{F.T.}[l_i'(\tau)] &= \frac{v_i T}{c}\int_{-\infty}^{+\infty} \mathrm{rect}(\tau)(T\tau + \frac{T}{2})e^{2\pi i f(T\tau+\frac{T}{2})}d\tau + 5.10^9\frac{T}{c}\int_{-\infty}^{+\infty}\mathrm{rect}(\tau)e^{2\pi i f(T\tau+\frac{T}{2})}d\tau \\ &= \frac{v_i T}{c}e^{\pi i F}\int_{-\infty}^{+\infty} \mathrm{rect}(\tau)(T\tau + \frac{T}{2})e^{2\pi i F\tau}d\tau + 5.10^9\frac{T}{c}e^{\pi i F}\int_{-\infty}^{+\infty}\mathrm{rect}(\tau)e^{2\pi i F\tau}d\tau\,, \end{aligned} \tag{5.10}$$

where we have introduced $F = fT$. According to [48], the Fourier transform of the rectangle function is equal to $\sin(\pi F)/\pi F$ so that:

$$\begin{aligned}\widetilde{F.T.}[l_i'(t)] &= \frac{v_i T^2 e^{\pi i F}}{2\pi i c}\frac{d}{dF}\left[\frac{\sin(\pi F)}{\pi F}\right] + T\left[v\frac{T}{2} + 5\times 10^9\right]e^{\pi i F}\frac{\sin(\pi F)}{\pi F} \\ &= v_i e^{\pi T i f}\frac{\pi T f\cos(\pi T f) - sin(\pi T f)}{2\pi^2 i c f^2} + \left[v_i\frac{T}{2} + 5\times 10^9\right]e^{\pi T i f}\frac{\sin(\pi T f)}{\pi c f}\,. \end{aligned} \tag{5.11}$$

This formula gives the Fourier transform of the arm length for integration time sufficiently short relative to the orbital motion.

Bibliography

[1] J. D. Anderson, P. A. Laing, E. L. Lau, A. S. Liu, M. M. Nieto and S. G. Turyshev, "Indication, from Pioneer 10/11, Galileo, and Ulysses Data, of an Apparent Anomalous, Weak, Long-Range Accelerattion," Phys. Rev. Lett. **81** (1998) 2858 [arXiv:gr-qc/9808081].

[2] J. D. Anderson, P. A. Laing, E. L. Lau, A. S. Liu, M. M. Nieto and S. G. Turyshev, "Study of the anomalous acceleration of Pioneer 10 and 11," Phys. Rev. D **65**, 082004 (2002) [arXiv:gr-qc/0104064].

[3] C. B. Markwardt, "Independent Confirmation of the Pioneer 10 Anomalous Acceleration," arXiv:gr-qc/0208046.

[4] A. Rathke, "Testing for the Pioneer anomaly on a Pluto exploration mission," arXiv:astro-ph/0409373.

[5] Einstein, A., "Über Gravitationswellen" Königlich Preußische Akademie der Wissenschaften (Berlin). Sitzungsberichte **8** (1918) 154-167.

[6] R. P. Feynman, F. B. Morinigo, W. G. Wagner and B. Hatfield (ed.), *Feynman lectures on gravitation,* (Reading, USA, Addison-Wesley 1995) p. XXV.

[7] J. W. Armstrong, L. Iess, P. Tortora and B. Bertotti, "Stochastic gravitational wave background: Upper limits in the 10^{-6} Hz – 10^{-3} Hz band," Astrophys. J. **599** (2003) 806.

[8] The LISA study team, *Laser Interferometer Space Antenna: A cornerstone mission for the observation of Gravitational waves*, System and technology study report, ESA-SCI(2000)11, July 2000.

[9] P.Bender, K. Danzmann, and the LISA study team, Laser Interferometer Space Antenna for the detection of Gravitational Waves, Pre-phase A report No. MPQ233, Max-Planck-Institüt für Quantenoptik, Garching, 1998.

[10] Dornier Satellitensysteme GmbH, Matra Marconi Space, Alenia Aerospazio, *Study of the Laser Interferometer Space Antenna: Final Technical Report* (ESTEC Contract no. 13631/99/NL/MS Report No. LI-RP-DS-009 April 2000).

[11] J. L. Rosales, "The Pioneer effect: a cosmological Foucault's experiment," arXiv:gr-qc/0212019.

[12] J. L. Rosales, "The Pioneer's Anomalous Doppler Drift as a Berry Phase," arXiv:gr-qc/0401014.

[13] J. L. Rosales, "The Pioneer Anomaly: The Measure of a Topological Phase Defect of Light in Cosmology," arXiv:quant-ph/0501041.

[14] A. F. Ranada, "The Pioneer anomaly as acceleration of the clocks," Found. Phys. **34** (2005) 1955 [arXiv:gr-qc/0410084].

[15] D. Izzo and A. Rathke, "Options for a non-dedicated test of the Pioneer anomaly," arXiv:astro-ph/0504634.

[16] C. Talmadge, J. P. Berthias, R. W. Hellings and E. M. Standish, "Model independent constraints on possible modifications of newtonian gravity," Phys. Rev. Lett. **61**, 1159 (1988).

[17] J. D. Anderson, E. L. Lau, T. P. Krisher, D. A. Dicus, D. C. Rosenbaum and V. L. Teplitz, "Improved bounds on nonluminous matter in solar orbit," Astrophys. J. **448** (1998) 885 [arXiv:hep-ph/9503368].

[18] F. I. Cooperstock, V. Faraoni and D. N. Vollick, "The influence of the cosmological expansion on local systems," Astrophys. J. **503** (1998) 61 [arXiv:astro-ph/9803097].

[19] S. Reynaud and M. T. Jaekel, "Testing the Newton law at long distances," arXiv:gr-qc/0501038.

[20] G. F. R. Ellis and J. P. R. Uzan, "'c' is the speed of light, isn't it?," Am. J. Phys. **73** (2005) 240 [arXiv:gr-qc/0305099].

[21] T. Buchert and M. Carfora, "Cosmological parameters are dressed," Phys. Rev. Lett. **90** (2003) 031101 [arXiv:gr-qc/0210045].

[22] M.V. Berry,"Quantal phase factors accompanying adiabatic changes," Proc. R. Soc. London, Ser. A **392**, 45 (1984).

[23] J. Samuel and R. Bhandari, Phys. Rev. D **58** (1987) 1593.

[24] N. Mukunda and R. Simon, *Ann. Phys.* **228**, 20 (1993).

[25] Y. S. Wu and H. Z. Li, "Observable effects of the quantum adiabatic phase for noncyclic evolution," Phys. Rev. B **38**, 11907 (1988).

[26] A. K. Pati,"Adiabatic Berry Phase and Hannay Angle for Open Paths," arXiv:quant-ph/9804057.

[27] C. M. Will and N. Yunes, "Testing alternative theories of gravity using LISA," Class. Quant. Grav. **21** (2004) 4367 [arXiv:gr-qc/0403100].

[28] R. Schilling, "Angular and frequency response of LISA," Class. Quant. Grav. **14** (1997) 1513.

[29] S. V. Dhurandhar, K. Rajesh Nayak, S. Koshti and J. Y. Vinet, "Fundamentals of the LISA stable flight formation," Class. Quant. Grav. **22** (2005) 481 [arXiv:gr-qc/0410093].

[30] Giacomo Giampieri, Ronald W. Hellings, Massimo Tinto, James E. Faller,"Algorithms for unequal-arm Michelson interferometers," Optics communications **123** (1996) 669.

[31] G. Giampieri, R. W. Hellings, L. Maleki, M. Tinto, K. Danzmann, J. Hough, D. Robertson: Optics communications **124** (1996) 313.

[32] M. Tinto and F. B. Estabrook, "Parallel beam interferometric detectors of gravitational waves," Phys. Rev. D **52** (1995) 1749.

[33] M. Tinto, "Spacecraft to spacecraft coherent laser tracking as a xylophone interferometer detector of gravitational radiation," Phys. Rev. D **58** (1998) 102001.

[34] M. Tinto and J. W. Armstrong, "Cancellation of laser noise in an unequal-arm interferometer detector of gravitational radiation," Phys. Rev. D **59** (1999) 102003.

[35] F. B. Estabrook, M. Tinto and J. W. Armstrong, "Time delay analysis of LISA gravitational wave data: Elimination of spacecraft motion effects," Phys. Rev. D **62** (2000) 042002.

[36] M. Tinto, F. B. Estabrook and J. W. Armstrong, "Time-delay interferometry for LISA," Phys. Rev. D **65** (2002) 082003.

[37] F. B . Estabrook and H. Wahlquist, Gen. Rel. Grav. **6** (1975) 439.

[38] H. Wahlquist, "The Doppler Response To Gravitational Waves From A Binary Star Source," Gen. Rel. Grav. **19** (1987) 1101.

[39] J.W. Armstrong, F.B. Estabrook, and M. Tinto,"Time delay interferometry for space-based gravitational wave searches," Astrophys. J. **527**, 814(1999).

[40] R. W. Hellings, "Elimination of clock jitter noise in spaceborn laser interferometers," Phys. Rev. D **64** (2001) 022002 [arXiv:gr-qc/0012013].

[41] W. M. Folkner, T. H. Sweetser, M. A. Vincent, F. Hechler and P. L. Bender, "LISA orbit selection and stability," Class. Quant. Grav. **14** (1997) 1405.

[42] N. J. Cornish and R. W. Hellings, "The Effects of orbital motion on LISA time delay interferometry," Class. Quant. Grav. **20** (2003) 4851 [arXiv:gr-qc/0306096].

[43] D. A. Shaddock, M. Tinto, F. B. Estabrook and J. W. Armstrong, Phys. Rev. D **68** (2003) 061303 [arXiv:gr-qc/0307080].

[44] M. Tinto, F. B. Estabrook and J. W. Armstrong, "Time delay interferometry with moving spacecraft arrays," Phys. Rev. D **69** (2004) 082001 [arXiv:gr-qc/0310017].

[45] C. Salomon, D. Hills and J. L. Hall: J. Opt. Soc. Am. B/Vol. 5, No 8 (August 1988).

[46] Y. De Rop: *Introduction à la relativité générale* (Liege University course, 2004).

[47] P. R. Saulson: *Fundamentals of interferometric gravitational wave detectors* (World Scientific Publishing, Singapore, 1994).

[48] N.C. Geçkinli and D. Yavuz; *Discrete fourier transformation and its applications to power spectra estimation* (Elsevier scientific publishing company, Amsterdam, 1983).

[49] G.M. Jenkins and D.G. Watts, *Spectral analysis and its applications* (Holden-Day, San Fransico, 1968).

[50] ESA scientific website: http://sci.esa.int/

[51] NASA website on LISA: http://lisa.jpl.nasa.gov/

Glossary and Acronyms

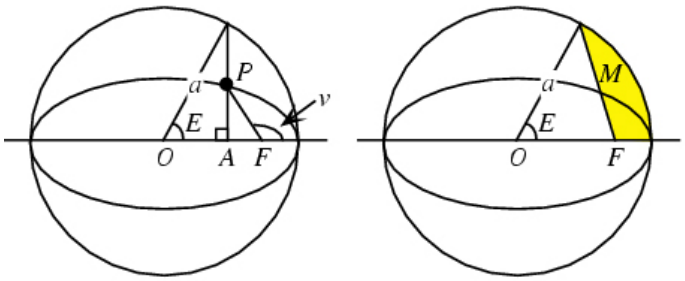

Figure 5.4: Definition of the eccentric anomaly E.

Amplitude power spectrum Square root of the *power spectral density*, defined here after.

Berry phase In quantum mechanics, phase acquired by quantum states when subjected to adiabatic processes, resulting from the geometrical properties of the parameter space of the Hamiltonian.

Black hole object with a concentration of mass great enough that the force of gravity prevents anything from escaping from it except through quantum tunneling behavior. The gravitational field is so strong that the escape velocity near it exceeds the speed of light. This implies that nothing, not even light, can escape its gravity, hence the word "black."

Cassegrain Combination of a prime concave and a secondary convex mirror, both aligned axially. The prime mirror is usually featuring a hole in the centre thus permitting the light to reach an eyepiece, a camera, or a light detector.

Cataclysmic white dwarf White dwarf, which accretes mass spilling over from a low mass hydrogen-burning secondary.

Dark matter Unseen matter that may make up more than ninety percent of the universe. As the name implies, dark matter does not interact with light or other electromagnetic radiation, so it cannot be seen directly, but it can be detected by measuring its gravitational effects. It is believed that dark matter was instrumental in forming galaxies early in the Big Bang.

Drag-free System aimed at shielding a *proof mass* from gas drag and solar radiation pressure (see Section 2.2.1 for more details).

Eccentric anomaly The angle E obtained by drawing the auxiliary circle of an ellipse with center O and focus F, and drawing a line perpendicular to the semimajor axis and intersecting it at A. The angle E is then defined as illustrated above.

Fabry-Perot cavity Optical resonator in which feedback is accomplished by two parallel planes.

Geodesic A curve, which is everywhere locally a distance minimizer, in metric geometry.

LIGO Laser Interferometer Gravitational wave Observatory. A set of two gravitational wave detectors in the USA.

MBH Massive Black Hole. *Black hole* with a mass in the range of millions to billions Solar masses. See also *supermassive black hole*.

Michelson interferometer Classic setup for optical interferometry and invented by Albert Abraham Michelson.

Nd:YAG Neodymium-doped Yttrium-Aluminium Garnet.

Neutron star Celestial body consisting of the superdense remains of a massive star that has collapsed with sufficient force to push all of its electrons into the nuclei that they orbit, thus leaving only neutrons, and having a powerful gravitational attraction from which only neutrinos and high-energy photons can escape, rendering the body detectable only by its X-ray emission.

Optical bench It is a rigid structure made of ultra-low expansion material on which, for rigidity, the optical components are embedded (see Section 2.2.1 for more details).

pc Unit of astronomical length based on the distance from Earth at which stellar parallax is one second of arc and equal to 3.258 light-years, 3.086×10^{13} kilometers.

Power spectral density For a given signal, it gives a plot of the portion of a signal's power (energy per unit time) falling within given frequency ranges.

Proof mass It consists in highly polished cube allowed to float freely within the spacecraft and shielded from external and internal disturbances so that they detect only the force of gravity (see Section 2.2.1 for more details).

Quasar Extremely distant, and thus old, celestial object whose power output is several thousand times that of our entire galaxy. The name is short for "quasistellar radio source."

RTG Radioisotope Thermoelectric Generator.

Sagnac effect Time shift for signals circulating around a closed path.

Sensitivity band Fourier frequency range, in which LISA will be sensitive to gravitational waves (10^{-4} Hz to 1 Hz).

Spectral leakage Release of power between different frequencies due to the finite observation time.

Super massive black hole *Black hole* with a mass in the range of millions to billions solar masses. Most if not all galaxies are thought to host a *supermassive black hole* in their center.

TDI. Time Delay Interferometry.

Weak equivalence principle Einstein's principle, which states that the (local) effects of a gravitational field are identical in all respects to the effect of uniform acceleration. It is a central principle in the theory of general relativity.

White dwarf Remnant of a star, that has collapsed, having an extremely dense state with no empty space between its atoms, but not reaching the extremely dense state of a *neutron star* or black hole.

Yukawa force Possible modification of gravity from a massive attractive field that leads to the following non-relativistic gravitational potential

$$V(r) = -\frac{GMm}{(1+\alpha)r}[1 + \alpha e^{-r/\lambda}]$$

where α is the new coupling strength relative to Newtonian gravity and λ is the new force's range.